AD737127

AFOSR - TR - 72 - 0378

STUDY OF ACOUSTIC-GRAVITY WAVE GENERATION BY NUCLEAR DETONATIONS

By

B. L. Murphy
A. D. Zalay

MT. AUBURN RESEARCH ASSOCIATES, INC.
385 Elliot Street
Newton Upper Falls, Massachusetts 02164

DDC
RECEIVED
FEB 23 1972
B

Sponsored by

Advanced Research Projects Agency
ARPA Order No. 1502

Monitored by

Air Force Office of Scientific Research
under Contract No. F44620-71-C-0086

Reproduced by
NATIONAL TECHNICAL
INFORMATION SERVICE
Springfield, Va. 22151

30 September 1971

Approved for public release;
distribution unlimited.

BEST
AVAILABLE COPY

Unclassified
Security Classification

DOCUMENT CONTROL DATA - R & D

(Security classification of title, body of abstract and indexing annotation must be entered when the overall report is classified)

1. ORIGINATING ACTIVITY (Corporate author)

MT. AUBURN RESEARCH ASSOCIATES, INC.
385 Elliot Street
Newton Upper Falls, Massachusetts 02164

2a. REPORT SECURITY CLASSIFICATION

Unclassified

2b. GROUP

3. REPORT TITLE

STUDY OF ACOUSTIC-GRAVITY WAVE GENERATION BY NUCLEAR DETONATIONS

4. DESCRIPTIVE NOTES (Type of report and inclusive dates)

Scientific----------Interim (Semi-Annual Technical) 2/16/71-8/16/71

5. AUTHOR(S) (First name, middle initial, last name)

Brian L. Murphy
Andrew D. Zalay

6. REPORT DATE	7a. TOTAL NO OF PAGES	7b. NO. OF REFS
30 September 1971	139	

8a. CONTRACT OR GRANT NO	F44620-71-C-0086	9a. ORIGINATOR'S REPORT NUMBER(S)
b. PROJECT NO.	AO 1502	
c.		9b. OTHER REPORT NO(S) (Any other numbers that may be assigned this report)
d.		

10. DISTRIBUTION STATEMENT

Approved for public release; distribution unlimited.

11. SUPPLEMENTARY NOTES	12. SPONSORING MILITARY ACTIVITY
TECH, OTHER	Air Force Office of Scientific Research 1400 Wilson Boulevard (NPG) Arlington, Virginia 22209

13. ABSTRACT

Three different acoustic phenomena relevant to nuclear test detection and diagnostics are discussed in this report: (1) The generation of long period (3-10 minute) acoustic-gravity waves is analyzed in terms of a Lamb mode propagation theory. One result of the analysis is that yield-amplitude proportionality is predicted to break down for very large yield detonations. (2) The generation and propagation of short period (1-60 seconds) acoustic pulses is treated by means of weak shock theory. Yield and height of burst scaling laws are derived for the far-field period. The dependence of period on atmospheric conditions and propagation path is also discussed. (3) The variation of long range Rayleigh wave amplitude with yield and height of burst is discussed for detonations at lower altitudes than previously treated.

DD FORM 1 NOV 65 1473

Unclassified
Security Classification

14 KEY WORDS	LINK A		LINK B		LINK C	
	ROLE	WT	ROLE	WT	ROLE	WT
Acoustic-Gravity Waves						
Infrasonics						
Nuclear Explosions						
Rayleigh Waves						

STUDY OF ACOUSTIC-GRAVITY WAVE GENERATION BY NUCLEAR DETONATIONS

By

B. L. Murphy
A. D. Zalay

MT. AUBURN RESEARCH ASSOCIATES, INC.
385 Elliot Street
Newton Upper Falls, Massachusetts 02164

Sponsored by

Advanced Research Projects Agency
ARPA Order No. 1502

Monitored by

Air Force Office of Scientific Research

Program Code:	1F10
Effective Date of Contract:	16 February 1971
Contract Expiration Date:	15 April 1972
Amount of Contract Dollars:	$78,441.00
Contract No:	F44620-71-C-0086
Principal Investigator:	Dr. Brian L. Murphy
Telephone Number:	(617) 969-7150
Type of Report:	Semi-annual Technical
Period Covered:	16 February 1971 through 31 August 1971

30 September 1971

FORWARD

We wish to acknowledge many helpful discussions with Drs. S. L. Kahalas and A. D. Pierce during the course of this work.

ABSTRACT

Three different acoustic phenomena relevant to nuclear test detection and diagnostics are discussed in this report: (1) The generation of long period (3-10 minute) acoustic-gravity waves is analyzed in terms of a Lamb mode propagation theory. One result of the analysis is that yield-amplitude proportionality is predicted to break down for very large yield detonations. (2) The generation and propagation of short period (1-60 seconds) acoustic pulses is treated by means of weak shock theory. Yield and height of burst scaling laws are derived for the far-field period. The dependence of period on atmospheric conditions and propagation path is also discussed. (3) The variation of long range Rayleigh wave amplitude with yield and height of burst is discussed for detonations at lower altitudes than previously treated.

TABLE OF CONTENTS

Table of Contents (continued)

1. INTRODUCTION

This report is concerned with acoustic disturbances produced by nuclear detonations which are important in the problem of long range test detection and diagnostics. The phenomena we treat, although they are different at large distances, all originate in the detonation blast wave. The basic method of our treatment has been to determine how the blast wave characteristics, and hence the detonation parameters such as yield and height of burst, determine the far-field acoustic disturbance. We have, in addition, attempted to indicate how atmospheric conditions and propagation path ultimately determine the far-field disturbance.

Three types of phenomena are considered:

a. In Section 2 we treat long period (3-10 minute) acoustic disturbances in terms of a theory based on Lamb's atmospheric edge mode. A detailed consideration of how the near-field shock wave evolves into the Lamb mode suggests that the far-field amplitude will increase somewhat faster than directly proportional to yield for very large yield explosions. The exact yield dependence is, however, determined by direction of propagation and atmospheric conditions near the burst point.

b. In Section 3 we discuss the dependence of short period (1-60 second) acoustic signals on source and propagation parameters. We find that the signal period varies approximately as the cube root of yield, is relatively independent of burst height, and is very much affected by the direction of propagation relative to the high altitude winds.

c. In Section 4 we consider the variation of far-field Rayleigh wave amplitude with yield and height of burst for atmospheric explosions. This section is primarily an extension of previous work to lower

heights of burst than were formerly considered. Our principal new finding is that the amplitude for low altitude detonations is a much more rapidly increasing function of yield than for higher altitude detonations.

Overall conclusions reached are presented in Section 5.

2. SOURCE MODELS FOR THE EXCITATION OF LAMB'S ATMOSPHERIC EDGE MODE BY NUCLEAR EXPLOSIONS

2.1 Introduction

The acoustic waveform observed several thousand kilometers away from a megaton range nuclear detonation begins with several cycles having a dominant period of from about 3 to 10 minutes. The amplitude of this portion of the acoustic signal has previously been predicted to be proportional to explosion yield.[1] Recently these first few cycles of the waveform have been analyzed by Pierce and Posey[2] under the hypothesis that the acoustic pulse propagates as the real atmosphere's counterpart of Lamb's edge mode. In the material which follows we rely heavily on the Pierce-Posey theory. This theory appears to be in at least qualitative agreement with test data.[3] When it has been tested against multimode numerical calculations the theory has also produced good agreement for the first few cycles of the waveform.[2] For our purposes the significant feature of this theory is that it is analytic. This allows us, for the first time, to analyze in some detail the relationship between the near-field shock wave and the resulting far-field waveform.

Specifically we ask the following question: At what distance from the detonation and in what direction should one utilize the shock wave parameters to begin a linear propagation theory? Obviously a linear theory is inadequate when the shock is strong. For a 1 MT detonation at sea level, for example, the shock becomes weak (the relative overpressure is .1) at a distance of about 9 km.[4] Since this is larger than the sea-level atmospheric scale height, the effects of atmospheric inhomogeneity might reasonably be expected to play a role. In other words, the weak shock parameters such as relative overpressure and positive phase duration will be different in different directions. Therefore we want to know whether a particular portion of the shock front dominates excitation of the Lamb mode and, if so, we want to know what the shock parameters are for this portion of the front.

The question of what parts of the shock front are most important in determining the far field waveform is not the only question we have to answer. The distance at which we match the weak shock to a linear propagation theory will also make a difference in the far-field result which the theory predicts. For example, consider the difference that occurs if we take the horizontally propagating shock wave from a 1 MT sea-level explosion at two places: (1) 9 km, where the relative overpressure is .1, and (2) 58 km where it is .01.[4] For a weak shock in a homogeneous atmosphere $\bar{\pi}Rt_+$ is a constant.[5] $\bar{\pi}$ is the peak relative overpressure, R is the distance, and t_+ is the positive phase duration. In the present example t_+ must increase by a factor of about 1.55 between 9 km and 58 km. The energy in the low frequency portion of the pulse $\left(\frac{2\pi}{\omega} >> t_+\right)$, which is responsible for the long period portion of the far-field waveform, is proportional to $\bar{\pi}Rt_+^2$. This result follows from Fourier analysis of a weak shock profile such as the so-called Glasstone pulse.[6] Since $\bar{\pi}Rt_+$ is a constant, the low frequency energy is proportional to t_+ and must also increase by a factor of 1.55 between 9 km and 58 km. We conclude that if we chose to match a linear propagation theory to the shock wave at $\bar{\pi}$ = .01 rather than at .1, we would predict far field amplitudes which are greater by a factor of 1.55 The difficulty is <u>not</u> that we have not gone to small enough $\bar{\pi}$. For a weak shock $\bar{\pi}$ never becomes so small that the propagation is linear; that is, the Fourier amplitudes at different frequencies are never frozen relative to each other. The energy in the low frequency portion of the pulse continues to increase proportional to t_+, which quantity increases asymptotically as $\sqrt{\ell nR}$ for a horizontally propagating shock.[5]

In the sequel we use the Pierce-Posey theory to investigate how the far-field waveform evolves from the near-field shock. Specific conclusions reached are: (a) The shock front extending over a number of scale heights in altitude is of almost equal importance in exciting Lamb's atmospheric edge mode. A consequence of this fact is that

features peculiar to a limited portion of the shock front cannot dominate the excitation. An example of what we mean by a feature peculiar to a limited portion of the shock front is the existence of a shock precursor region near the ground within which shock parameters are drastically altered. This occurs when a low altitude detonation occurs over a heat absorbing surface.[6] (b) For small yields, the appropriate distance for matching increases as $Y^{1/3}$, where Y is the explosion yield. For large yields the appropriate distance for matching increases more rapidly than $Y^{1/3}$. This produces a yield dependence in the far-field amplitudes which varies approximately as $Y\left[1+\frac{\sqrt{2}}{3}\sqrt{2n\frac{Y}{Y^*}}\right]$ for $Y > Y^*$, and as Y for $Y < Y^*$. Typically, Y^*, which depends on atmospheric conditions near the burst and on the direction of propagation, is the order of 10 Mt.

In the next section we outline the method used and the major assumptions made in calculating the far-field Lamb mode amplitude from the near field shock parameters. The calculation itself is contained in an appendix.

Then in Section 2.3 we compare the above theoretical prediction (b) with the test data. While the results of this comparison are not conclusive we find that there is indeed a strong indication that on occasion very large yields do produce anomalously large far-field amplitudes.

Finally, we summarize the results of this study, and indicate where we believe extensions of the analysis would be most fruitful, in the conclusions presented in Section 2.4.

2.2 Method of Calculation of the Far-Field Lamb Mode Amplitude

In this section we outline the method used and the major assumptions made in calculating the far field Lamb mode amplitude. The actual calculation is done in Appendix A.

The fundamental assumption of the theory, the justification for which has been discussed by Pierce and Posey, is that the long

period acoustic pulse observed at great distances propagates in the real atmosphere's counterpart of Lamb's edge mode.

To extract this mode from the near field shock wave we pick a cylindrical matching radius r_o, in a manner described below, and decompose the shock pressure pulse into a modal sum, one of whose terms is the desired Lamb mode. This Lamb mode term is then taken to propagate linearly to the observation point, a great circle distance r from the burst, in accordance with the Lamb mode dispersion equation. Because we are primarily interested in modeling the source, we do not attempt to incorporate a realistic atmospheric model in the theory, i.e., one which would include effects such as acoustic ray refraction. Horizontal refraction of the Lamb mode may be an important effect, but this can be treated independently from the source modeling.

To simplify the analysis several assumptions are made concerning the properties of the near field shock wave:

a. The weak shock is characterized as a Glasstone pulse whose peak overpressure $\bar{\pi}$ and positive phase duration t_+ are taken to be functions of altitude and range as described below. It must be admitted that the choice of a Glasstone pulse is made for lack of any better analytic representation of the detonation shock wave. To our knowledge no detailed analysis has ever been made of how adequately the Glasstone pulse represents the very low frequency components of the detonation shock wave.

b. Based on test observations it is assumed that t_+ is much smaller than the far-field period T. Use is made of this assumption in expanding the far-field amplitude as a series in $\frac{t_+}{T}$ and keeping only the first non-zero term.

c. The shock front, except where it intersects the ground, is assumed to be spherical. This assumption is only intended to apply to the portion of the shock which is effective in exciting the Lamb mode. It need not apply, for example, to the upward going shock front.

This assumption will be correct if the shock becomes essentially sonic within an effective scale height in the direction in question.

d. For low altitude detonations the secondary shock which results when the direct shock is reflected from the ground is assumed to make a contribution to the far-field amplitude equal to that of the direct shock. The justification for this assumption is that for a low altitude detonation the secondary shock at sufficiently large distances from the burst point has essentially the same amplitude and radius of curvature as the direct shock. Furthermore, the secondary shock follows the direct shock within a time which is small compared to the periods observed in the far field. For a contact or surface burst the secondary and direct shock are of course the same, although the amplitude may be reduced due to energy expended in digging a crater, etc. This assumption restricts the present theory to low altitude detonations (less than say 15 km). For sufficiently high altitudes the radius of curvature of the two shocks may be very different and the time lag between the shocks may be comparable to the far field period. In this case we would expect interference effects to occur. The high altitude case has not been investigated.

The result of the preceding steps and assumptions is Eq. (A-30) of the Appendix:

$$P_L = - P_s \frac{r_o^{\frac{1}{2}}}{r_e^{\frac{1}{2}} \left(\sin \frac{r}{r_e}\right)^{\frac{1}{2}}} \frac{2(2-\gamma)}{\gamma \sqrt{\pi}} \frac{1}{H \tau_d^2}$$

$$\int_0^\infty A_1' \left[\frac{-t}{\tau_d} + \frac{\sqrt{\Delta z^2 + r_o^2} - r_o}{c \tau_d}\right] e^{-\frac{z}{\gamma H}} \bar{\pi}(r_o, z) t_+^2 (r_o, z)\, dz \qquad \text{(A-30)}$$

where:

P_L = pressure amplitude of the far field Lamb mode

P_s = sea level pressure

r_o = cylindrical matching radius (to be discussed below)

r_e = earth radius

r = great circle distance

γ = ratio of specific heats

H = scale height

τ_d = characteristic dispersion time which is approximately a quarter of the far field period T.

A_i' = derivative of Airy function with respect to its argument.

t = time after arrival of the far-field acoustic signal

c = sound speed

Δz = vertical distance relative to height of burst

z = altitude relative to sea level

$\bar{\pi}$ = peak overpressure of weak shock

t_+ = positive phase duration of weak shock

To proceed from Eq. (A-30) it is necessary to assume a specific spatial dependence for $\bar{\pi}$ and t_+. We take t_+ to be given at a small radius R_o, where $\bar{\pi}(R_o) = .1$, by the problem M results for a homogeneous atmosphere with ambient pressure equal to the ambient pressure at the burst point. R_o is also taken from the problem M results and both $t_+(R_o)$ and R_o are scaled according to Sachs scaling. At the spherical radii $\sqrt{\Delta z^2 + r_o^2} \geq R_o$ where $\bar{\pi}$ and t_+ are required in Eq. (A-30) these quantities are obtained from the values at R_o by using Reed's theory for weak shock propagation in an exponential atmosphere.[5] After some labor it is found that Eq. (A-30) can be reduced to be written solely in terms of the horizontal values of the shock parameters $\bar{\pi}$ and t_+:

$$P_L = \frac{-P_s}{r_e^{1/2}\left(\sin\frac{r}{r_e}\right)^{1/2}} \sqrt{\frac{2}{\pi}}\,\frac{2-\gamma}{\gamma}\,\frac{c^{1/2}}{\mathrm{II}\tau_d^{3/2}}\left(\frac{P_b}{P_s}\right)^{1/\gamma}$$

$$\bar{\pi}\,(r_o, \bar{z})\,t_+^2\,(r_o, \bar{z})\,r_o \int_o^\infty \frac{dy}{\sqrt{y}}\; A_1'\left[\frac{-t}{\tau_d} + y\right] \qquad \text{(A-44)}$$

where $\bar{z}$ is the height of burst and the new integration variable

$$y = \frac{\sqrt{\Delta z^2 + r_o^2} - r_o}{c\tau_d} .$$

Equation (A-44) is essentially identical to the result of Pierce and Posey. This is in spite of the fact that we have used a distinctly different shock model, one which includes the effects of an exponential atmosphere. This result occurs because in the integral of Eq. (A-30) the effect of the exponential atmosphere on the shock parameters tends to be cancelled by the Lamb mode weighting factor $e^{-z/\gamma H}$ as well as other purely geometrical effects.

Now, the first maximum of the far-field amplitude $P_L\left(\frac{t}{\tau_d}\right)$ occurs at about $t = \tau_d$. For $t = \tau_d$ the quantity $\frac{A_1'[-1+y]}{\sqrt{y}}$ occurring in Eq. (A-39) is shown to be significant only between about $0 \lesssim y \lesssim 2$. Truncating the y integration at y=2 corresponds to an effective upper limit on the Δz values of interest of $\Delta z \gtrsim 2c\tau_d$, that is about a half wavelength of the far-field disturbance. Typically this means that the shock at Δz values of at least up to 60 km contribute almost equally to the Lamb mode excitation. This is the basis for our statement that features peculiar to a limited portion of the shock front, such as the existence of a precursor region near the ground, cannot dominate the Lamb mode excitation.

It now remains to choose the matching radius r_o which occurs in Eq. (A-44). Physical arguments are given in the Appendix that this

should be done in the following way: We make a Fourier analysis of the Glasstone pulse and assume that each frequency component within the pulse propagates at a group velocity given by the Lamb mode dispersion equation. The matching radius r_o is determined by requiring that at r_o the low frequencies $\left(\omega \sim \frac{1}{\tau_d(r)}\right)$ which will be important in the far field must have propagated ahead of the largest amplitude frequency components of the weak shock $\left(\omega \sim \frac{1}{t_+(r_o)}\right)$. The basis for this criterion is that while the low frequency components are located behind the shock front they will gain energy from the higher frequency components, but once they move ahead of the higher frequencies their propagation should be amenable to a linear treatment. A more detailed statement of this argument is given in the Appendix.

This criterion assumes the form:

$$t_+(r_o) \simeq \tau_d(r_o) \tag{A-54}$$

which serves to determine r_o. Equation (A-54) has an additional interpretation: Suppose we start with the near field disturbance and follow its development to increasing radii by means of weak shock theory. In addition suppose we take the far-field disturbance and carry it back toward the detonation by means of the Lamb mode theory. According to Eq. (A-54) the matching radius is the distance at which the dominant frequency content of the two disturbances becomes equal.

It turns out that for small yields $\tau_d(r) > t_+(r)$ for all r at which the shock is weak. In this case we use conventional Sachs scaling $r_o \alpha \left(\frac{Y}{P_b}\right)^{1/3}$, where Y is the detonation yield. The constant of proportionality is chosen to make $r_o\left(\frac{Y}{P_b}\right)$ a continuous function in making the transition to the large yield case where Eq. (A-54), rather than Sachs scaling, is used to determine r_o.

The detonation shock parameters enter into Eq. (A-44) in the form $\bar{\pi}(r_o,\bar{z})t_+^2(r_o,\bar{z})r_o$. Since for a weak shock the quantity

$\bar{\pi}(r,\bar{z})t_+(r,\bar{z})r$ is proportional to $\left(\frac{Y}{P_b}\right)^{2/3}$ and independent of r this means that the far-field amplitude P_L is just proportional to $\left(\frac{Y}{P_b}\right)^{2/3} t_+(r_o)$ which increases more rapidly than $\frac{Y}{P_b}$ when r_o is determined by Eq. (A-54). The result of this analysis is the following*:

$$P_L = \frac{-4.7 \times 10^{-5}}{r_o^{1/2} \left|\sin \frac{r}{r_e}\right|^{1/2}} \frac{1}{(cr_d)^{3/2}} \left(\frac{P_b}{P_s}\right)^{1/\gamma-1}$$

$$Y\, Q\left(\frac{Y}{P_b}\right) \int_0^\infty \frac{dy}{\sqrt{y}}\, A_1'\left[-\frac{t}{\tau_d} + y\right] \qquad \text{(A-69)}$$

where P_L is in atmospheres, Y in kT, and cr_d and r_e in km. The "correction factor" Q is:

$$Q\left(\frac{Y}{P_b}\right) = 1 + \frac{\sqrt{2}}{3} \ln \frac{Y}{Y^*} \frac{P_b^*}{P_b}\Bigg]^{1/2}, \quad \frac{Y}{P_b} \geq \frac{Y^*}{P_b^*}$$

$$= 1, \quad \frac{Y}{P_b} \leq \frac{Y^*}{P_b^*} \qquad \text{(A-75)}$$

The critical yield to pressure ratio is given in terms of Pierce and Posey's dispersion parameter h_{kk} by:

$$\frac{Y^*}{P_b^*} = 400(h_{kk})^{3/2} \frac{\text{Mt}}{\text{atmosphere}} \frac{\text{sec}^{3/2}}{\text{km}^{9/2}} \qquad \text{(A-71)}$$

---

* The corresponding constant in the work of Pierce and Posey[2] would appear to be 3.2×10^{-5} rather than our value of 4.7×10^{-5}. This difference probably arises primarily from their choice of $\bar{\pi}t_+^2 r_o$ as $(3.4 \times 10^{-2})(.33)^2(1.61) = 6.1 \times 10^{-3}$ km/sec^2 for a 1 kT sea level detonation. Based on problem M[4] we have taken $\pi t_+^2 r_o = (.1)(1/3)^2(.9) = 10^{-2}$.

The quantity h_{kk} is independent of frequency but is a function of atmospheric conditions near the burst (we only require h_{kk} in Eq. (A-66) out to the distance r_o) as well as the direction of propagation. For this reason it appears that $\frac{Y^*}{p_{\ell}^{*}}$ can only be calculated numerically in conjunction with a detailed atmospheric model for conditions near the burst point.

Nevertheless, as discussed in the next section, it is possible to see some evidence in the low altitude test data of the breakdown of yield-amplitude proportionality for very large yield detonations.

2.3 Comparison of Theory with Test Data for Large Yields

There is at least a suggestion in the test data that very large yields do on occasion produce anomalously large far-field amplitudes. According to Eq. (A-64) the quantity $\frac{P_{\ell}(t=\tau_d)\sqrt{\sin r/r_e}}{Y\,\eta(Y)}\,\tau_d^{2/3}$ is supposed to be a constant for near surface detonations. Taking $P_{\ell}(t=\tau_d)$ to be about half the pressure amplitude first peak to through P_{fpt}, and τ_d to be about a quarter of the far-field period T, we have used the data presented in Ref. 4 to plot Y vs. $\frac{P_{fpt}}{Y}\sqrt{\sin r/r_e}\;T^{3/2}$ in Fig. 2.1. Note that the plot is semi logarithmic. The detonations used are the Soviet explosions of (a) 10 September, (b) 11 September, (c) 14 September, (d) 4 October, (e) 6 October, (f) 20 October, (g) 23 October, (h) 30 October, (i) 31 October, 1961, and the U. S. explosions of (j) 4 May, (k) 10 June, (l) 12 June, (m) 27 June, and (n) 11 July, 1962. Some detonations occur in Fig. 2.1 more than once because data from several stations are used.

The vertical lines in Fig. 2.1 have been arbitrarily drawn at $\frac{P_{fpt}}{Y}\sqrt{\sin r/r_e}\;T^{3/2} = 25 \cdot 10\,\frac{\mu\text{-bar}}{\text{kt}}\,(100\text{ sec})^{3/2}$. The average value

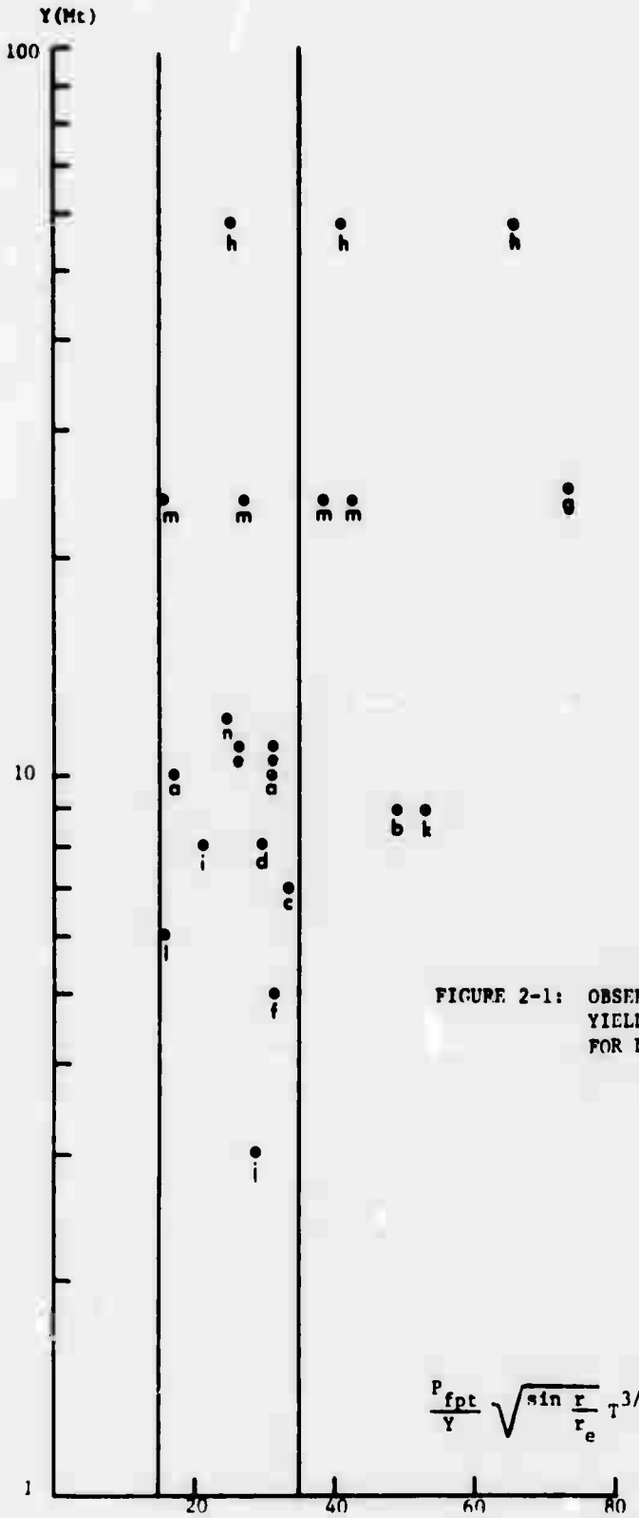

FIGURE 2-1: OBSERVED DEVIATION FROM YIELD-AMPLITUDE PROPORTIONALITY FOR LARGE YIELDS

$$\frac{P_{fpt}}{Y}\sqrt{\sin\frac{r}{r_e}}\,T^{3/2}\left(\frac{\mu bar}{Mt} - (100\ sec)^{3/2}\right)$$

of 25 $\frac{\mu\text{-bar}}{\text{Mt}}$ (100 sec)$^{3/2}$ corresponds to a choice of sound speed c = .31 km/sec in Eq. (A-64). The detonations which lie outside the large amplitude boundary do tend to be large yield detonations. For example, 58 and 24 Mt at two stations lie outside, 25 Mt and two 9Mt detonations also lie outside.

Figure 2.1 provides some indication of the possible breakdown of yield-amplitude proportionality. However, we should caution that some of the deviations may be caused by propagation rather than source effects and furthermore that some of the yield estimates, which are based on seismic data, may be in error.

2.4 Conclusions

We have found that the shock front extending from the ground to many scale heights above the ground is of almost equal importance in determining the far-field Lamb mode amplitude. Because of this, the far-field amplitude should be relatively independent of phenomena peculiar to any small portion of the shock front. In particular, ground effects such as the presence of a precursor should not play a very important role.

For large yield, low altitude detonations we have found a far-field amplitude dependence which varies as $Y\left[1 + \frac{\sqrt{2}}{3}\sqrt{\ell n \frac{Y}{Y^*}}\right]$, where typically Y* is the order of 10 Mt for a sea level detonation. This dependence arises from a detailed consideration of the mechanism by which the low frequency components of the near-field (shock) disturbance become spatially separated from the high frequency components. The precise value of the critical yield Y* where yield-amplitude proportionality breaks down is determined by atmospheric conditions near the burst as well as the direction of propagation and must be determined by detailed numerical calculations. Nevertheless, in analyzing the test data we have seen some evidence that very large yields do on occasion produce anomalously large far-field amplitudes.

Finally, we note that a number of potentially important source effects can be explored within the framework of the present theory. The most important of these effects, which we have not investigated, are probably related to the presence of a secondary shock front due to ground reflection. We expect that at low altitudes the effect of the secondary shock in determining the far-field amplitudes is approximately equal to that of the direct shock, but for higher altitude detonations interference or destructive effects between the two shocks may occur. It would be desirable to subject these ideas to a quantitative analysis.

3. VARIATION OF FAR-FIELD HIGH FREQUENCY ACOUSTIC PERIODS WITH YIELD AND HEIGHT OF BURST

3.1 Introduction

This portion of the report is concerned with detonation-produced infrasonic signals which have periods between about 1 second and 1 minute. These signals have been far less extensively studied than the long period (3-10 minute) acoustic-gravity waves discussed in Section 2.

The short period disturbances are difficult to treat theoretically because their propagation is sensitive to small-scale meteorological phenomena. For example, Meecham[7,8] has calculated that signals in the second to minute period range have a substantial probability of encountering a diffracting wind duct in propagating between the ground and an upper boundary at about 50 km altitude. On each encounter the acoustic signal is split and a small fraction of the energy is lost from the main pulse. According to Meecham, since the propagation path to large distances involves a large number of transits between the ground and the upper boundary, the main pulse eventually becomes so degraded at large ranges that it becomes lost in the multiplicity of pulses. In fact, as Meecham notes, the far-field signal is observed to consist of a large number of apparent pulses extending over a time interval of an hour or more. He attributes the extended signal duration to horizontal refraction by large-scale weather fronts.

Meecham's findings are related to the degradation of pulse amplitude with range. We are concerned with the far-field pulse period and here the situation is quite different. We believe that the period of the main pulse is relatively unaffected by pulse splitting phenomena. In particular we find, as outlined in the subsequent sections, that the disturbance period is essentially determined after only a few transits between the ground and the upper boundary; that is, before

pulse splitting has had an appreciable effect. A corollary to this finding is that the far-field periods have a very weak dependence on range.

The model on which the analysis is based follows Meecham in describing the upper boundary as a reflecting plane at about 50 km altitude. This is the mode of long-range propagation observed for infrasound from rockets.[9] The precise altitude of reflection, which is an important parameter in the theory, is determined primarily by the direction of signal propagation relative to the winds at about 50 km altitude.

In our model the period observed in the far-field is proportional to the positive phase duration of the near-field shock wave. The positive phase duration increases as the shock propagates and this effect is calculated by means of weak shock theory. This is the novel feature of our analysis, namely that it includes nonlinear weak shock effects over large distances.

To obtain starting values for the application of weak shock theory we use modified Sachs scaling. This procedure has been demonstrated to be superior to ordinary Sachs scaling for prediction of peak overpressures in an inhomogeneous atmosphere. We extend the concept of modified Sachs scaling to apply to prediction of positive phase duration as well as peak overpressure.

In Section 3.2 we develop the weak shock propagation model and in Section 3.3 we obtain starting values for this model using modified Sachs scaling. The theory is then used in Section 3.4 to derive scaling laws for the far-field period. Specifically we find:

a. The height of burst dependence is very weak; for detonations in the lower atmosphere it is the order of $\left|1 + \frac{\bar{z}}{45.7}\right|$ where $\bar{z}$ is the height of burst in kilometers.

b. For yields small enough that both weak shock theory and modified Sachs scaling are valid the yield dependence is approximately $Y^{1/3}$. For very large yields the situation is uncertain.

c. Far field periods are found to depend on the altitude of the upper reflecting boundary, z_o, approximately as $e^{z_o/4H_s}$, where H_s is the atmospheric scale height. The altitude z_o is itself primarily determined by the direction of propagation relative to the winds at about 50 km.

3.2 Propagation Model

In this section we derive the basic equation relating the period of the far-field high frequency acoustic signal to the near-field shock parameters.

We assume that the signals of interest in the far field are the ones of largest amplitude. Furthermore, we assume that the period of these signals corresponds to the period of the largest amplitude Fourier components of the weak shock wave. Characterizing the shock wave as a Glasstone pulse[6] with positive phase duration t_+ we find that the largest amplitude Fourier component has a period:

$$T = 2\pi t_+ \ . \tag{3-1}$$

The problem is thus to calculate t_+, which quantity will increase with increasing distance from the detonation. To calculate the evolution of t_+ we use Reed's weak shock equations for an inhomogeneous atmosphere:[5]

$$\frac{\Delta P}{P(r)} = \frac{\Delta P_o}{P(r_o)} \frac{r_o}{r} \frac{t_+^o}{t_+} \sqrt{\frac{P(r_o)}{P(r)}} \ , \tag{3-2}$$

$$\frac{t_+}{t_+^o} = \left[1 + \frac{\gamma+1}{2\gamma} \frac{\Delta P_o}{P(r_o)} \frac{r_o}{ct_+^o} \int_{r_o}^{r} \sqrt{\frac{P(r_o)}{P(r)}} \frac{dr}{r} \right]^{\frac{1}{2}}, \qquad (3\text{-}3)$$

where $\frac{\Delta P}{P(r)}$, t_+, and $P(r)$ are the values of relative overpressure, positive phase duration, and ambient pressure at a distance r from the detonation. $\frac{\Delta P_o}{P(r_o)}$, t_+^o, and $P(r_o)$ are the same quantities at a smaller distance r_o, γ is the ratio of specific heats, and c is the sound speed.

These equations are written for a spherical shockwave. In the real atmosphere the shock wave is refracted and becomes non-spherical. However, hydrodynamic calculations at the Air Force Weapons Laboratory have shown that to a very high degree of approximation, for an exponential atmosphere each portion of the shock front can be regarded as propagating independently with its own radius of curvature.[10] The equations are also written for an N wave pulse form. Groves has examined the difference between N wave and Glasstone pulse propagation laws. He finds the difference to be very small.[11]

The dependence of t_+ on values at r_o may be eliminated by taking the logarithmic derivatives of Eqs. (3-2) and (3-3) and combining to obtain:

$$t_+ = \frac{-\frac{\gamma+1}{4\gamma c} r \frac{\Delta P}{P(r)}}{\left[1 + \frac{r}{2} \frac{\partial}{\partial r} \ln P(r) + r \frac{\partial}{\partial r} \ln \frac{\Delta P}{P(r)} \right]} \qquad (3\text{-}4)$$

For an exponential atmosphere this becomes:

$$t_+ = \frac{-\frac{\gamma+1}{4\gamma c} \frac{\Delta P}{P(r)} r}{\left[1 + \frac{r}{2H} + n \right]} \qquad (3\text{-}5)$$

where

$$n = r \frac{\partial}{\partial r} \ln \frac{\Delta P}{P(r)} , \tag{3-6}$$

and H is the effective scale height in the direction of interest from the burst. The negative and positive signs in Eq. (3-5) correspond to upward and downward shock propagation, respectively.

Applying Eq. (3-5) at the starting radius r_o above the burst and substituting back in Eq. (3-2) yields:

$$t_+(r) = \frac{-\frac{\gamma+1}{4\gamma} \frac{\Delta P_o}{P(r_o)} \frac{r_o}{c}}{\left[1 - \frac{r_o}{2H} + n(r_o)\right]} \left\{ 1 - 2 \left[1 - \frac{r_o}{2H} + n(r_o) \right] e^{-r_o/2H} \int_{r_o}^{r} \sqrt{\frac{P_b}{P(r)}} \frac{dr}{r} \right\}^{\frac{1}{2}} \tag{3-7}$$

where P_b is the ambient pressure at the burst altitude $\bar{z}$.

The range dependence of t_+ is contained in the integral:

$$I = \int_{r_o}^{r} \sqrt{\frac{P_b}{P(r)}} \frac{dr}{r} , \tag{3-8}$$

which is to be done over a propagation path such as illustrated in Fig. 3-1.

It is convenient to rewrite Eq. (3-8) as:

$$I = \sum_{\ell=1}^{L} I_\ell , \tag{3-9}$$

where the index ℓ corresponds to each straight line segment as shown in Fig. 3-1, and L is a large number for the far-field disturbance. We now

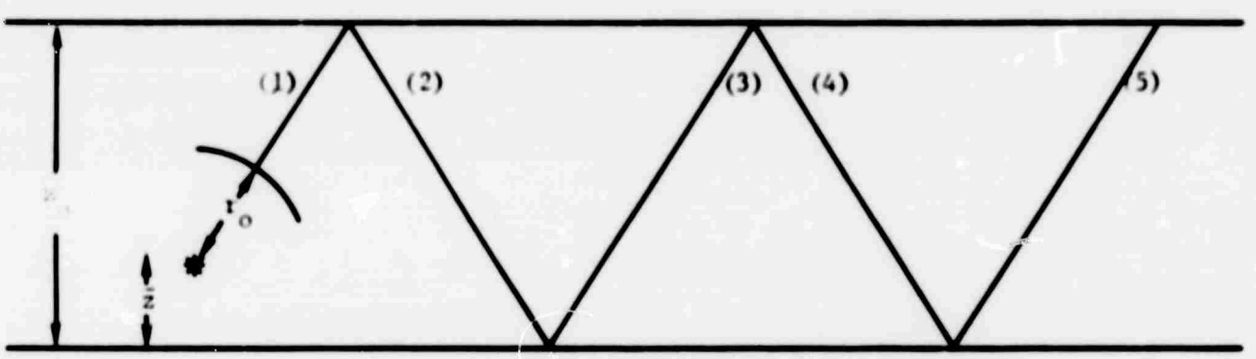

FIGURE 3-1: ASSUMED PROPAGATION PATH

turn to the task of summing the series in Eq. (3-9). Assuming that the radius of curvature is unaltered upon reflection we obtain for each term:

$$I_1 = E_i\left[\frac{z_o - \bar{z}}{2H_s}\right] - E_1\left[\frac{r_o}{2H}\right] , \tag{3-10}$$

$$I_{\substack{\ell \\ \ell\text{odd} \\ \ell\neq 1}} = e^{-(\ell-1)z_o/2H_s}\left\{E_i\left[\frac{\ell z_o - \bar{z}}{2H_s}\right] - E_1\left[\frac{(\ell-1)\ z_o - \bar{z}}{2H_s}\right]\right\} \tag{3-11}$$

$$I_{\substack{\ell \\ \ell\text{even}}} = e^{-\bar{z}/H_s}\, e^{\ell z_o/2H_s}\left\{E_1\left[\frac{(\ell-1)\ z_o - \bar{z}}{2H_s}\right] - E_1\left[\frac{\ell z_o - \bar{z}}{2H_s}\right]\right\} , \tag{3-12}$$

where H_s is the atmospheric scale height in the vertical direction and the exponential integrals E_i and E_1 are defined as:

$$E_1(y) = \int_y^\infty \frac{e^{-t}}{t}\, dt , \tag{3-13}$$

$$E_i(y) = -\int_{-\infty}^{y} \frac{e^{t}}{t}\, dt . \tag{3-14}$$

For large y Eqs. (3-13) and (3-14) can be approximated as:

$$E_1(y) \approx \frac{e^{-y}}{y} \tag{3-15}$$

$$E_i(y) \approx \frac{e^{y}}{y} \tag{3-16}$$

On the assumption that $\frac{z_o - \bar{z}}{2H_s} >> 1$ we may then neglect the second terms in Eqs. (3-11) and (3-12) since these are smaller than the first terms by a factor of $\exp - \frac{(z_o - \bar{z})}{2H_s}$. Physically this is related to the fact that most of the contribution to the integral I, and hence most of the positive phase lengthening, occurs at the upper reflecting boundary where the quantity $\sqrt{\frac{P_b}{P(r)}}$ occurring in Eq. (3-8) is largest.

Using the asymptotic forms, Eqs. (3-15) and (3-16), for the remaining exponential integrals which are functions of z_o we obtain the following expression for I:

$$I = -E_i\left[\frac{r_o}{2H_s}\right] + 2H_s \exp\left(\frac{z_o - \bar{z}}{2H_s}\right)\left[\sum_{\substack{\ell=1 \\ \ell \text{odd}}}^{L} \frac{1}{\ell\bar{z} - z_o} + \sum_{\substack{\ell=2 \\ \ell \text{even}}}^{L} \frac{1}{(\ell-1)z_o - \bar{z}}\right]$$

$$= -E_i\left[\frac{r_o}{2H_s}\right] + 4H_s \exp\left(\frac{z_o - \bar{z}}{2H_s}\right) \sum_{\substack{\ell=1 \\ \ell \text{odd}}}^{L} \frac{1}{\ell z_o - \bar{z}} \quad . \tag{3-17}$$

The summation can be further approximated for $z_o \geq \bar{z}$ (12)

$$\sum_{\substack{\ell=1 \\ \ell \text{odd}}}^{L} \frac{1}{\ell z_o - \bar{z}} = \frac{1}{z_o} \sum_{m=1}^{m} \frac{1}{2m-1}$$

$$= \frac{1}{z_o}\left[\frac{1}{2}(\Gamma + \ell n\, m) + \ell n\, 2 + \frac{B_1}{8m^2} - \frac{7}{64}\frac{B_2}{m^4} + - -\right]$$

$$= \frac{1}{z_o}\left[1 + \ell n \sqrt{m}\right] , \tag{3-18}$$

where Γ is Euler's constant (.57721) and B_1, B_2 -- are Bernoulli numbers (1/6, 1/30, --).

The first term in this last expression comes from I_1; hence a somewhat better approximation than (3-17) is:

$$I \approx E_1\left[\frac{z_o - \bar{z}}{2H_s}\right]\left[1 + \ln \sqrt{m}\right] - E_1\left[\frac{r_o}{2H}\right], \qquad (3\text{-}19)$$

where m is the number of reflections occurring at the upper boundary.

Combining Eqs. (3-1), (3-7), (3-8), and (3-19) we finally obtain:

$$T = \frac{-\frac{\pi}{2}\frac{\gamma+1}{\gamma}\frac{\Delta P_o}{P(r_o)}\frac{r_o}{c}}{\left[1 - \frac{r_o}{2H} + n(r_o)\right]}\left\{1 - 2\left[1 - \frac{r_o}{2H} + n(r_o)\right]e^{-r_o/2H}\right.$$

$$\left.\left[1 + \ln \sqrt{m} \quad E_1\left(\frac{z_o - \bar{z}}{2H_s}\right) - E_1\left(\frac{r_o}{2H}\right)\right]\right\}^{\frac{1}{2}}. \qquad (3\text{-}20)$$

3.3 Starting Values for Weak Shock Parameters

It now remains to determine the shock wave parameters $\frac{\Delta P_o}{P(r_o)}$ and $n(r_o)$ at r_o. To do this we use modified Sachs scaling. According to modified Sachs scaling the relative overpressure, in an inhomogeneous atmosphere, at a distance r from an explosion where the ambient pressure is P(r), is just the same as if the explosion had occurred in a homogeneous atmosphere with ambient pressure P(r). That is:

$$\frac{\Delta P}{P(r)} = f\left\{r\left[\frac{P(r)}{\gamma}\right]^{1/3}\right\} \qquad (3\text{-}21)$$

where Y is the explosion yield and f is the function which gives the relative overpressure in a homogeneous atmosphere.

Modified Sachs scaling appears to be much better for shocks which propagate downward in an exponential atmosphere than for those which propagate upward. Nevertheless, modified Sachs scaling is superior to ordinary Sachs scaling (where P(r) on the right side of Eq. (3-21) is replaced by P_b) and it is our hope that by using it we can obtain some additional accuracy in our calculations.

The accuracy of modified Sachs scaling is best illustrated by a particular example. In Fig. 3-2 we have compared the predictions of modified Sachs scaling for the relative overpressure of the upward going shock with the results of SAP and SHELL calculations for the shock propagation at 45^o from the horizontal due to a 4 Mt isothermal sphere at sea level.[13] The SHELL calculation gives somewhat higher relative overpressures than does SAP because it includes the effects of fireball rise which SAP does not. The rising fireball, particularly for large yields, prevents the shock from relieving backwards. At very small angles from the horizontal the differences between SHELL and SAP are negligible.

The modified Sachs scaling curve in Fig. 3-2 has been constructed under the following assumptions:

a. The 4 Mt isothermal sphere is assumed to correspond to a 4/.7 = 5.72 Mt detonation. This is based on the value of .7 for the effective yield for weak shock production from nuclear explosions in real air relative to ideal air given in Ref. 14.

b. The 1962 Standard atmosphere is used for the ambient pressure.

c. The homogeneous atmosphere calculations of Lehto and Larson are used to provide the function f occurring in Eq. (3-21).[14]

For reasons which appear below we will choose r_o to be the distance at which $\frac{\Delta P_o}{P(r_o)} = .2$. It can be seen from Fig. 3-2 that for

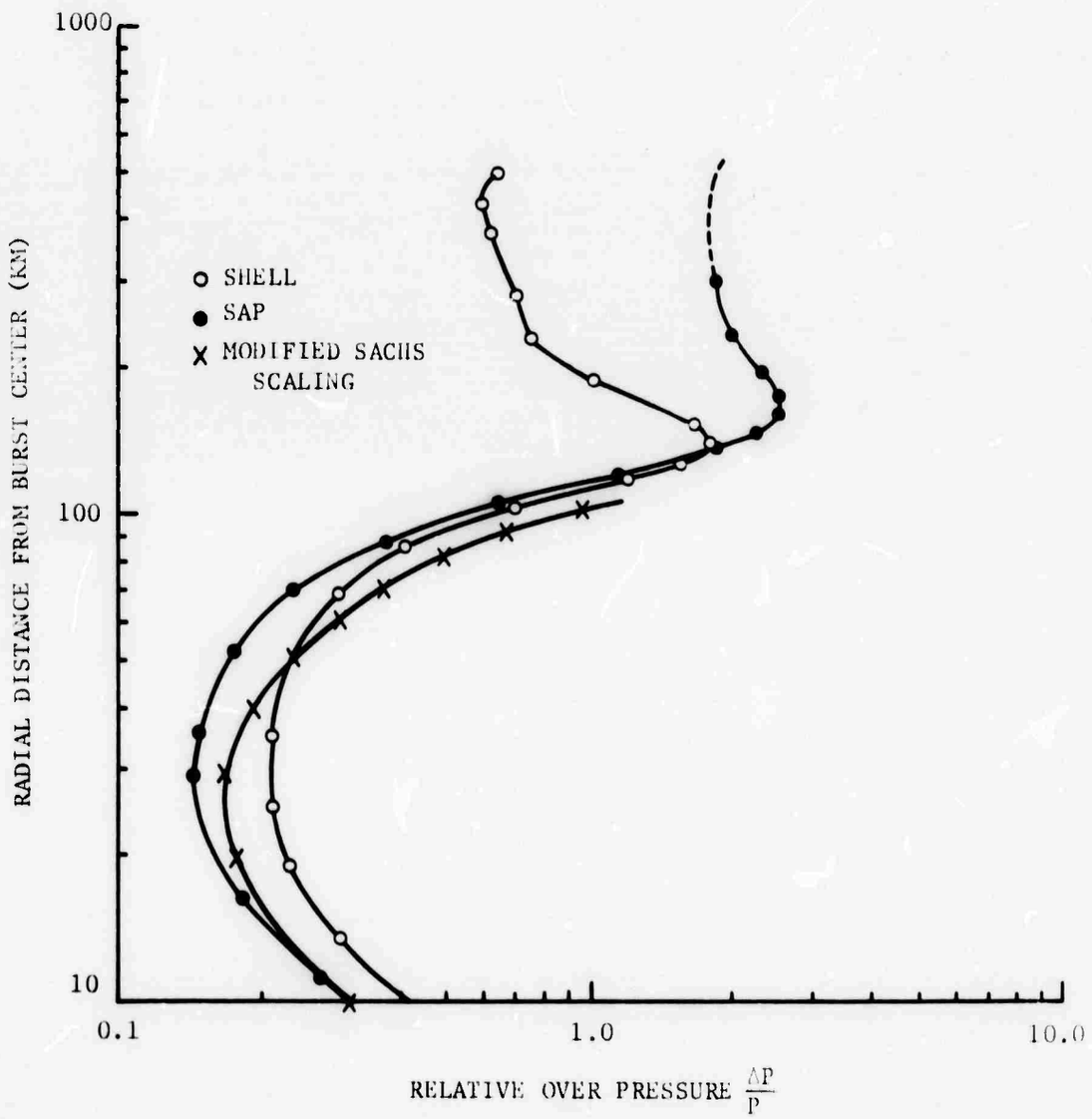

FIGURE 3-2: COMPARISON OF SHELL AND SAP CODES AT 45° WITH MODIFIED SACHS SCALING FOR 4 Mt SEA LEVEL ISOTHERMAL SPHERE (After Reference 13)

this particular case modified Sachs scaling overestimates r_o by perhaps 5-10% compared to the SAP calculation. The function $n(r_o)$ which is the reciprocal of the slope of the curve in Fig. 3-2 appears to be a smaller negative number than given by the SAP result. Quantitative comparison of the modified Sachs scaling result with the SHELL calculation cannot be done using Fig. 3-2 for directions of propagation other than 45^o. However, for angles less than 45^o the agreement between SHELL and modified Sachs scaling will be better than shown in Fig. 3-2.

In any case we would expect modified Sachs scaling to become more accurate in predicting the radius r_o at which $\frac{\Delta P_o}{P(r_o)} = .2$ when the yield becomes small. The reasons for this are:

a. $r_o \propto Y^{1/3}$ and hence the atmosphere encountered by the shock in propagating to r_o is more nearly homogeneous for small Y.

b. The interaction of the rising fireball with the upward going shock is less important for small yields.[13]

Returning to Eq. (3-21) and putting $P(r) = P_b\, e^{-r/H}$ we calculate n(r)

$$n(r) = r \frac{\partial}{\partial r} \ell n \frac{\Delta P}{P(r)} = \left[1 - \frac{r}{3H}\right] \left(\frac{P_b}{Y}\right)^{1/3} r \frac{f'}{f}$$

$$= \left[1 - \frac{r}{3H}\right] n_h \quad , \tag{3-22}$$

where f' is the derivative of f with respect to its argument and n_h is the value of n for a homogeneous atmosphere ($H \to \infty$). The quantity n_h is plotted vs. relative overpressure in Fig. 3-3 which is based on Ref. 14.

We take $\frac{\Delta P_o}{P(r_o)} = .2$ for which, according to Fig. 3-3, $n_h = -3/2$. Eq. (3-22) then gives:

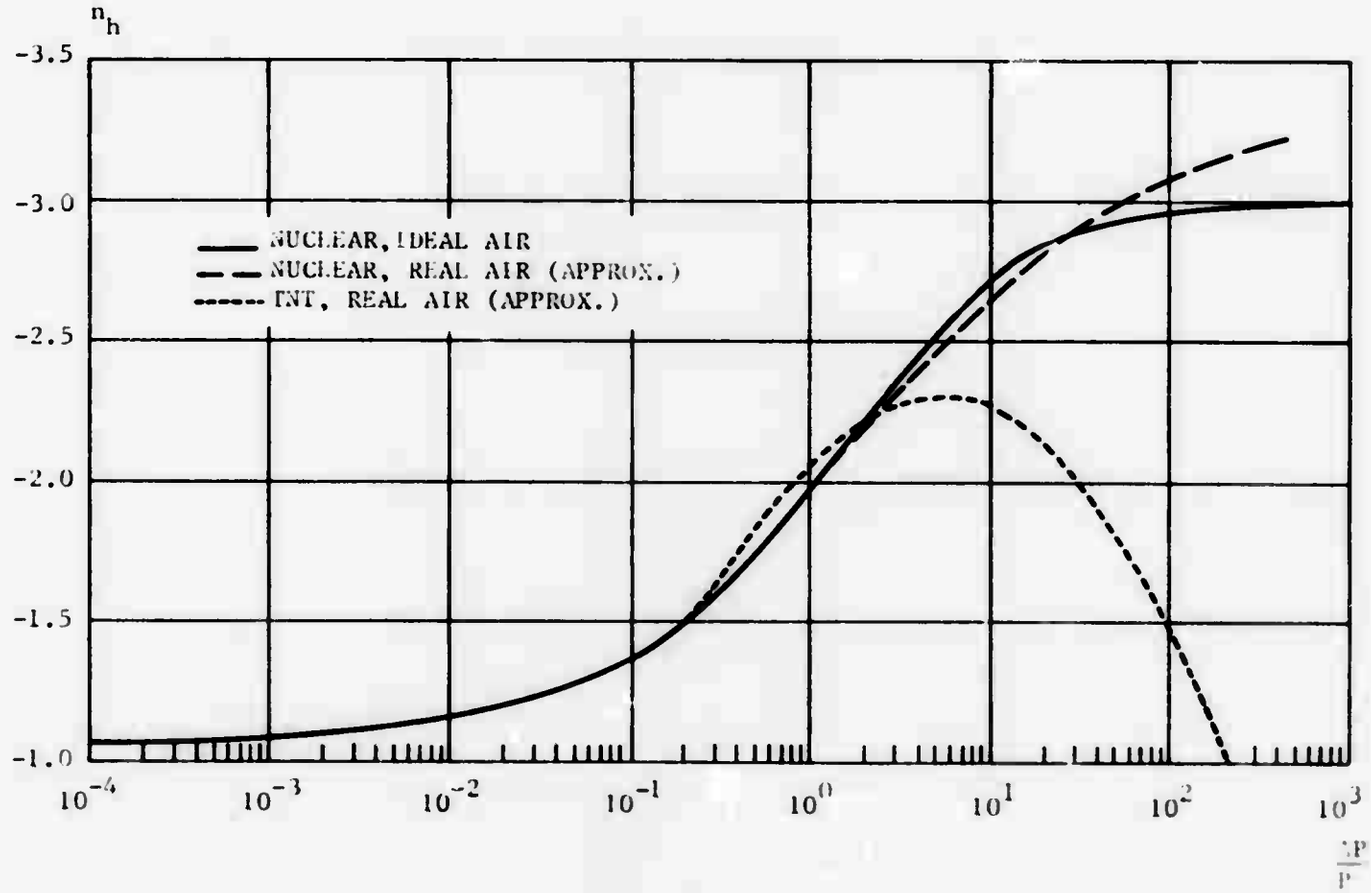

FIGURE 3-3: THE PARAMETER n_h VS. RELATIVE OVERPRESSURE
(After Reference 15)

$$n(r_o) = -\frac{3}{2} + \frac{r_o}{2H} \tag{3-23}$$

The radius r_o is given by modified Sachs scaling as:

$$r_o = .53 \left(\frac{Y}{P(r_o)}\right)^{1/3} \text{ km} , \tag{3-24}$$

where Y is in kT and $P(r_o)$ is in atmospheres. The constant appearing in Eq. (3-24) is obtained from Ref. 14.

Substitution of Eq. (3-23) in Eq. (3-20) with $\frac{\Delta P_o}{P(r_o)} = .2$ gives:

$$T = \pi \frac{\gamma+1}{\gamma} (.2) \frac{r_o}{c} \left\{ 1 + e^{-r_o/2H} \left[\left[1 + \ln \sqrt{m} \right] E_i \left(\frac{z_o - \bar{z}}{2H_s} \right) - E_i \left(\frac{r_o}{2H} \right) \right] \right\}^{\frac{1}{2}} \tag{3-25}$$

where according to (3-24):

$$r_o e^{-r_o/3H} = .53 \left(\frac{Y}{P_b} \right)^{1/3} = .53 e^{\bar{z}/3H_s} Y^{1/3} \tag{3-26}$$

since P_b is measured in atmospheres.

Combining Eqs. (3-25) and (3-26) we obtain the basic equation relating far-field periods to detonation and propagation path parameters:

$$T = \frac{.571}{c} e^{r_o/3H} c^{\bar{z}/3H_s}$$

$$\left\{ 1 + e^{-r_o/2H} \left[(1 + \ln \sqrt{m})\, E_i\left(\frac{z_o - \bar{z}}{2H_s}\right) - E_i\left(\frac{r_o}{2H}\right) \right] \right\}^{1/2} \qquad (3\text{-}27)$$

For detonations in the lower atmosphere $\frac{z_o - \bar{z}}{2H_s} > 1$ the term involving $E_i\left(\frac{z_o - \bar{z}}{2H_s}\right)$ is dominant and Eq. (3-27) becomes:

$$T = \frac{.571}{c} Y^{1/3} \; e^{r_o/12H} \; e^{\bar{z}/3H_s} \; \sqrt{1 + \ln \sqrt{m}} \; \sqrt{E_i\left(\frac{z_o - \bar{z}}{2H_s}\right)} \quad , \qquad (3\text{-}28)$$

or using the large argument approximation given by Eq. (3-16) for $E_i\left(\frac{z_o - \bar{z}}{2H_s}\right)$:

$$T \propto Y^{1/3} \; e^{r_o/12H} \; e^{\bar{z}/3H_s} \; \sqrt{(1 + \ln \sqrt{m}} \; \frac{\exp\left(\frac{z_o - \bar{z}}{4H_s}\right)}{\sqrt{z_o - \bar{z}}}$$

$$= Y^{1/3} \; e^{r_o/12H} \; e^{\bar{z}/12H_s} \; \sqrt{1 + \ln \sqrt{m}} \; \frac{e^{z_o/4H_s}}{\sqrt{z_o - \bar{z}}} \qquad (3\text{-}29)$$

Equations (3-28) and (3-29) provide the basis for the discussion of scaling laws which follows.

3.4 Scaling Laws for the Far Field Period

3.4.1 Range Scaling

The range dependence in Eqs. (3-28) and (3-29) is contained in the factor $\sqrt{1 + \ln \sqrt{m}}$. Since m is the number of reflections from the upper boundary this factor is approximately $\sqrt{1 + \frac{1}{2} \ln \frac{R}{d}}$, where R is the range and d is the distance between ground reflections. Based on ray tracing calculations for infrasonic propagation in a realistic atmosphere[10] a typical value of d would seem to be about 200 km. The factor $\sqrt{1 + \frac{1}{2} \ln \frac{R}{d}}$ would then be equal to 1.47 at 2,000 km, 2.62 at 5,000 km, and 1.72 at 10,000 km; that is, an increase of 17% between 2,000 and 10,000 km.

Actually, this is the largest range dependence we would expect since processes we have not considered would tend to inhibit the increase of period with range. These processes operate in two ways: (a) They decrease the weak shock amplitude, for example by pulse splitting due to wind ducts, and this decreases the importance of nonlinear effects of which period lengthening is a manifestation. (b) Nonlinear effects are also decreased in importance by erosion of the weak shock front, that is, by an increase in the rise time at the front. This could be caused, for example, by ambient turbulence particularly at higher altitudes where there is large wind shear. If the shock front is sufficiently eroded the shock will no longer satisfy the Rankine-Hugoniot relations on which Eqs. (3-2) and (3-3) are based and we would expect pulse lengthening to be less rapid than these equations predict.

In summary the range dependence should be very weak. Furthermore, the exact dependence is probably affected by meteorological conditions along the propagation path.

3.4.2 Height of Burst Scaling

The dependence of far-field period on height of burst $\bar{z}$ for detonations in the lower atmosphere is given by Eq. (3-29):

$$T \propto \frac{e^{\bar{z}/12\,H_s}}{\sqrt{z_o - \bar{z}}} \approx \frac{1}{z_o}\left(1 + \frac{\bar{z}}{12H_s} + \frac{\bar{z}}{2z_o}\right) \propto \left(1 + \frac{\bar{z}}{45.7}\right), \qquad (3\text{-}30)$$

where $\bar{z}$ is measured in kilometers and where we have set the scale height $H_s = 7$ km and the altitude of the upper boundary $z_o = 50$ km.

The origin of this weak height of burst dependence can be seen by inspection of Eq. (3-29). The dependence on height of burst occurs in two factors: (a) $e^{\bar{z}/3H_s} P_b^{-1/3}$, which is due to the fact that the initial positive phase duration t_+^o increases with increasing height of burst according to hydrodynamic (Sachs) scaling.

(b) $\dfrac{\exp\left(\dfrac{z_o - \bar{z}}{4H_s}\right)}{\sqrt{z_o - \bar{z}}}$ which represents the increase in positive phase duration from the initial value t_+^o to the value at the upper reflecting boundary. This factor is a decreasing function of height of burst since the higher the burst altitude the shorter the path length over which the positive phase duration can increase. As shown by Eq. (3-30) these two effects nearly cancel for detonations in the lower atmosphere.

3.4.3 Yield Dependence

According to Eq. (3-26) $r_o < H_s < H$ for

$$Y \cdot P_b \left(\frac{H_s}{.53}\right)^3 = 2.3 \text{ Mt}, \qquad (3\text{-}31)$$

for $H_s = 7$ km and $P_b = 1$.

For sea level detonations of yield much less than 2.3 Mt $r_o \ll H$ and Eq. (3-28) gives:

$$T \alpha Y^{1/3} \tag{3-32}$$

For larger yields the factor $e^{r_o/12H}$ occurring in Eq. (3-28) would make T increase more rapidly than $Y^{1/3}$. Before this factor can become effective, however, several other effects occur. First, the upward going shock becomes strong. The maximum value of r_o allowed by Eq. (3-26) is $r_o = 3H$. The reason for this is that according to modified Sachs scaling the upward going shock never reaches a value of $\frac{\Delta P_o}{P(r_o)}$ as small as .2 for $r_o > 3H$. We conclude that if weak shock theory is to be valid r_o must be considerably less than 3H and hence the factor $e^{r_o/12H}$ would not be very important.

Second, as noted by Greene and Whitaker in Ref. 13, and as demonstrated by the comparison between SAP and SHELL calculations in Fig. 3-2, the rising fireball from large yield detonations interacts with the upward going shock and prevents it from relieving backwards. The effect of this phenomenon should be to decrease the near-field positive phase duration and hence to decrease the far-field period. This would offset and conceivably could dominate the factor of $e^{r_o/12H}$.

3.4.4 Dependence on High Altitude Winds

When the signal propagation is in the direction of the winds near 50 km (downwind) we expect the reflection altitude (z_o) to be lower than when the winds are perpendicular (crosswind) or opposite (upwind) the direction of signal propagation. The reflection altitude occurs in Eq. (3-29) in the factor $e^{z_o/4H_s}$. Therefore, if H_s is taken as 7 km, a 10 km change in z_o will produce about a 40% change in T.

This effect would appear to be among the most significant sources of variation in the far-field period for a given yield and height of burst. Note that the far-field periods will be different in different directions for the same detonation.

In the case of upwind propagation, ray tracing calculations indicate that reflection may not occur at the 50 km level. There is, however, a reflecting boundary at about 100 km altitude.[10] Applying Eq. (3-29) for a sea level detonation the period of signals propagating in this channel is found to be a factor $\frac{e^{100/4H_s}}{\sqrt{100}} \frac{\sqrt{50}}{e^{50/4H_s}} = 4.2$ times as large as for signals propagating in the 50 km channel.

Finally we return to Eq. (3-28) to obtain a numerical estimate for the far-field periods. According to what has been said regarding yield scaling we neglect the factors $e^{r_o/12H}$. We take the sound speed c = .31 km/sec and the scale height H_s = 7 km. We treat the case of a burst near sea level (z = 0). Results for other burst heights can be accomplished by means of Eq. (3-30). Equation (3-28) becomes:

$$\frac{T}{Y^{1/3}} = 1.84 \quad E_i\sqrt{\frac{z_o}{14}} \quad 1 + \ell n \sqrt{m} \quad \frac{\text{sec}}{(kT)^{1/3}} \qquad (3\text{-}33)$$

where z_o is in kilometers.

In Fig. 3-4 we plot $\frac{T}{Y^{1/3}}$ vs z_o, for z_o between 40 and 60 km and for m = 1,2,10, and 25. The value m=1 neglects pulse lengthening effects beyond the first reflection at the upper boundary. The values m=2,10, and 25 would correspond to weak shock propagation, without pulse splitting, to larger distances. For a skip distance d = 200 km the corresponding ranges would be 400, 2000, and 5000 km.

Figure 3-4 predicts the far-field period to be the order of 10 sec for a 1kT low altitude detonation. A more precise

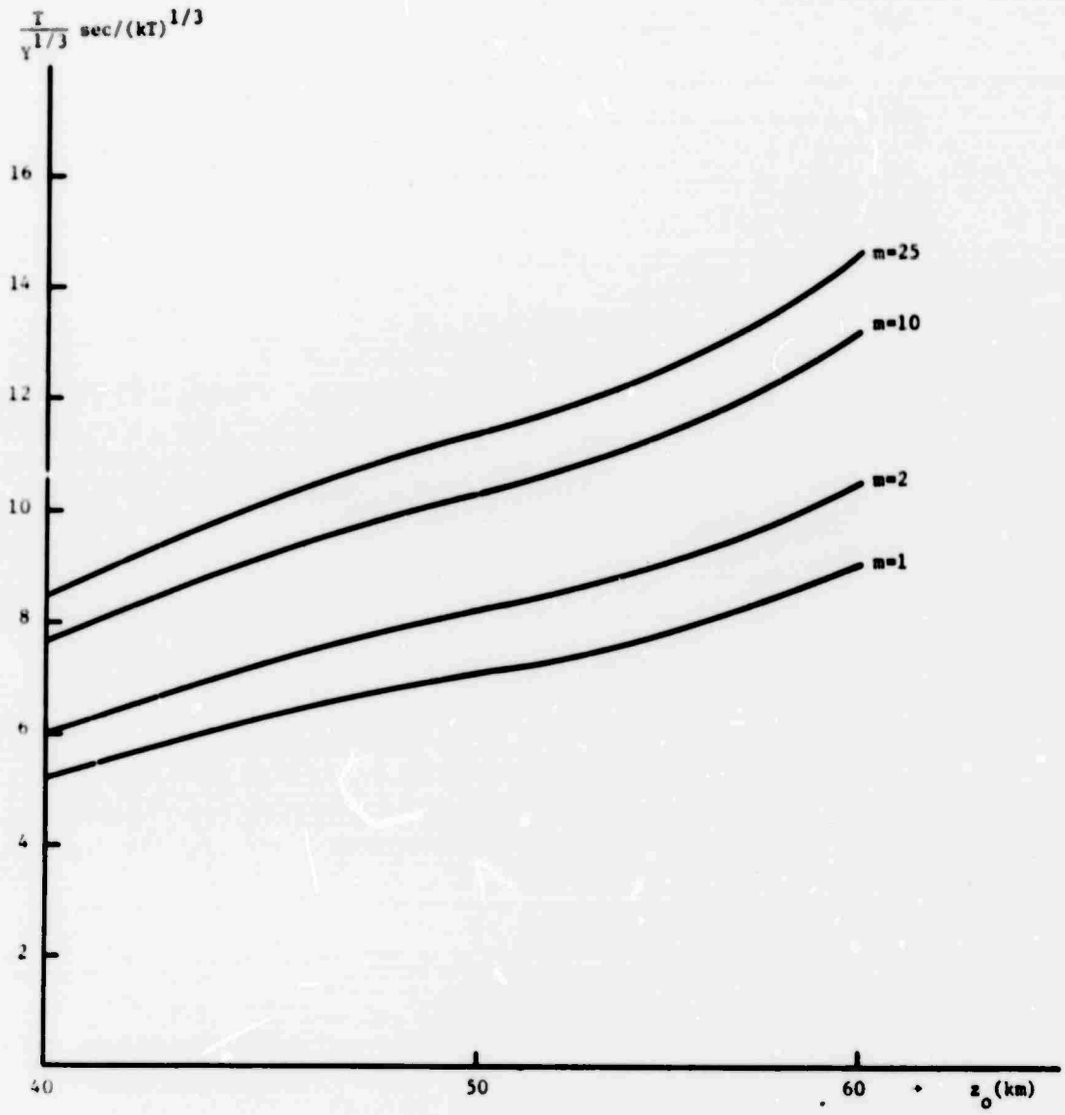

FIGURE 3-4: SCALED PERIOD VS. ALTITUDE OF THE UPPER REFLECTING BOUNDARY

estimate would require detailed information concerning the altitude of the upper reflecting boundary as well as the approximate number of transits between this boundary and the ground for which pulse lengthening effects are important. Determination of the reflection altitude can be accomplished by ray tracing. Determination of the appropriate m value is more complex since detailed meteorological effects such as pulse splitting by wind ducts must be considered. However, the far-field period is insensitive to the exact value of m and so only a rough estimate need be given.

3.5 Conclusions

Based on the theoretical model outlined in the text we have reached the following conclusions concerning the short period detonation-produced infrasound observed at large distances:

a. The period for a 1 kT detonation is the order of 10 seconds.

b. For small yields the period scales as $Y^{1/3}$. For large yields the scaling is uncertain. The interaction of the rising fireball from high yield detonations with the upward going shock needs to be investigated before the large yield scaling can be determined.

c. The range dependence of far-field periods is extremely weak, as an absolute maximum about a 17% increase in going from 2,000 to 10,000 km. Pulse splitting by wind ducts and the effects of other small scale meteorological phenomena are expected to make the actual dependence even weaker than the above value.

d. The period dependence on height of burst is also extremely weak. The dependence is given approximately as: $T \alpha \left(1 + \frac{\bar{z}}{45.7}\right)$, where $\bar{z}$ is the burst height in km.

e. Probably the most significant variation in far-field period, other than that caused by variations in yield, is caused by the direction

of signal propagation relative to the winds at about 50 km altitude. For downwind propagation the signal reflection occurs at a lower altitude than for cross wind or upwind propagation. The dependence of period on reflection altitude is approximately given by: $T \propto e^{z_o/28}$, where z_o is the reflection altitude in kilometers. A 10 km variation in z_o produces about a 40% variation in T. The altitude z_o needs to be determined by ray tracing for the appropriate atmospheric conditions and direction of propagation.

4. GENERATION OF RAYLEIGH WAVES BY ATMOSPHERIC NUCLEAR DETONATIONS

4.1 Introduction

This section is an extension of work contained in a previous report[15] and which will also be presented elsewhere.[16] For convenience Ref. 16 has been included as Appendix B of this report. In this earlier work contained in Appendix B we calculated the source strength for Rayleigh wave excitation, which is defined below, for intermediate altitude detonations. These previous calculations were limited to burst heights between about 30 and 100 km altitude.

In the present work we extend these calculations to lower burst altitudes. Specifically in the case of a 10 kT detonation we now have results as low as .5 km altitude and for a 1 Mt detonation as low as 2 km altitude.

The extension to lower altitudes is not trivial. As discussed below, we have had to develop different methods of calculation than were used for detonations above 30 km altitude.

Our definition of the source strength for Rayleigh wave excitation is based on the work of Toksöz and Ben-Menahem.[17] They have considered the far-field Rayleigh wave amplitudes excited by a point source in a homogeneous atmosphere. For three-dimensional propagation in the absence of nonlinear effects, the source parameters contribute to the amplitudes almost entirely through a factor

$$|L(\omega)| = \left| \int_{-\infty}^{\infty} \delta p(t)\, e^{-i\omega t}\, dt \right| \qquad (4\text{-}1)$$

which is the Fourier transform of the point source pressure fluctuation $\delta p(t)$. In the case of linear pressure pulse propagation, $\delta p(t) \propto \delta p_g(t)\, r$, where $\delta p_g(t)$ is the time dependent pressure pulse on the ground a distance r beneath the source.

Even in the case where the pressure pulse propagation is nonlinear, because of pulse lengthening and dissipative effects we expect that the source strength for Rayleigh wave excitation will be proportional to the Fourier transform of $\delta p_g(t)$ r. The reason is simply that the source strength can only depend on parameters at the ground and not on the previous history of the pulse propagation.

For reasons which will become evident, we therefore define the dimensionless source strength to be

$$S(\tau) = \frac{2\pi r}{\tau\, p_g h} \left| \int_0^\infty \delta p(t)\, e^{-i\omega t}\, dt \right| \qquad (4\text{-}2)$$

where $\tau = 2\pi/\omega$ is the Rayleigh wave period of interest, p_g is the sea level pressure, and h is the atmospheric scale height. We assume a Glasstone pulse[6] at the ground

$$\delta p_g(t) = \Delta p \left(1 - \frac{t}{t_+}\right) e^{-t/t_+} \qquad (4\text{-}3)$$

where Δp is the peak overpressure and t_+ is the positive phase duration.

We then obtain the following result from Eqs. (4-2) and (4-3):

$$S(\tau) = \frac{\Delta p\, r}{\left[1 + \left(\frac{\tau}{2\pi t_+}\right)^2\right] p_g h} \qquad (4\text{-}4)$$

Equation (4-4), which is identical to the definition used in our previous work (Eq. (B-19) of Appendix B), is the basis for the subsequent analysis. In deriving Eq. (4-4) we have not considered details of Rayleigh wave propagation, so that we are unable to provide absolute values of far-field Rayleigh wave amplitudes (or phases). The present

analysis is directly applicable only to estimating relative yields or heights of burst for situations in which source and receiver locations are the same for two or more detonations. However, the shock parameters at the earth's surface, which are calculated in the theory, are suitable as inputs to existing Rayleigh wave propagation models such as those of Harkrider and Flinn[18] and Nickel and Whitaker.[19]

In Section 4.2 we calculate Δp and t_+ as functions of yield and height of burst. The fact that the earth's atmosphere is inhomogeneous plays a major role in determining these shock parameters, at least when the height of burst is comparable to a scale height. In order to treat this effect we use the numerical shock propagation calculations of Lutzky and Lehto[20], for an exponential atmosphere, in conjunction with weak shock theory. For burst heights of much less than a scale height the atmosphere may be treated as homogeneous but the shock becomes strong. In this case we use the problem M results to determine the shock parameters.[4]

In Section 4.3 these values of Δp and t_+ are used in Eq. (4-4) to determine the source strength for Rayleigh wave excitation as a function of yield and height of burst. The dependence on detonation parameters is quite complex, but in general we find:

a. The dependence on yield is stronger for lower altitude detonations. For example, for a Rayleigh wave period of 20 sec and for yields between 500 kT and 1 Mt the source strength varies as $Y^{.95}$ when the burst height is 2 km. When the burst height is 10 km $S \alpha Y^{.63}$ for the same Rayleigh wave period and over the same yield range.

b. The variation of source strength with height of burst can be quite significant. For example, for a Rayleigh wave period of 20 sec and a yield of 100 kT the source strength increases by a factor of about 2.3 as the height of burst is raised from 4 km to 20 km. For this yield and Rayleigh wave period, S then

continues to increase slowly reaching a maximum (about 3 times the value at 4 km) at 65 km. S then decreases with increasing height of burst.

4.2 Calculation of Shock Parameters

We use three different methods of calculating the quantities Δp and t_+ required by Eq. (4-4). The method used depends on the burst height as outlined in the following discussion.

(a) As in our previous work, contained in Appendix B, we base our analysis on the numerical calculations of Lutzky and Lehto[20] for the case of intermediate altitude detonations. These one-dimensional calculations are for downward shock propagation in an ideal gas, exponential atmosphere due to a point explosion.

The Lutzky and Lehto calculations are extrapolated to smaller overpressures on the ground than were treated numerically by means of weak shock theory. The basic equations for this procedure, which are derived in Appendix B, are as follows:

$$t_+ = \frac{h}{c}\, g(x) \tag{4-5}$$

$$\frac{\Delta p}{p_g} = \frac{h}{r}\, f(x)\; e^{-r/2h} \quad , \tag{4-6}$$

where t_+ and Δp are the positive phase duration and overpressure at the earth's surface from a detonation at altitude r, h is the atmospheric scale height, c is the speed of sound, and p_g is the sea level pressure. The functions g(x) and f(x) are given by:

$$g(x) = -\left(\frac{\gamma+1}{2\gamma}\,\frac{\Delta p_o}{p_o}\right)\frac{x}{1+x+n}\left\{1-2\left[1+x+n\right]\epsilon^{x}\left[E_1(x) - E_1\left(\frac{r}{2h}\right)\right]\right\}^{\frac{1}{2}} \tag{4-7}$$

$$f(x) = \left(\frac{\Delta p_o}{p_o}\right) \frac{xe^x}{\left\{1-2\left[1+x+n\right] e^x \left[E_1(x) - E_1\left(\frac{r}{2h}\right)\right]\right\}^{\frac{1}{2}}} \qquad (4\text{-}8)$$

where γ is the ratio of specific heats, $\frac{\Delta p_o}{p_o}$ is the relative overpressure at a distance $r_o \leq r$ beneath the burst, and E_1 is the exponential integral, $E_1(x) = \int_x^\infty \frac{e^{-t}}{t}\, dt$. The quantities x and n are starting values obtained from the numerical calculations:

$$x = \frac{r_o}{2h} \qquad (4\text{-}9)$$

$$n = \left(r \frac{\partial}{\partial r} \ln \frac{\Delta p}{p}\right)_{r=r_o} \qquad (4\text{-}10)$$

Equations (4-5) and (4-7) are equivalent to Eq. (B-10) of Appendix B, and Eqs. (4-6) and (4-8) are equivalent to Eq. (B-11) of Appendix B.

The calculations of Lutzky and Lehto are parameterized by the quantity:

$$\sigma_h = h\left(\frac{p_b}{E}\right)^{1/3} , \qquad (4\text{-}11)$$

where p_b is the ambient pressure at the burst point and E is the energy released by the point explosion. According to Ref. (14) a nuclear explosion in real air is expected to be .7 times as effective in producing a given weak shock overpressure at large distances as the idealized point source with $\gamma = 1.4$. Accordingly, we take $Y_{kT} = .7\, E_{kT}$ and Eq. (4-11) becomes:

$$\sigma_h = h \left[\frac{p_b(mb)}{29.4\ Y_{kT}}\right]^{1/3} = h\, e^{-r/3h} \left[\frac{p_g(mb)}{29.4\ Y_{kT}}\right]^{-1/3} \qquad (4\text{-}12)$$

The starting values x and n obtained for the particular values of σ_h used by Lutzky and Lehto are shown in Table 4-1.

TABLE 4-1

STARTING VALUES AT $\Delta p_o/p_o = .1$ FOR APPLICATION OF THEORY AS OBTAINED FROM NUMERICAL CALCULATIONS

σ_h	x	n
.05	3.11	-4.26
.1	2.55	-3.84
.2	1.96	-3.29
.5	1.26	-2.82
2.0	.502	-1.9

According to Eq. (4-12) a given yield Y and height of burst r determine σ_h. When the yield and height of burst are chosen to produce σ_h values occurring in Table 4-1 we obtain values of x and n and hence determine t_+ and Δp by means of Eqs. (4-4) - (4-8). This is what we have done for intermediate altitude detonations, $r \gtrsim 30$ km.

The calculational procedure is identical to that of Appendix B with two exceptions: (i) We retain the term $E_1(r/2h)$ in Eqs. (4-7) and (4-8) for increased accuracy. This term was previously omitted. (ii) The ambient pressure at the burst point, p_b in Eq. (4-11), was previously determined by using the 1962 Standard Atmosphere. For the sake of consistency we now determine p_b by assuming that the

atmosphere is truly exponential as indicated in Eq. (4-12). These differences produce no significant changes in our previous values of S which are given in Appendix B for intermediate altitude detonations.

The above procedure does not work at low altitudes, however. For example, for a yield of 1 Mt there are no σ_h values in Table 4-1 corresponding to altitudes between sea level and 30 km. To use the method we have outlined for low altitude detonations, we need x and n for additional σ_h values (particularly $\sigma_h > 2$). How these additional values are obtained is described below.

(b) For detonations at low altitudes corresponding to $\sigma_h > 2$ we extend Table 4-1 by adding an additional value of σ_h, namely, $\sigma_h = \infty$ corresponding to a homogeneous atmosphere ($h = \infty$). For this value of σ_h we have, of course, x=0 and from numerical calculations[14] (see Fig. 2-3) we obtain n = -1.38.

According to Eq. (4-12) there is no altitude or yield (other than Y=0) corresponding to $\sigma_h = \infty$. However, we add $\sigma_h = \infty$ to Table 4-1 in order to interpolate to σ_h values between 2 and ∞. We now describe how this interpolation is done.

In Fig. 4-1 we plot $1/\sigma_h + 1$ vs. x using the data of Table 4-1 as well as $\sigma_h = \infty$, x = 0. Note that the plot, which is semi-logarithmic, is very nearly a straight line, i.e., $\ell n(1/\sigma_h + 1) \propto x$. Figure 4-2 shows a plot of n vs. x using the same x values, again the plot is very nearly a straight line, i.e., $n = n_o + ax$, where n_o and a are constants.

Based on the empirical evidence contained in Figs. 4-1 and 4-2 we use a linear interpolation of $\ell n(1/\sigma_h + 1)$ vs. x to obtain x given σ_h. We then use a linear interpolation of n vs. x to obtain the corresponding value of n. This procedure works not only for σ_h between ∞ and 2 but also for example between .5 and 2. Thus, Eqs. (4-5) through (4-8) can now be used for arbitrary yield and height of burst provided that the shock at the ground is weak. When the shock at the ground is strong we must use still a different procedure as described below.

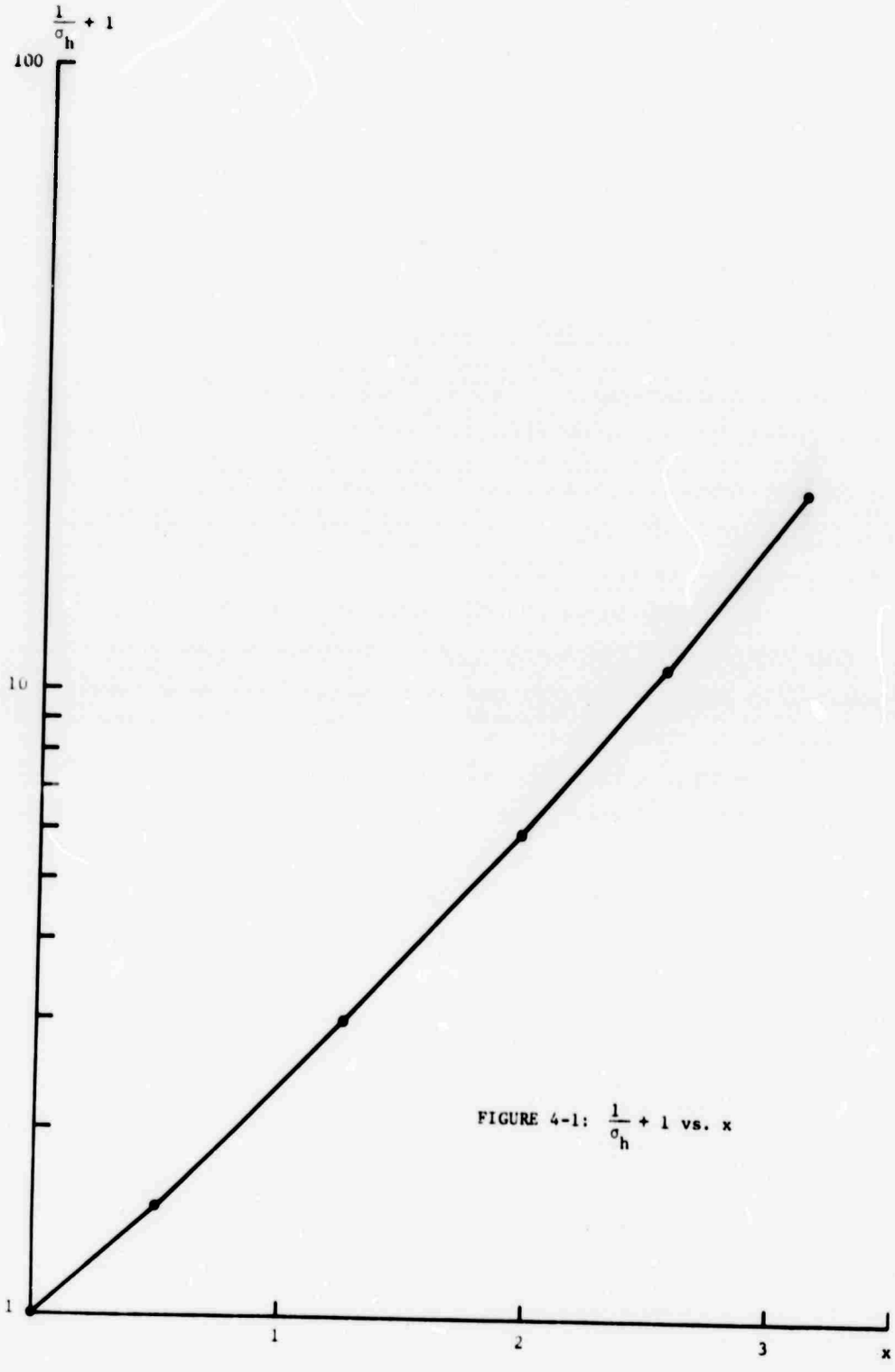

FIGURE 4-1: $\frac{1}{\sigma_h} + 1$ vs. x

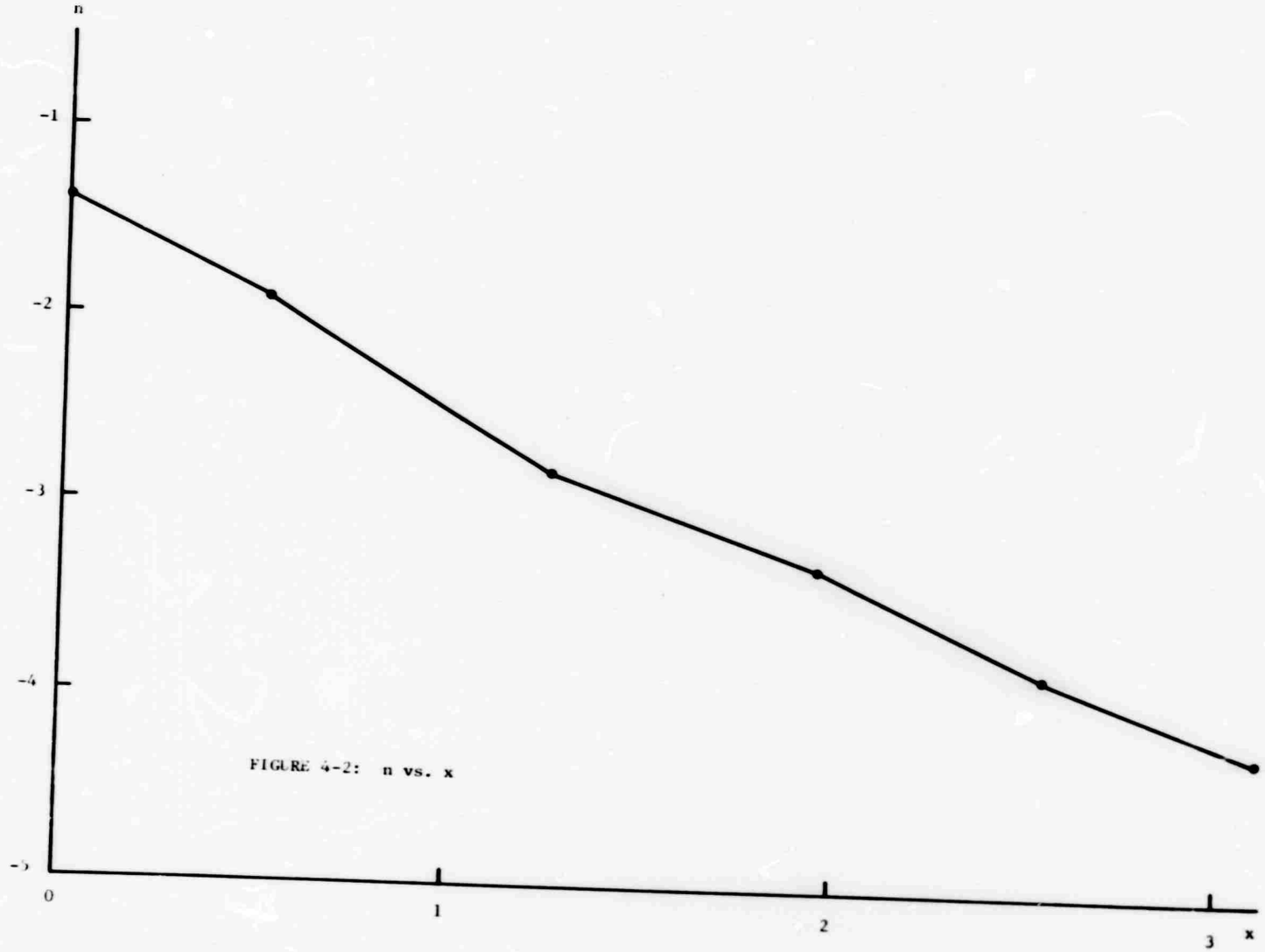

FIGURE 4-2: n vs. x

c. When the shock at the ground is strong ($\Delta p/p_g \sim 1$) Eqs. (4-5) - (4-8) are no longer valid. This situation arises, of course, for low altitude detonations. In general, the height of burst is the order of, or less than, an atmospheric scale height. This suggests that values of the shock parameters obtained from numerical calculations with a homogeneous atmosphere will be reasonably accurate.

We have used Δp and t_+ values as computed in problem M[4] with the ambient pressure of the homogeneous atmosphere taken as p_g, the sea level pressure. Scaling to sea level rather than burst point conditions corresponds to modified Sachs scaling. This scaling has been shown to be very accurate in predicting the overpressure Δp.[20] The validity of modified Sachs scaling for strong shocks in predicting the value of positive phase duration t_+ has not been investigated. However, as will be seen, this procedure does give values of t_+ which match smoothly to the values given by weak shock theory using the calculational procedures (a) and (b).

Figures 4-3 and 4-4 shown $\Delta p/p_g$ and t_+ as functions of r for five different yields based on this combination of weak shock theory and problem M results. We have taken $\gamma = 1.4$, $h = 7$ km, and $c = .34$ km/sec, the value used in problem M, in constructing these curves. In Fig. 4-4 when neither weak shock theory nor the problem M results can strictly apply ($\Delta p/p_g \approx 1$, $r \approx h$) we have used a best fit by eye. The deviations from this best fit which arise from applying weak shock theory at too large a value of $\Delta p/p_g$ and applying the problem M results at too large a value of r are indicated by dashed curves for the 10 kT case. In all cases the region fit by eye (or "extrapolated") is indicated. For reasons described below we do not treat values of $\Delta p/p_g > 1$.

The solid curves in Figs. 4-3 and 4-4 give the values of $\Delta p/p_g$ and t_+ which are used in Section 4.3 to predict the source strength for Rayleigh wave excitation.

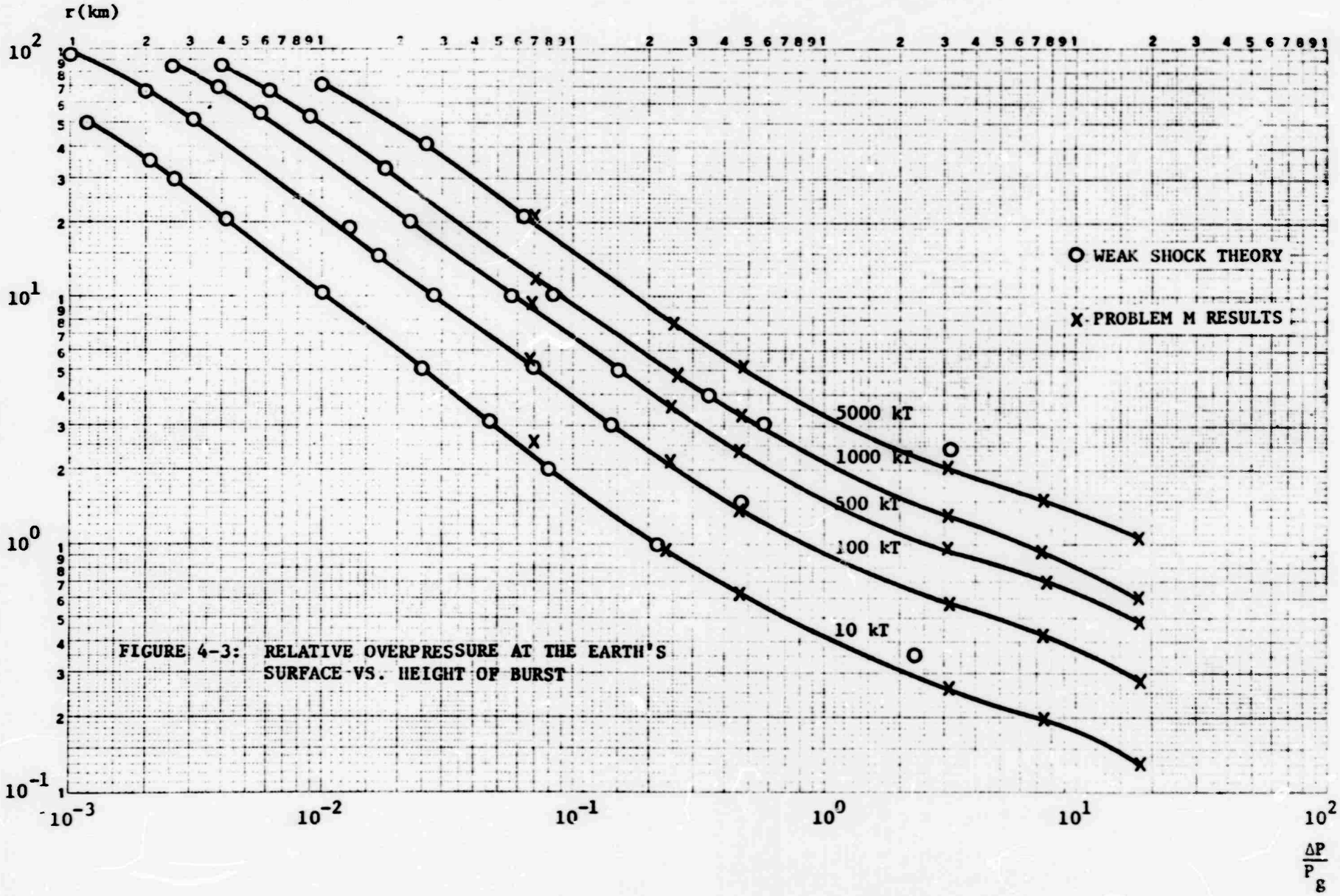

FIGURE 4-3: RELATIVE OVERPRESSURE AT THE EARTH'S SURFACE VS. HEIGHT OF BURST

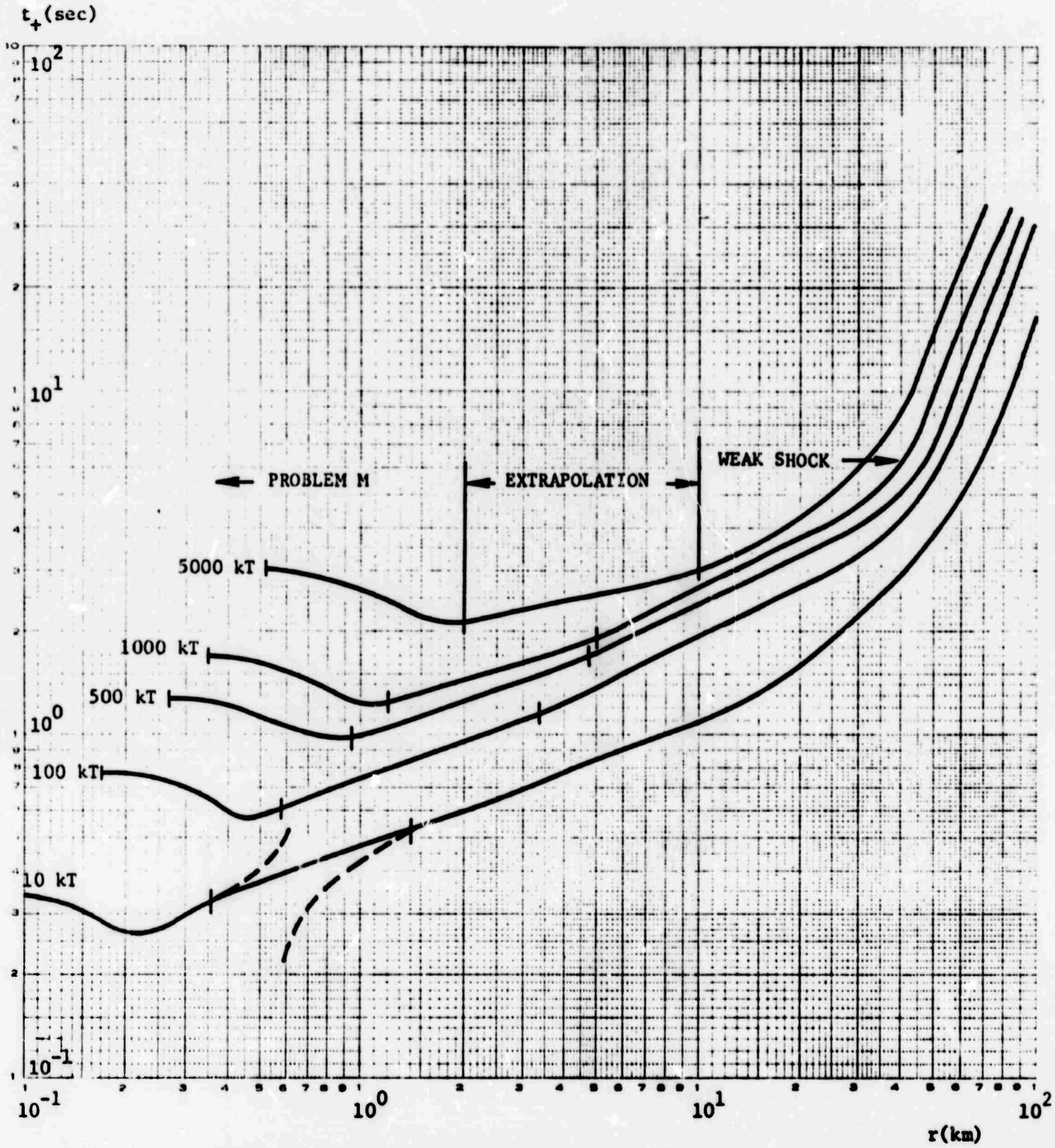

FIGURE 4-4: DURATION OF POSITIVE PHASE AT THE EARTH'S SURFACE VS. HEIGHT OF BURST

4.3 Results

To obtain the source strength for Rayleigh wave excitation we have substituted the values of $\Delta p/p_g$ and t_+ shown in Figs. 4-3 and 4-4 into Eq. (4-4).

Figures 4-5 through 4-9 show the source strength as a function of altitude for yields of 10, 100, 500, 1000, and 5000 kT. In each figure the source strength is shown for Rayleigh wave periods of 10, 20, and 40 seconds. At altitudes above perhaps 40 km the yield referred to should be considered to be an effective yield. This may be less than the nominal yield due to radiative or other energy loss mechanisms.

The highest altitude shown on these plots corresponds either to the smallest value of σ_h at our disposal ($\sigma_h = .05$ in Table 4-1) or to an altitude of 100 km. Our reason for stopping at 100 km is that above this altitude the real atmosphere cannot be characterized by a constant scale height h as assumed in the theory.

The lowest altitude shown has been arbitrarily taken to correspond to $\Delta p/p_g = 1$. Using the problem M results we could continue the curves to still lower altitudes. However, in every case we find that S rapidly goes to infinity. This is the result of the fact that for a strong shock $\Delta p \propto 1/r^3$ so that $\Delta pr \propto 1/r^2 \to \infty$ as $r \to 0$. The difficulty seems to be that, while the shock description is correct, S no longer represents the source strength for Rayleigh wave excitation. This is not unexpected since the theory of Toksöz and Ben-Menahem which we have used in defining S is based on a linear model of wave propagation. A different model of the excitation itself is required to go to still lower altitudes. Ideally this model, which would include effects such as cratering, would extend through the "trans-surface" regime. That is, it would match smoothly not only to our results but also to results obtained for contained underground explosions.

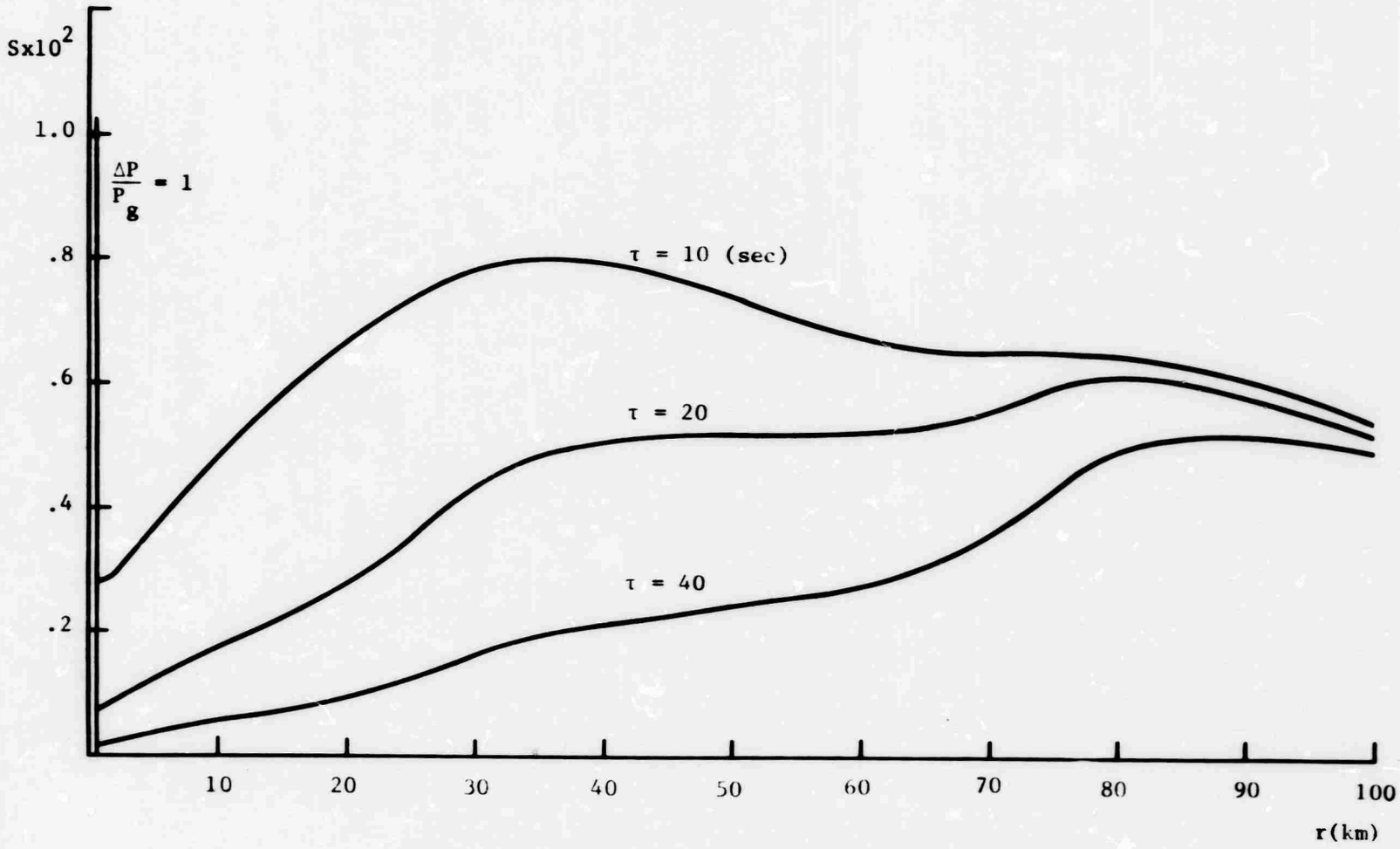

FIGURE 4-5 DIMENSIONLESS SOURCE STRENGTH AS A FUNCTION OF ALTITUDE FOR Y = 10 KT

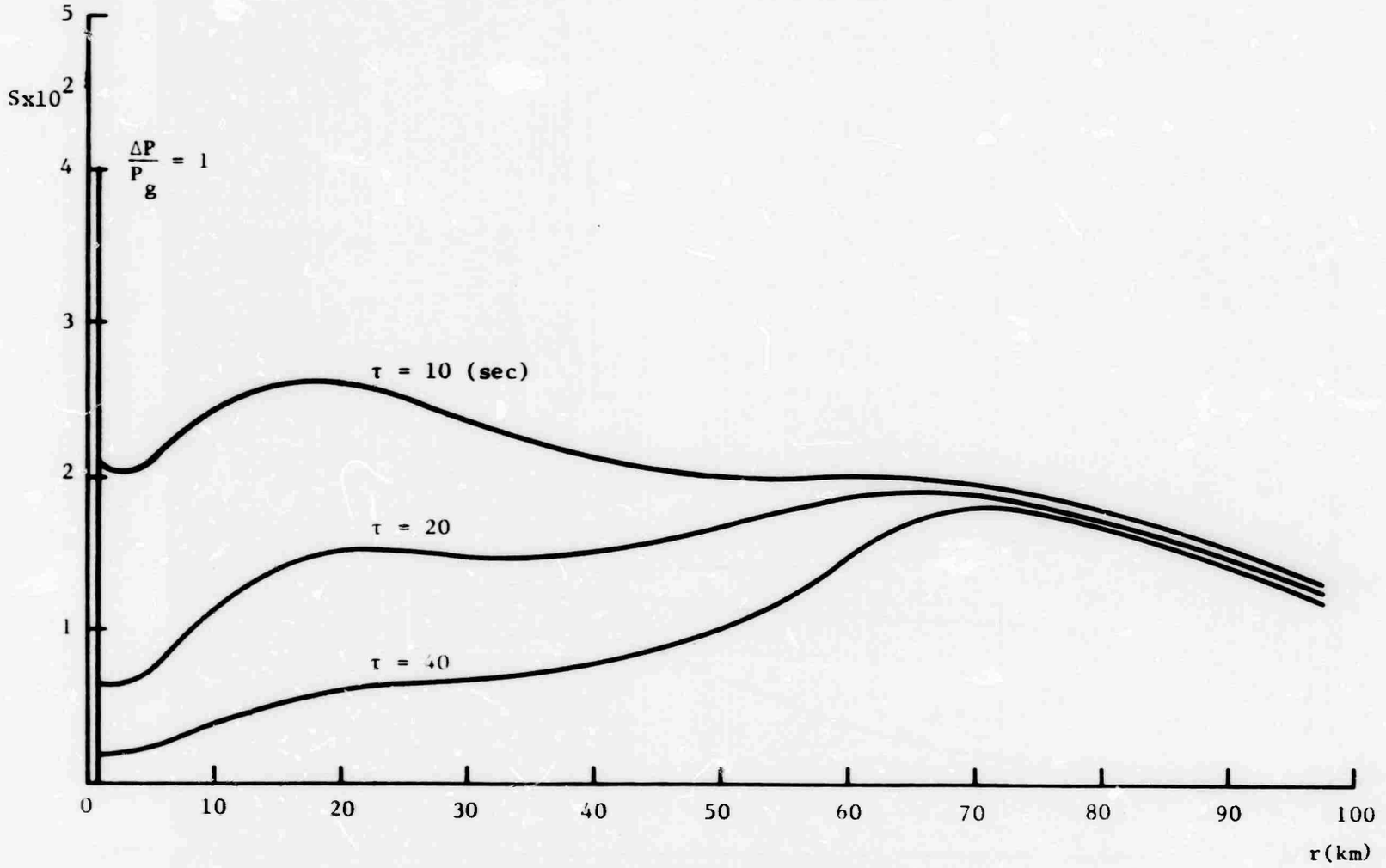

FIGURE 4-6: DIMENSIONLESS SOURCE STRENGTH AS A FUNCTION OF ALTITUDE FOR Y = 100 KT

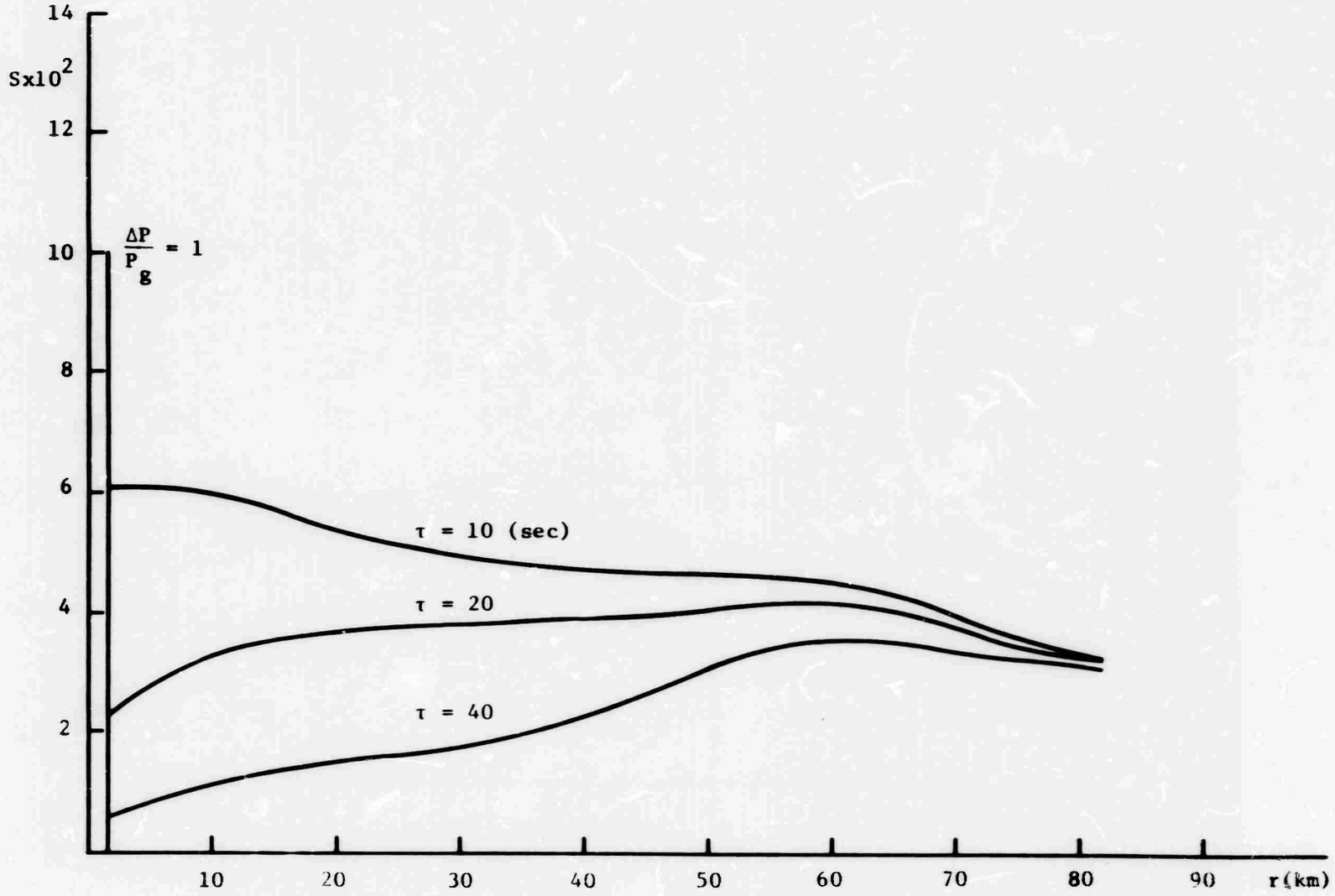

FIGURE 4-7: DIMENSIONLESS SOURCE STRENGTH AS A FUNCTION OF ALTITUDE FOR Y = 500 KT

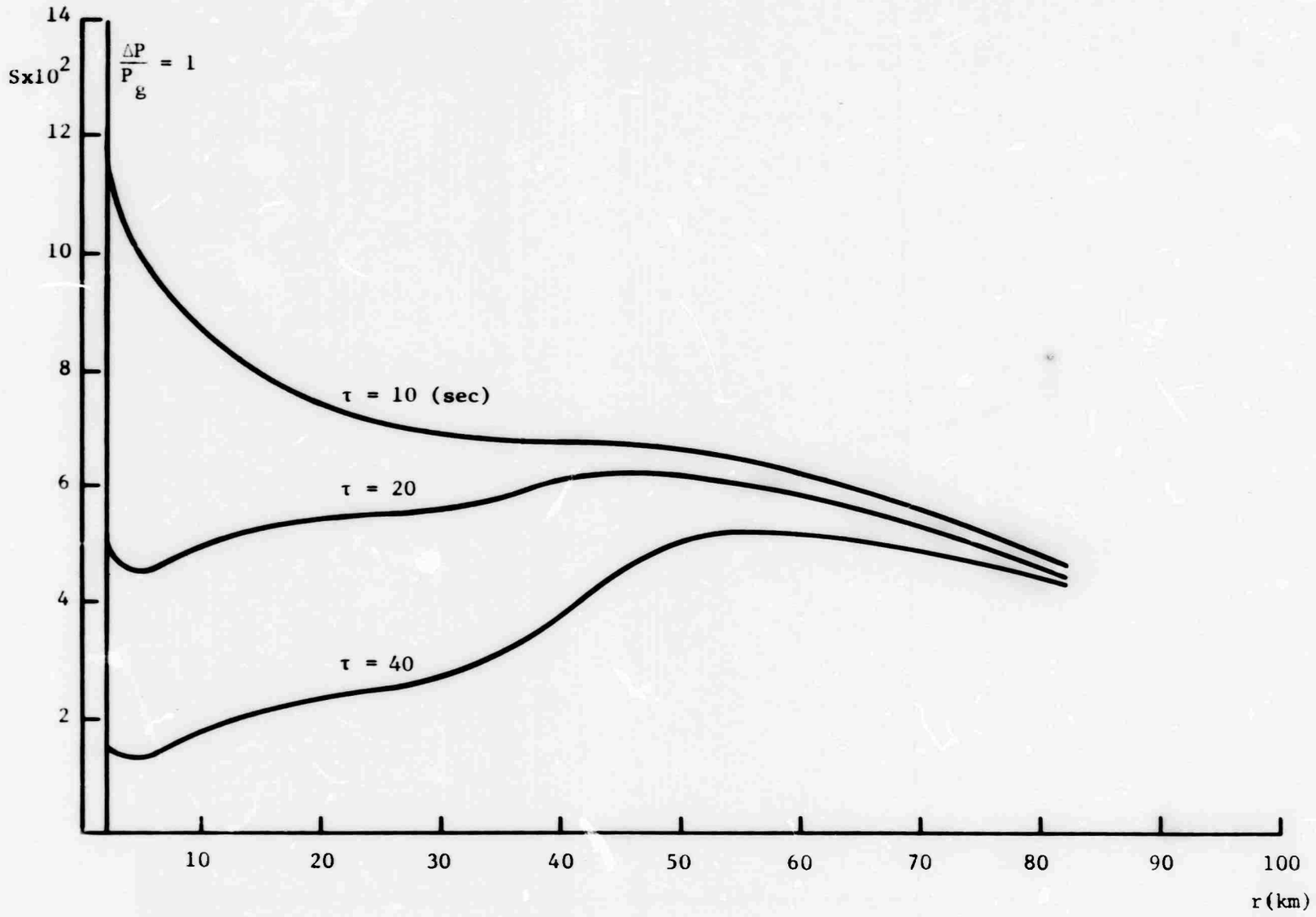

FIGURE 4-8: DIMENSIONLESS SOURCE STRENGTH AS A FUNCTION OF ALTITUDE FOR Y = 1 MT

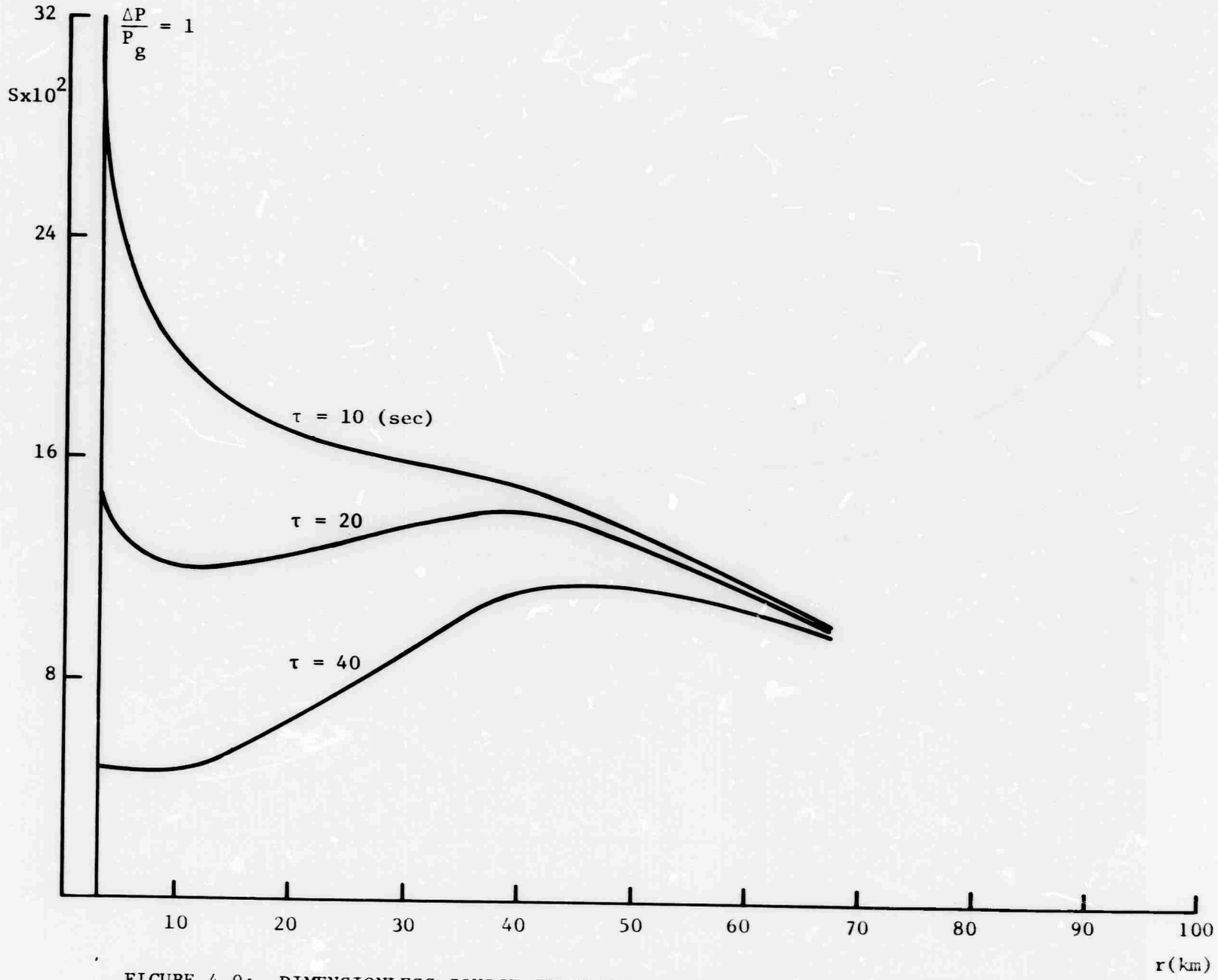

FIGURE 4-9: DIMENSIONLESS SOURCE STRENGTH AS A FUNCTION OF ALTITUDE FOR Y = 5 MT

In any case, the curves in Figs. 4-5 through 4-9 generally exhibit a maximum at intermediate altitudes (the exceptions are $Y \geq 500$ kT for $\tau = 10$ sec). This behavior may be understood in terms of Eq. (4-4) in the following way: At altitudes above the altitude of the maximum $2\pi t_+ >> \tau$ and $S \alpha \Delta pr$, which is a decreasing function of r. For altitudes somewhat below the altitude of the maximum $2\pi t_+ << \tau$ and $S \alpha \Delta pr\ t_+^2$. The positive phase duration t_+ decreases more rapidly with decreasing r than Δpr increases and hence S decreases with decreasing r. The situation is reversed at sufficiently low altitudes, however, and Δpr increases more rapidly with S than t_+^2 decreases. Hence S may start to increase with decreasing r. This behavior is exhibited, for example, by the 5 Mt curve with $\tau = 20$ sec and $r < 10$ km.

For large yields and short periods (i.e., $Y \geq 500$ kT, $\tau = 10$ sec) the condition $2\pi t_+ \geq \tau$ holds at all altitudes and hence $S \sim \Delta pr$ which is a monotonic decreasing function of r.

Table 4-2 gives the burst altitude at which the maximum occurs for various yields and Rayleigh wave periods. As shown in Table 4-2 the altitude of the maximum increases with increasing period and decreases with increasing yield.

TABLE 4-2

HEIGHT OF BURST AT WHICH
MAXIMUM SOURCE STRENGTH OCCURS

Period τ (sec) → \ Yield, Y(kT) →	10	100	500	1000	5000
10	36	17	--	--	--
20	81	65	55	45	39
40	89	71	62	57	45

The increase in source strength between the value at low altitudes (say at $\Delta p/p_g = 1$) and the value at the maximum can be substantial, particularly for smaller yields. For a Rayleigh wave period $\tau = 20$ sec the increase is a factor of 7.6 for 10 kT, 3.0 for 100 kT, 1.9 for 500 kT, 1.2 for 1 Mt, and 1.0 for 5 Mt.

We turn now to a discussion of the yield dependence exhibited by S. Figure 4-10 shows the source strength as a function of yield for burst heights of 2, 5, 10, 40, and 60 km.

It is apparent that in general S increases more rapidly with Y for small heights of burst than for large. This behavior is brought our more clearly in Table 4-3 where we show the value of n that results from assuming a dependence $S \alpha Y^n$ over particular yield intervals and heights of burst.

TABLE 4-3

VALUES OF n ASSUMING $S \alpha Y^n$ FOR $\tau = 20$ SEC

Yield Interval (kt-kt)	Height of Burst (km)				
	2	5	10	40	60
10-100	.87	.78	.83	.48	.57
100-500	.93	.89	.68	.61	.61
500-1000	.95	.85	.63	.63	.58
1000-5000		.65	.56	.50	.50

This functional dependence of S on Y can be qualitatively understood in terms of Eq. (4-4). For high altitudes we have the limiting case $2\pi t_+ >> \tau$ and $S \alpha \Delta pr$. If modified Sachs scaling is approximately valid, which Fig. 4-3 indicates is the case, and if the shock is weak when it strikes the earth's surface then $\Delta pr \alpha Y^{1/3}$,

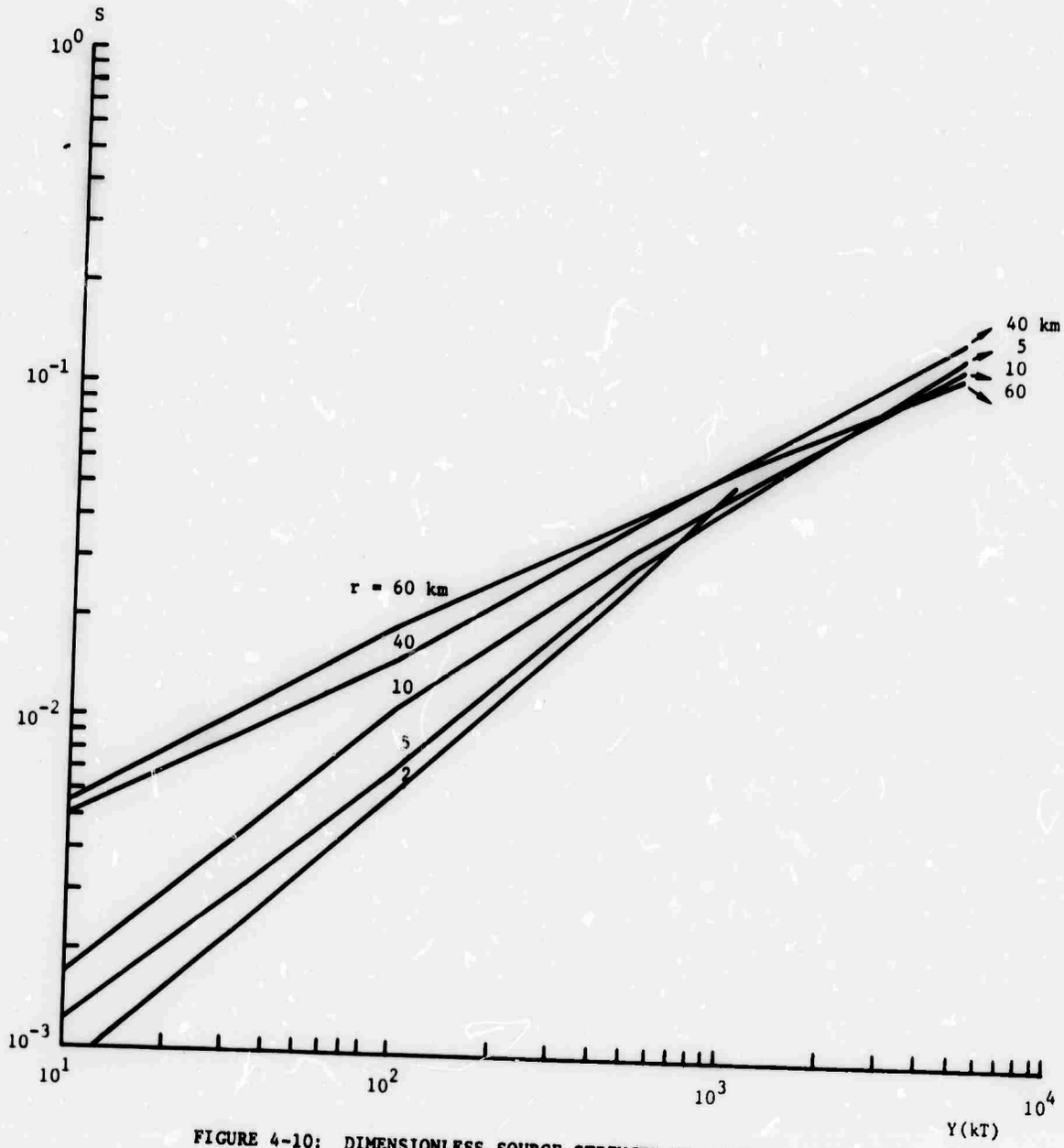

FIGURE 4-10: DIMENSIONLESS SOURCE STRENGTH VS. YIELD. τ = 20 sec.

i.e., $S \alpha Y^{1/3}$. At low altitudes the limiting case is $2\pi t_+ << \tau$ and $S \alpha (\Delta pr)\, t_+^2$. Since t_+ should scale approximately as $Y^{1/3}$ we would expect $S \alpha Y$, again provided the shock is weak when it strikes the earth's surface.

4.4 Conclusions

Our detailed conclusions are contained in the previous section in the form of plots of source strength for Rayleigh wave excitation vs. yield and height of burst. Some general conclusions based on these plots are as follows:

a. The source strength S increases less rapidly with yield Y the higher the burst altitude. For example, for a Rayleigh wave period of 20 sec and for yields between 100 and 500 kT we find $S \alpha Y^{.93}$ for detonations at 2 km altitude, $S \alpha Y^{.89}$ at 5 km, $S \alpha Y^{.68}$ at 10 km, and $S \alpha Y^{.61}$ at 40 km.

b. For large yields and short Rayleigh wave periods τ (for example, $Y > 500$ kT for $\tau = 10$ sec) the source strength is a monotonic decreasing function of height of burst. For larger yields or longer Rayleigh wave periods S is maximized for a particular height of burst. The altitude at which the maximum occurs increases with increasing τ and decreasing Y. For $Y = 1$ Mt and $\tau = 20$ sec the maximum occurs at about 45 km altitude.

c. The variation of S with height of burst can be appreciable. For example, for $\tau = 20$ sec and $Y = 100$ kT, S increases by a factor of 2.3 as the height of burst is raised from 4 km to 20 km.

5. REPORT CONCLUSIONS

Three different kinds of acoustic phenomena related to nuclear test detection and diagnostics have been discussed in this report. They are: (1) Long period (3-10 minutes) acoustic-gravity waves which propagate in the real atmosphere's counterpart to Lamb's edge mode. (2) High frequency (1-60 second period) acoustic pulses which result from the degeneration of the detonation blast wave into a weak shock. (3) Rayleigh or surface seismic waves which result when the detonation shock wave strikes the earth. Conclusions reached for each of these phenomena are given below.

5.1 Lamb Mode Analysis

(a) The shock front extending from the ground to many scale heights above the ground is of almost equal importance in determining the far-field Lamb mode amplitude. Because of this, the far-field amplitude should be relatively independent of phenomena peculiar to any small portion of the shock front. In particular, ground effects such as the presence of a precursor should not play a very important role.

(b) For large yield, low altitude detonations we have found a far-field amplitude dependence which varies as $Y\left[1 + \frac{\sqrt{2}}{3}\sqrt{\ell n \frac{Y}{Y^*}}\right]$, where typically Y* is the order of 10 Mt for a sea level detonation. This dependence arises from a detailed consideration of the mechanism by which the low frequency components of the near-field (shock) disturbance become spatially separated from the high frequency components. The precise value of the critical yield Y* where yield-amplitude proportionality breaks down is determined by atmospheric conditions near the burst as well as the direction of propagation and must be determined by detailed numerical calculations. Nevertheless, in analyzing the test data we have seen some evidence that very large yields do on occasion produce anomalously large far-field amplitudes.

(c) A number of potentially important source effects can be explored within the framework of the Lamb mode theory. The most important of these effects, which we have not investigated, are probably related to the presence of a secondary shock front due to ground reflection. We expect that at low altitudes the effect of the secondary shock in determining the far-field amplitudes is approximately equal to that of the direct shock, but for higher altitude detonations interference or destructive effects between the two shock may occur.

5.2 High Frequency Acoustic Periods

(a) At large distances the dominant acoustic pulse period for a 1 kT detonation is the order of 10 seconds.

(b) For small yields the period scales as $(\text{yield})^{1/3}$. For large yields the scaling is uncertain. The interaction of the rising fireball from high-yield detonations with the upward going shock needs to be investigated before the large yield scaling can be determined.

(c) The range dependence of far-field periods is extremely weak, as an absolute maximum about a 17% increase in going from 2,000 to 10,000 km. Pulse splitting by wind ducts and the effects of other small scale meteorological phenomena are expected to make the actual dependence even weaker than the above value.

(d) The period dependence on height of burst is also extremely weak. The dependence is given approximately as: $T \alpha \left(1 + \frac{\bar{z}}{45.7}\right)$, where T is the period and $\bar{z}$ is the burst height in km.

(e) Probably the most significant variation in far-field period, other than that caused by variations in yield, is caused by the direction of signal propagation relative to the winds at about 50 km altitude. For downwind propagation the signal reflection occurs at a lower altitude than for crosswind or upwind propagation. The dependence of period on reflection altitude is approximately given by:

$T \alpha e^{z_o/28}$, where z_o is the reflection altitude in kilometers. A 10 km variation in z_o produces about a 40% variation in T. The altitude z_o needs to be determined by ray tracing for the appropriate atmospheric conditions and direction of propagation.

5.3 Rayleigh Wave Amplitudes

Our detailed conclusions are contained in the text in the form of plots of source strength for Rayleigh wave excitation vs. yield and height of burst. Some general conclusions are as follows:

(a) The source strength S increases less rapidly with yield Y the higher the burst altitude. For example, for a Rayleigh wave period of 20 sec and for yields between 100 and 500 kT we find $S \alpha Y^{.93}$ for detonations at 2 km altitude, $S \alpha Y^{.89}$ at 5 km, $S \alpha Y^{.68}$ at 10 km, and $S \alpha Y^{.61}$ at 40 km.

(b) For large yields and short Rayleigh wave periods τ (for example, $Y > 500$ kT for $\tau = 10$ sec) the source strength is a monotonic decreasing function of height of burst. For larger yields or longer Rayleigh wave periods S is maximized for a particular height of burst. The altitude at which the maximum occurs increases with increasing τ and decreasing Y. For $Y = 1$ Mt and $\tau = 20$ sec the maximum occurs at about 45 km altitude.

(c) The variation of S with height of burst can be appreciable. For example, for $\tau = 20$ sec and $Y = 100$ kT, S increases by a factor of 2.3 as the height of burst is raised from 4 km to 20 km.

(d) The present analysis of the Rayleigh wave excitation mechanism appears to break down when the shock striking the ground is strong. This occurs for 1 kT at burst heights below about .5 km and for 1 Mt at burst heights below about 2 km. A new model needs to be formulated between the altitude where our model no longer holds and the burial depth of a contained underground detonation.

6. REFERENCES

1. J. N. Hunt, R. Palmer, and W. Penny, Phil. Trans. Roy. Soc. London, 252, 275, 1960.

2. A. D. Pierce and J. W. Posey, Geophys. J. Roy. Astron. Soc. (to be published).

3. J. W. Posey and A. D. Pierce, Nature, 232, 253, 1971.

4. "Problem M" results as contained in Nuclear Weapons Blast Phenomena, Vol. 1, DASA 1200-1, compiled by P. A. Ellis, D. C. Sachs, F. H. Shelton, and J. F. Moulton, 1 March 1971 (S-RD).

5. S. G. Reed, J. Acous. Soc. Am., 31, 1265, 1959.

6. S. Glasstone, Ed., The Effects of Nuclear Weapons, U. S. Atomic Energy Commision, Washington, D. C., 1962.

7. W. C. Meecham, J. Geophys. Res., 73, 377, 1968.

8. W. C. Meecham in Acoustic-Gravity Waves in the Atmosphere, Symposium Proceedings, T. M. Georges, Ed., Boulder, Colorado, 15-17 July, 1968, pg. 337.

9. N. K. Balachandran, W. L. Donn, and G. Kaschak, J. Acous. Soc. Am., 50, 397, 1971.

10. W. W. Troutman and C. W. Davis, Jr., "The Two-Dimensional Behavior of Shocks in the Atmosphere," Air Force Weapons Laboratory Technical Report, AFWL-TR-65-151, September 1965.

11. G. V. Groves, "Acoustic Pulse Characteristics from Explosive Releases in the Upper Atmosphere," Project Firefly 1962-1963, N. W. Rosenberg, Ed., AFCRL-64-364.

12. L. B. W. Jolley, Summation of Series, Dover Publication, Inc., New York, N. Y., 1961, pg. 16, Series No. 87.

13. J. S. Greene and W. A. Whitaker, in Acoustic-Gravity Waves in the Atmosphere, Symposium Proceedings, T. M. Georges, Ed., Boulder, Colorado, 15-17 July, 1968, pg. 45.

14. D. L. Lehto and R. A. Larsen, "Long Range Propagation of Spherical Shockwaves from Explosions in Air," Naval Ordnance Laboratory Report, NOLTR 69-88, July, 1969.

15. B. L. Murphy, T. Fohl, and S. L. Kahalas, "Nuclear Source Mechanisms for Acoustic-Gravity Waves (U)," Mt. Auburn Research Associates, Inc. MARA-SRD-147, Final Report Contract No. F44620-70-C-0043, ARPA Order No. 1520, 1970 (S-RD).

16. B. L. Murphy, "Variation of Rayleigh Wave Amplitude with Yield and Height of Burst for Intermediate Altitude Nuclear Detonations," to be published in The Journal of Geophysical Research.

17. M. N. Toksöz and A. Ben-Menahem, J. Geophys. Res., 69, 1639, 1964.

18. D. G. Harkrider and E.A. Flinn, Rev. Geophys. and Space Phys. 8, 501, 1970.

19. G. Nickel and W. Whitaker, "Distant Seismic Waves from a High Altitude Source," Air Force Weapons Laboratory Technical Report, AFWL-TR-67-125, 1968.

20. M. Lutzky and D. L. Lehto, Phys. Fluids, 11, 1466, 1968.

APPENDIX A: DERIVATION OF THE BASIC EQUATIONS FOR PREDICTION OF FAR-FIELD LAMB MODE AMPLITUDES

A.1 Introduction

In this appendix we develop the theoretical basis for the equations discussed in the text. The analysis is heavily based on the work of Pierce and Posey described in Ref. 1, and, where possible, we use the notation of this reference. However, because we are primarily concerned with the source model rather than with the propagation theory we make several simplifying assumptions. Specifically:

(a) We neglect the effects of acoustic ray refraction and assume that all rays follow great-circle paths between source and observation point. This is not necessarily a good assumption. However, the corrections necessary to incorporate a realistic atmospheric propagation model do not affect the way in which the source model is incorporated into the theory.

(b) On the assumption that the various "sound speeds" occurring in the Pierce-Posey theory are of approximately equal magnitude we do not distinguish them. In the notation of Ref. 1 this means that the altitude dependent sound speed $c(z)$, the sound speed averaged in altitude over the Lamb mode weighting function c_L, and the effective sound speed c_e which incorporates effects such as those due to winds, are all denoted by c. At the same time, and this is consistent with the above assumption, the major effect of differences between these quantities, namely a frequency dependent group velocity, is taken into account.

A.2 Isolation of the Lamb Mode in the Near-Field Disturbance

According to Pierce and Posey, if the upper atmosphere is considered to be bounded at some large altitude, z_m, by a rigid ceiling then an acoustic disturbance may be expanded as a sum of guided modes.

one of which is the analogue of Lamb's mode. That is:

$$\Delta P(\vec{r},t) = P_L(\vec{r},t) + \Psi(\vec{r},t), \tag{A-1}$$

where ΔP is the overpressure of the disturbance, P_L is the contribution of the Lamb mode, and Ψ represents the contribution of other modes. The Lamb mode is characterized by an altitude dependence such that P_L can be factored as:

$$P_L(\vec{r},t) = P_s\, e^{-z/\gamma H}\, F(r,t), \tag{A-2}$$

where P_s is the sea-level pressure, z is the altitude, γ is the ratio of specific heats, and H is the scale height. F(r,t) is a function only of time and of the great-circle distance r.

The height profiles of the various modes contained in Ψ satisfy an orthogonality relation such that:

$$\int_0^{z_m} e^{\frac{\gamma-1}{\gamma}\frac{z}{H}}\, dz = 0 \tag{A-3}$$

Turning now to the case in which $\Delta P(\vec{r},t)$ represents the detonation shock wave, we define r_o to be the appropriate horizontal distance for matching the shock to the linear propagation theory. How this distance is to be determined is left for subsequent discussion. Suppose that at distance r_o and time t_o the shock extends between altitudes z_1 and z_2. It will be shown below that for detonations in the lower atmosphere $z_1 = 0$ (i.e., sea level) and $z_2 >> H$ is, in fact, the situation of interest. Under these circumstances we assume that Eq. (A-3) is approximately correct with the limits, $0, z_m$ replaced by z_1, z_2.

Multiplying Eq. (A-1) by $e^{\frac{\gamma-1}{\gamma}\frac{z}{H}}$, integrating from $z=z_1$ to $z=z_2$, and using Eq. (A-2) we then obtain:

$$\int_{z_1}^{z_2} \Delta P(r_o,z,t_o)\, e^{\frac{\gamma-1}{\gamma}\frac{z}{H}}\, dz = F(r_o,t_o)\, P_s \int_{z_1}^{z_2} e^{\frac{\gamma-2}{\gamma}\frac{z}{H}}\, dz$$

$$= F(r_o,t_o) P_s \frac{\gamma H}{\gamma-2} e^{\frac{\gamma-2}{\gamma}\frac{z}{H}} \Bigg|_{z_1}^{z_2}$$

$$\simeq F(r_o,t_o) P_s \frac{\gamma H}{2-\gamma}\,, \qquad \text{(A-4)}$$

where we have assumed $\frac{2-\gamma}{\gamma}\frac{z_1}{H} \ll 1$ and $\frac{2-\gamma}{\gamma}\frac{z_2}{H} \gg 1$.

Putting $\frac{\Delta P(r_o,z,t_o)}{P_s} e^{z/H} = \pi(r_o,z,t_o)$ where π is the relative overpressure, we may rewrite Eq. (A-4)

$$F(r_o,t_o) = \frac{2-\gamma}{\gamma H} \int_{z_1}^{z_2} \pi(r_o,z,t_o)\, e^{-\frac{z}{\gamma H}}\, dz. \qquad \text{(A-5)}$$

We retain the limits z_1, z_2 rather than setting them to 0, ∞ as a reminder of the assumptions made.

In the Pierce-Posey theory the geometrical acoustics approximation is made that F may be factored into amplitude and waveform functions:

$$F(r_o,t_o) = A(r_o)\, \psi(r_o,t_o) \qquad \text{(A-6)}$$

and similarly at some r,t corresponding to a larger distance and a later time:

$$F(r,t) = A(r)\ \psi\ (r,t). \tag{A-7}$$

For Eq. (A-7) to be valid the spatial variation of A(r) must be on a scale large compared to the disturbance wavelength. This will be the case for the effect of earth curvature which produces a dependence:

$$A(r) \propto \left[r_e \sin \frac{r}{r_e}\right]^{-\frac{1}{2}}, \tag{A-8}$$

where r_e is the earth's radius and where r is again the great circle distance.

A.3 Propagation of the Lamb Mode to the Far Field

The waveform function ψ is representable as a Fourier integral:

$$\psi(r,t) = 2R_e \int_0^\infty \hat{\psi}(k)\ e^{-i(\omega t - kr)}\ dk, \tag{A-9}$$

The quantities ω and k are related through the Lamb mode dispersion equation:

$$\omega = c\ k - k^3\ h_{kk}, \tag{A-10}$$

where c is taken as an average sound speed and the quantity h_{kk} is not a function of k and is due to deviations of sound speed and wind velocity from vertically averaged values. The second term on the right side of Eq. (A-10) is much smaller than the first.

Combining Eqs. (A-9) and (A-10) we obtain:

$$\frac{\partial \psi}{\partial t} + c \frac{\partial \psi}{\partial r} + h_{kk} \frac{\partial^3 \psi}{\partial r^3} = 0 \qquad \text{(A-11)}$$

The last and smallest term in Eq. (A-11), $h_{kk} \frac{\partial^3 \psi}{\partial r^3}$, which represents dispersive effects, may be rewritten by replacing $\frac{\partial}{\partial r}$ to lowest order by $\frac{1}{c} \frac{\partial}{\partial t}$. Thus:

$$\frac{1}{c} \frac{\partial \psi}{\partial t} + \frac{\partial \psi}{\partial r} + \frac{h_{kk}}{c^4} \frac{\partial^3 \psi}{\partial t^3} = 0 \qquad \text{(A-12)}$$

Following Pierce and Posey we now introduce the parameters:

$$\bar{t} = t - \int^r \frac{dr}{c} , \qquad \text{(A-13)}$$

$$\bar{r} = \int^r \frac{h_{kk}}{c^4} dr , \qquad \text{(A-14)}$$

so that $\frac{\partial \psi}{\partial t} = \frac{\partial \psi}{\partial \bar{t}}$ and $\frac{\partial \psi}{\partial r} = \frac{-1}{c} \frac{\partial \psi}{\partial \bar{t}} + \frac{h_{kk}}{c^4} \frac{\partial \psi}{\partial \bar{r}}$. Thus Eq. (A-12) becomes:

$$\frac{\partial \psi}{\partial \bar{s}} - \frac{\partial^3 \psi}{\partial \bar{t}^3} = 0 \qquad \text{(A-15)}$$

Equation (A-15) may be solved to obtain ψ at r,t $(\bar{r},\bar{t})$ from $\psi(t_o)$ at r_o $\left[\psi(\bar{t}_o)\right.$ at $\left.\bar{r}_o\right]$.

$$\psi(\bar{r},\bar{t}) = \frac{1}{\sqrt{\pi}\,(3\bar{r})^{1/3}} \int_{-\infty}^{\infty} A_i\left[\frac{\bar{t}_o - \bar{t}}{(3\bar{r})^{1/3}}\right] \psi(\bar{r}_o,\bar{t}_o)\, d\bar{t}_o \qquad \text{(A-16)}$$

where A_i is the Airy function.

We now define the waveform arrival time:

$$\tau_a = t - \bar{t} \qquad \text{(A-17)}$$

and the characteristic dispersion time:

$$\tau_d = (3\bar{r})^{1/3} \qquad \text{(A-18)}$$

in terms of which Eq. (A-16) may be written

$$\psi(r,t) = \frac{1}{\sqrt{\pi}\,\tau_d} \int_{-\infty}^{\infty} A_i\left[\frac{\tau_a - t + t_o}{\tau_d}\right] \psi(t_o,r_o)dt_o \qquad \text{(A-19)}$$

In writing Eq. (A-19) we have put $\bar{t}_o = t_o$ since t_o is being measured at r_o, the distance at which the Lamb mode theory is presumed to just begin to be applicable.

The far-field overpressure at sea level is given by combining Eqs. (A-2), (A-7), and (A-19)

$$\begin{aligned} P_L(r,t) &= P_s\, F(r,t) \\ &= P_s\, A(r)\, \psi(r,t) \\ &= P_s\, A(r)\, \frac{1}{\sqrt{\pi}\,\tau_D} \int_{-\infty}^{\infty} A_i\left[\frac{\tau_a - t + t_o}{\tau_d}\right] \psi(t_o,r_o)dt_o \end{aligned} \qquad \text{(A-20)}$$

Henceforth we will measure the time t relative to the arrival time τ_a. Now $\psi(r_o,t_o) = \dfrac{F(r_o,t_o)}{A(r_o)}$, where $F(r_o,t_o)$ is given by Eq. (A-5). Thus we obtain:

$$P_L = P_s \frac{A(r)}{A(r_o)} \frac{(2-\gamma)}{\gamma H\sqrt{\pi}} \frac{1}{\tau_d} \int_{-\infty}^{\infty} A_i \left[\frac{\bar{t}_o - t}{\tau_d}\right] \left[\int_{z_1}^{z_2} \pi(r_o,z,t_o)\, e^{-z/\gamma H} dz\right] dt_o \qquad \text{(A-21)}$$

A.4 The Shock Model

To proceed it is necessary to make some additional assumptions about the form of π. We assume that the detonation occurs at altitude $\bar{z}$ and that the shock front is spherical about the burst. For this assumption to be correct it is necessary that while the shock is strong and supersonic it encounters a nearly homogeneous atmosphere. When the shock is weak and sonic the shock parameters may vary drastically along the front, although the front will still be spherical.

The assumption of a single spherical shock front is admittedly an oversimplification. For detonations in the lower atmosphere there will be a second shock, due to reflection from the ground, which will follow the main shock. Near the ground the primary shock and the ground reflected shock may fuse and form a Mach stem. Very crudely the reflected shock may be considered as arising from a mirror detonation at $-\bar{z}$. The time lag between primary and reflected shocks will be less than $\simeq \dfrac{2\bar{z}}{c}$ and the difference in radius of curvature between the two shocks will be less than $2\bar{z}$. For small $\bar{z}$, then, the reflected

shock follows immediately behind the primary shock and has approximately the same curvature. The time lag between the two shocks will be less than a typical far-field quarter period ($\simeq$100 sec) for $\bar{z} \lesssim 15$ km. On this basis we expect that for low altitude detonations the effect of the ground reflected shock is to approximately double the far-field overpressure. Thus the effective yield of a low altitude detonation would be essentially the same as for a contact ($\bar{z}$=0) surface burst, although this is not exact since the contact detonation expends some energy in digging a crater, etc. This model must break down, however, for large heights of burst where the time lag between the two shocks becomes comparable with a far-field quarter period or where the radius of curvature of the two shocks at the matching radius r_o becomes very different.

The techniques we develop below should be adequate to treat this more complex shock structure in detail and we hope to do this in the future. However, in the present analysis we consider only a single spherical shock front and take the ground reflected shock into account by simply doubling the amplitude in Eq. (A-21). The geometry envisioned is shown in Fig. A-1.

Let the time t_o be measured from the arrival of the horizontal portion of the shock front at r_o. At time $t_o > 0$ the spherical shock radius is $r_o + ct_o$, where c is the sound speed, since the shock is assumed weak and near sonic at r_o.

For the situation illustrated in Fig. A-1 we must have $z < z_2 = \bar{z} + \sqrt{c^2 t_o^2 + 2r_o\, ct_o}$ and $z > z_1$ = larger of zero or $\bar{z} - \sqrt{c^2 t_o^2 + 2r_o\, ct_o}$. The integration in Eq. (A-21) occurs over the region of space and time within which the shock is located, that is $0 < t_o < \infty$, $z_1 < z < z_2$. This is equivalent to an integration over $0 < z < \infty$, $\dfrac{\sqrt{(z-\bar{z})^2 + r_o^2} - r_o}{c} < t_o < \infty$. Thus, switching the order of

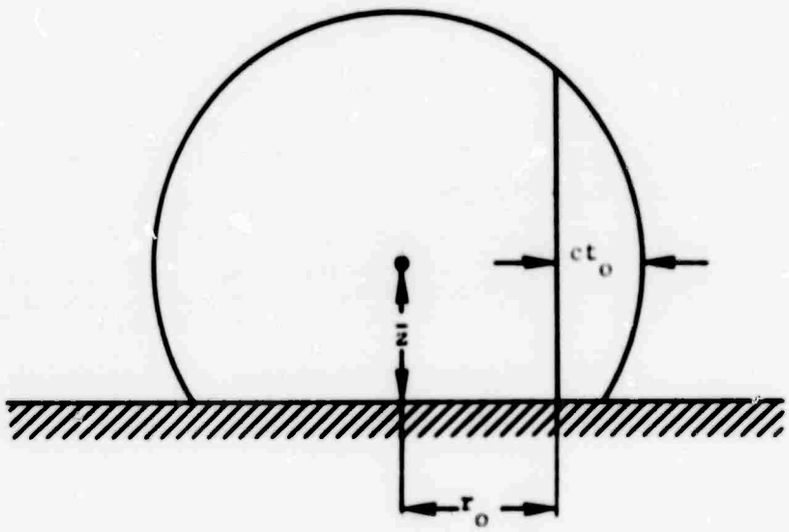

FIGURE A-1: SHOCK GEOMETRY NEAR THE BURST

integration we obtain:

$$P_L = P_s \frac{A(r)}{A(r_o)} \frac{2(2-\gamma)}{\gamma H \bar{z}} \frac{1}{\tau_d} \int_o^\infty dz\, e^{-z/\gamma H} \int_{\frac{\sqrt{(z-z^2)+r_o^2}-r_o}{c}}^\infty dt_o$$

$$A_i\left[\frac{t_o-t}{\tau_d}\right] \bar{\pi}(r_o,z,t_o), \qquad \text{(A-22)}$$

where a factor of 2 has been added to represent the contribution of the ground reflected shock.

We define the local time τ:

$$\tau = \frac{r_o + ct_o - \sqrt{\Delta z^2 + r_o^2}}{c} \qquad \text{(A-23)}$$

where $\Delta z = (z-\bar{z})$. The quantity τ is the time elapsed at r_o,z since the passage of the shock front.

Now we further assume that the relative overpressure at r_o,z has the form of a Glasstone pulse when written in terms of the local time:

$$\bar{\pi}(r_o,z,t_o) = \bar{\pi}(r_o,z)\, e^{-\tau/t_+(r_o,z)}\left(1 - \frac{\tau}{t_+(r_o,z)}\right) \qquad \text{(A-24)}$$

for $\tau > 0$. Equation (A-22) becomes:

$$P_L = P_s \frac{A(r)}{A(r_o)} \frac{2(2-\gamma)}{\gamma\sqrt{\pi}} \frac{1}{H\tau_d} \int_o^\infty \int_o^\infty A_i \left[\frac{\tau - t}{\tau_d} + \frac{-\sqrt{\Delta z^2 + r_o^2} - r_o}{c\tau_d} \right]$$

$$\bar{\pi}(r_o, z)\, e^{-\tau/t_+} (1 - \tau/t_+)\, e^{-z/\gamma H}\, d\tau\, dz \qquad (A\text{-}25)$$

As shown by Pierce and Posey the characteristic dispersion time τ_d is the order of the far-field waveform period which is much larger than the near field positive phase duration t_+. For τ comparable to τ_d the factor $e^{-\tau/t_+}$ occurring in the integrand of Eq. (A-25) is very small. Since the dominant contribution to the τ integration comes from $\tau << \tau_d$ we may expand A_i in a power series in $\frac{\tau}{\tau_d}$:

$$A_i = A_i \left(\frac{\tau}{\tau_d} = 0 \right) + A_i' \left(\frac{\tau}{\tau_d} = 0 \right) \frac{\tau}{\tau_d} + \cdots \qquad (A\text{-}26)$$

Putting $x = \frac{\tau}{t_+}$ we do the x integration, noting that:

$$\int_o^\infty e^{-x} (1-x)\, dx = 0, \qquad (A\text{-}27)$$

$$\int_o^\infty x\, e^{-x} (1-x)\, dx = -1 . \qquad (A\text{-}28)$$

The result is:

$$P_L = -P_s \frac{A(r)}{A(r_o)} \frac{2-\gamma}{\gamma\sqrt{\pi}} \frac{1}{H\tau_d^2}$$

$$\int_o^\infty A_1' \left[\frac{-t}{t_d} + \frac{\sqrt{(\Delta z^2 + r_o^2} - r_o}{ct_d} \right] e^{-z/\gamma H}$$

$$\bar{\pi}\,(r_o,z)\; t_+^2\,(r_o,z)\; dz \qquad \text{(A-29)}$$

Finally, using Eq. (A-8) under the assumption that $r_o << r_e$ we obtain:

$$P_L = -P_s \frac{r_o^{\frac{1}{2}}}{r_e^{\frac{1}{2}} \left| \sin \frac{r}{r_e} \right|^{\frac{1}{2}}} \frac{2(2-\gamma)}{\gamma\sqrt{\pi}} \frac{1}{H\tau_d^2}$$

$$\int_o^\infty A_1' \left[\frac{-t}{\tau_d} + \frac{\sqrt{\Delta z^2 + r_o^2} - r_o}{c\tau_d} \right] e^{-z/\gamma H}$$

$$\bar{\pi}(r_o,z)\; t_+^2\,(r_o,z)\; dz \qquad \text{(A-30)}$$

A.5 Form of the Shock Parameters $\bar{\pi}$, t_+

We wish to do the z integration in Eq. (A-30) using a simple shock model for $\bar{\pi}(r_o,z)$ and $t_+(r_o,z)$. The shock model assumes that at some small radius $R_o < r_o$ about the burst the shock parameters $\bar{\pi}(R_o)$, $t_+(R_o)$ are constant along the spherical shock front and that the shock is weak at R_o ($\bar{\pi}(R_o) << 1$). The geometry is shown in Fig. A-2. It is only necessary that this assumption apply to the portion of the shock

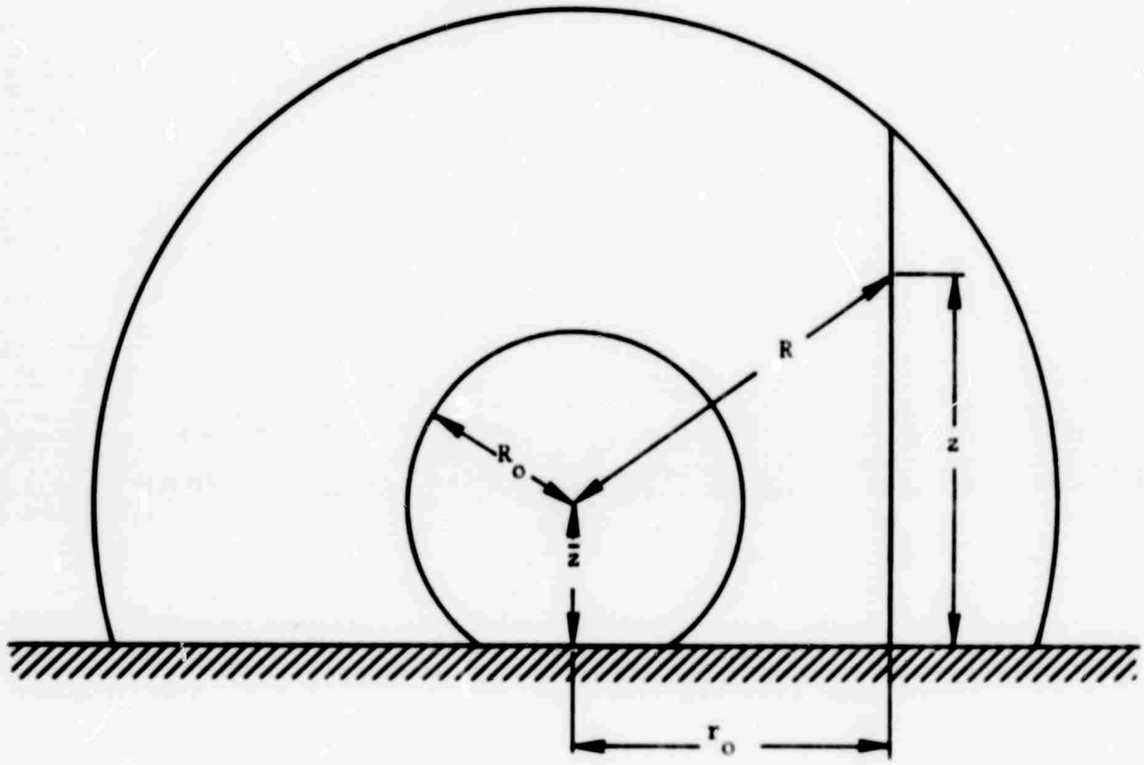

FIGURE A-2: SHOCK GEOMETRY AT SMALL RADIUS R_o WHERE ATMOSPHERIC INHOMOGENEITY IS NEGLECTED AND AT A LARGER RADIUS WHERE IT IS NOT

front that is effective in exciting the Lamb mode; that is, it need not apply, for example, to the vertically upward going portion of the shock front.

Beyond this small radius R_o the shock is assumed to evolve according to the weak shock equations. In particular at (r_o,z):[2]

$$\bar{\pi}(r_o,z) = \bar{\pi}(R_o)\,\frac{R_o}{\sqrt{r_o^2+\Delta z^2}}\,\frac{t_+(R_o)}{t_+(r_o,z)}\,\sqrt{\frac{P(R_o)}{P(r_o,z)}} \qquad \text{(A-31)}$$

$$t_+(r_o,z) = t_+(R_o)\left\{1+\frac{\gamma+1}{2\gamma}\,\frac{\bar{\pi}(R_o)R_o}{ct_+(R_o)}\int_{R_o}^{r_o,z}\sqrt{\frac{P(R_o)}{P(R)}}\,\frac{dR}{R}\right\}^{1/2} \qquad \text{(A-32)}$$

where $P(R_o)$ is the ambient pressure at R_o, $P(r_o,z)$ is the ambient pressure at the point r_o,z where matching to the Lamb mode propagation model occurs, and $P(R)$ is the ambient pressure at a spherical radius R, $R_o \leq R \leq \sqrt{r_o^2+\Delta z^2}$. Consistent with the assumption that R_o is a small radius (that is, that it is small compared with the effective scale height in the direction in question) we take $P(R_o) = P_b$, the ambient pressure at the burst point. Then $P(r_o,z) = P_b\, e^{\frac{-\Delta z}{H}}$ and Eq. (A-31) becomes:

$$\bar{\pi}(r_o,z) = \bar{\pi}_o\,\frac{R_o}{\sqrt{r_o^2+\Delta z^2}}\,\frac{t_+^o}{t_+(r_o,z)}\,e^{\frac{\Delta z}{2H}} \qquad \text{(A-33)}$$

where (except in the case of r_o) we use zero subscripts to denote values at R_o.

The integral occurring in Eq. (A-32) may be approximated as follows:

$$\int_{R_o}^{r_o,z} \sqrt{\frac{P(R_o)}{P(R)}}\,\frac{dR}{R} = \int_{R_o}^{\sqrt{r_o^2+\Delta z^2}} \frac{dR}{R}\exp\frac{(R-R_o)}{2H}\frac{\Delta z}{\sqrt{r_o^2+\Delta z^2}}$$

$$= e^{\frac{-R_o}{2H}\frac{\Delta z}{\sqrt{r_o^2+\Delta z^2}}} \sum_{n=o}^{\infty}\left[\frac{\Delta z}{2H\sqrt{r_o^2+\Delta z^2}}\right]^n \frac{1}{n!}\int_{R_o}^{\sqrt{r_o^2+\Delta z^2}} R^{n-1}\,dR \qquad (A-34)$$

$$= e^{\frac{-R_o}{2H}\frac{\Delta z}{\sqrt{r_o^2+\Delta z^2}}}\left\{\ln\frac{\sqrt{r_o^2+\Delta z^2}}{R_o} + \sum_{n=1}^{\infty}\left(\frac{\Delta z}{2H}\right)^n\frac{1}{nn!}\left[1-\left(\frac{R_o}{\sqrt{r_o^2+\Delta z^2}}\right)^n\right]\right\}$$

Consistent with the assumption that R_o is small, i.e.

$R_o \le \sqrt{r_o^2+\Delta z^2}$, $R_o << 2H\,\frac{\sqrt{r_o^2+\Delta z^2}}{|\Delta z|}$, Eq. (A-34) reduces to:

$$\int_{R_o}^{r_o,z} \sqrt{\frac{P(R_o)}{P(R)}}\,\frac{dR}{R} = \ell n\,\frac{\sqrt{r_o^2+\Delta z^2}}{R_o} + \sum_{n=1}^{\infty}\left(\frac{\Delta z}{2H}\right)^n \frac{1}{nn!} \qquad \text{(A-35)}$$

Thus Eq. (A-32) becomes:

$$t_+(r_o,z) = t_+^o\left\{1+\beta\left[\ell n\,\frac{\sqrt{r_o^2+\Delta z^2}}{R_o} + \sum_{n=1}^{\infty}\frac{1}{nn!}\left(\frac{\Delta z}{2H}\right)^n\right]\right\}^{\frac{1}{2}}, \qquad \text{(A-36)}$$

where we have defined $\beta \equiv \frac{\gamma+1}{2\gamma}\,\frac{\bar{\pi}_o R_o}{c\,t_+^o}$. The quantity β is nearly constant for a weak shock. Since we want R_o as small as possible consistent with the shock being weak we take $\bar{\pi}_o = .1$. Then $\beta = .67 \approx 2/3$ according to the problem M results with $\gamma = 1.4$ and $c = .34$ km/sec.[3] The other parameters used in computing β correspond to a distance of .9 km from a 1 Kf explosion where the positive phase duration is about 1/3 sec.

Now in our basic equation, Eq. (A-30), the shock parameters occur in the form $\bar{\pi}(r_o,z)\,t_+^2(r_o,z)$. Using Eqs. (A-33) and (A-36) we write this quantity in terms of the value at r_o, $z=\bar{z}$, that is the value for the horizontally propagating portion of the shock:

$$\bar{\pi}(r_o,z)\,t_+^2(r_o,z) = \bar{\pi}(r_o,\bar{z})\,t_+^2(r_o,\bar{z})\; e^{\frac{\Delta z}{2H}}\,\frac{r_o}{\sqrt{r_o^2+\Delta z^2}}\,\frac{\left\{1+\beta\left[\ell n\,\frac{\sqrt{r_o^2+\Delta z^2}}{R_o}+\sum_{n=1}^{\infty}\frac{1}{nn!}\left(\frac{\Delta z}{2H}\right)^n\right]\right\}^{\frac{1}{2}}}{\left\{1+\beta\,\ell n\,\frac{r_o}{R_o}\right\}^{\frac{1}{2}}} \qquad \text{(A-37)}$$

Thus Eq. (A-30) becomes:

$$P_L = - P_s \frac{r_o^{\frac{1}{2}}}{r_e^{\frac{1}{2}} \left(\sin \frac{r}{r_e}\right)^{\frac{1}{2}}} \frac{2(2-\gamma)}{\gamma\sqrt{\pi}} \frac{1}{H\tau_d^2} \left(\frac{P_b}{P_s}\right)^{1/\gamma}$$

$$\bar{\pi}(r_o, \bar{z})\ t_+^2(r_o, \bar{z}) \int_o^\infty dz\ A_i' \left[\frac{-t}{\tau_d} + \frac{\sqrt{\Delta z^2 + r_o^2} - r_o}{c\tau_d}\right]$$

$$\frac{r_o}{\sqrt{r_o^2 + \Delta z^2}}\ e^{-\frac{2-\gamma}{2\gamma}\frac{\Delta z}{H}} \frac{\left\{1 + \beta\ \ln \frac{\sqrt{r_o^2 + \Delta z^2}}{R_o} + \sum_{n=1}^{\infty} \frac{1}{nn!} \left(\frac{\Delta z}{2H}\right)^n\right\}^{\frac{1}{2}}}{\left\{1 + \beta\ \ln \frac{r_o}{R_o}\right\}^{\frac{1}{2}}} \qquad \text{(A-38)}$$

We now introduce the variable $y = \frac{\sqrt{\Delta z^2 + r_o^2} - r_o}{c\tau_d}$ and write $dz = dy \frac{\sqrt{\Delta z^2 + r_o^2}}{\sqrt{1 + \sqrt{1 + \frac{\Delta z^2}{r_o^2}}}} \sqrt{\frac{c\tau_d}{r_o y}} \frac{\Delta z}{|\Delta z|}$. The y integration consists of two parts:

$0 \leq y \leq \infty$ $(\Delta z \geq 0)$ and

$0 \leq y \leq \frac{\sqrt{\bar{z}^2 + r_o^2} - r_o}{c\tau_d}$ $(\Delta z \leq 0)$.

Equation (A-38) becomes:

$$P_L = -\frac{P_s}{r_e^{1/2}\left(\sin\frac{r}{r_e}\right)^{1/2}}\,\frac{(2-\gamma)}{\gamma}\sqrt{\frac{2}{\pi}}\,\frac{c^{1/2}}{H\tau_d^{3/2}}\left(\frac{P_b}{P_s}\right)^{1/\gamma}$$

$$\bar{\pi}(r_o,\bar{z})\; t_+^2(r_o,\bar{z})\; r_o \left\{ \int_{\substack{o \\ \Delta z \geq 0}}^{\infty} \frac{dy}{\sqrt{y}}\; A_i'\left[-\frac{t}{\tau_d}+y\right] G(y) \right.$$

$$\left. + \int_{\substack{o \\ \Delta z \leq 0}}^{\frac{\sqrt{\bar{z}^2+r_o^2}-r_o}{c\tau_d}} \frac{dy}{\sqrt{y}}\; A_i'\left[-\frac{t}{\tau_d}+y\right] G(y) \right\}, \qquad \text{(A-39)}$$

where in terms of the variable $\Delta z(y)$:

$$G = \frac{\sqrt{2}\; e^{\frac{-\Delta z}{\gamma H}}\; e^{\frac{\Delta z}{2H}}}{\sqrt{1+\sqrt{1+\frac{\Delta z^2}{r_o^2}}}} \left\{ 1 + \frac{\beta\left[\ell n\sqrt{1+\frac{\Delta z^2}{r_o^2}} + \sum_{n=1}^{\infty}\frac{1}{nn!}\left(\frac{\Delta z}{2H}\right)^n\right]}{1+\beta\,\ell n\frac{r_o}{R_o}} \right\}^{1/2} \qquad \text{(A-40)}$$

A.6 Reduction of Eq. (A-39)

We will demonstrate below that G(y) is a weak function of Δz and hence of y over the integration region of interest. Accordingly, as a first approximation, we take G(y) to be given by its value at y=0 (Δz=0) which is unity. The remaining integral for $\Delta z \geq 0$ is twice the function

$PP\left(\frac{t}{\tau_d}\right) = \int_0^\infty A_i'\left[-\frac{t}{\tau_d} + \alpha^2\right] d\alpha$ discussed by Pierce and Posey.[2]

They have shown by numerical computation that the first maximum of $PP\left(\frac{t}{\tau_d}\right)$ occurs at $\frac{t}{\tau_d} \simeq 1$. The remaining integral for $\Delta z \leq 0$ will be shown to be unimportant. Therefore, for consideration of the first maximum of the far field amplitude we may restrict our attention to times $t \simeq \tau_d$.

The integrand $\frac{A_i'[-1 + y]}{\sqrt{y}}$, which results from setting $t = \tau_d$, is plotted in Fig. A-3. Maximum contribution to the integral is seen to come from the region $0 \leq y \leq 2$ corresponding to $0 \leq |\Delta z| \leq 2c\tau_d\sqrt{1 + r_o/c\tau_d}$. Since τ_d is a quarter period observed in the far field a typical value is about 100 seconds. For $c \simeq .3$ km/sec we thus find that $|\Delta z|$ values up to at least 60 km contribute to the integral in Eq. (A-39). This justifies the initial assumption made in extracting the Lamb mode from the near-field pressure disturbance; namely, that the z integration extends to values much larger than a scale height, $z_2 >> \frac{\gamma}{2-\gamma} H$.

It remains for us to justify the assumption made above that $G(y) \simeq 1$ over the range of Δz of interest. First, however, we note the physical origin of the various factors composing G. These factors are:

a. $e^{\frac{-\Delta z}{\gamma H}}$ is the Lamb mode weighting factor.

b. $e^{\frac{\Delta z}{2H}}$ is due to the increase in relative overpressure π with altitude.

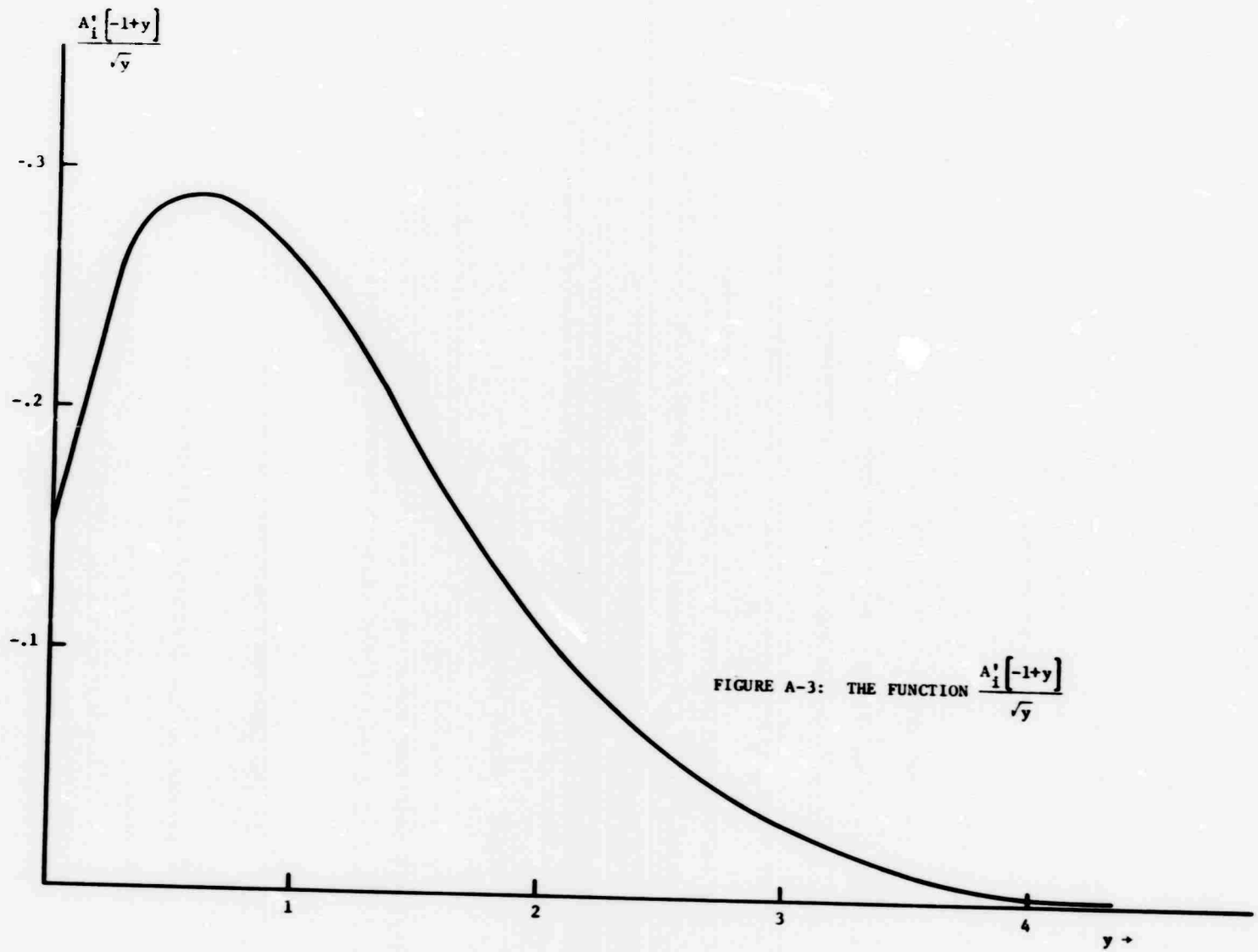

FIGURE A-3: THE FUNCTION $\frac{A_i'[-1+y]}{\sqrt{y}}$

c. $\left\{1 + \frac{\beta\left[\ell n \sqrt{1 + \frac{\Delta z^2}{r_o^2}} + \sum_{n=1}^{\infty} \frac{1}{nn!}\left(\frac{\Delta z}{2H}\right)^n\right]}{1 + \beta\, \ell n \frac{r_o}{R_o}}\right\}^{\frac{1}{2}}$ is due to the change in positive phase duration t_+ with altitude.

d. $\frac{\sqrt{2}}{\sqrt{1 + \sqrt{1 + \frac{\Delta z^2}{r_o^2}}}}$ is a geometrical factor arising from the assumption of a spherical shock front.

The relatively small variation of G(z) is best shown for a particular case by specifying values of H, r_o, cT_d, and Δz. Here we wish to give a more general demonstration based on the Taylor series expansion of G about $\Delta z = 0$. From Eq. (A-40) we obtain:

$$G(\Delta z) \simeq 1 + \frac{1}{2H}\left[\frac{\beta}{2\left(1 + \beta\, \ell n \frac{r_o}{R_o}\right)} - \frac{(2-\gamma)}{\gamma}\right]\frac{\Delta z}{H}$$

$$+ \frac{1}{4H^2}\left[\left(\frac{2-\gamma}{\gamma}\right)^2 + \frac{\beta}{1 + \beta\, \ell n \frac{r_o}{R_o}}\left(\frac{1}{8} - \frac{2-\gamma}{\gamma}\right)\right.$$

$$\left. - \frac{H^2}{r_o^2}\left(\frac{1}{2} - \frac{\beta}{1 + \beta\, \ell n \frac{r_o}{R_o}}\right)\right]\left(\frac{\Delta z}{H}\right)^2 + - - \qquad \text{(A-41)}$$

In the sequel we show that $r_o = R_o$. For $\beta = \frac{2}{3}$ and $\gamma = 1.4$; Eq. (A-41) then becomes:

$$G(\Delta z) = 1 - .048\,\frac{\Delta z}{H} - .0047\left(\frac{\Delta z}{H}\right)^2 - .04\left(\frac{\Delta z}{r_o}\right)^2 + \cdots \qquad \text{(A-42)}$$

The $\frac{\Delta z}{H}$ term becomes important at $\Delta z = 20H \approx 140$ km, the $\left(\frac{\Delta z}{H}\right)^2$ term at $\Delta z = 15H \approx 105$ km, and the $\left(\frac{\Delta z}{H}\right)^2$ term at $\Delta z = 5r_o \approx 5R_o = 45\ Y_M^{1/3}$ km for a sea level detonation, where Y_M is the yield in megatons. Recall that the maximum value of $|\Delta z|$ of interest is about $2c\tau_d\sqrt{1 + \frac{r_o}{c\tau_d}} \approx 60\sqrt{1 + \frac{9}{30}\,Y_M^{1/3}}$ km, for $c = .3$ km/sec and $\tau_d = 100$ sec. Thus we find that for reasonable yields of more than about 1.6 Mt at sea level the second and third terms in the Taylor series expansion of G are not important over the range of Δz or interest.

The cancellation of the various factors which make up $G(\Delta z)$ can also be seen by examining Eq. (A-40) for Δz large. For example, for Δz large and positive $\sum_{n=1}^{\infty} \frac{1}{n!}\left(\frac{\Delta z}{2H}\right)^n \approx e^{\frac{\Delta z}{2H}}$ and the square root of this factor combines with the factors $e^{\frac{-\Delta z}{\gamma H}}$ and $e^{\frac{\Delta z}{2H}}$ to produce a very weak exponential dependence of $e^{\left(\frac{3\gamma-4}{4\gamma}\right)\frac{\Delta z}{H}} = e^{.036\,\Delta z/H}$.

The point is not that G(y) in Eq. (A-39) is exactly constant. Doubtless there are effects which could be explored which depend on deviations of G from unity. The point is that since G(y) is a slowly varying function all values of y from zero to 2, and hence all values of z extending to many scale heights above sea level, are of nearly equal importance in Eq. (A-39). Physically this means that the shock front extending from sea level to many scale heights above sea level is of nearly equal importance in determining the far-field Lamb

mode amplitudes. The significance of this is that for the first maximum of the far-field waveform at times like $t \approx \tau_d$ the peculiar features of the shock near the ground such as the presence of a precursor should not be of particular importance.

Finally, we return to Eq. (A-39) with $G(y) \equiv 1$:

$$P_L = -\frac{P_s}{r_e^{1/2}\left(\sin\frac{r}{r_e}\right)^{1/2}}\frac{(2-\gamma)}{\gamma}\sqrt{\frac{2}{\pi}}\frac{c^{1/2}}{H\,\tau_d^{2/3}}\left(\frac{P_b}{P_s}\right)^{1/\gamma}$$

$$\bar{\pi}(r_o,\bar{z})\; t_+^2(r_o,\bar{z})\; r_o \left[\int_0^{\frac{\sqrt{\bar{z}^2+r_o^2}-r_o}{c\tau_d}} \frac{dy}{\sqrt{y}} A_i'\left(-\frac{t}{\tau_d}+y\right) + \int_{\frac{\sqrt{\bar{z}^2+r_o^2}-r_o}{c\tau_d}}^{\infty} \frac{dy}{\sqrt{y}} A_i'\left(-\frac{t}{\tau_d}+y\right)\right] \qquad \text{(A-43)}$$

The second integral in Eq. (A-43) is always unimportant compared with the first for the following reasons. We have previously observed that for $t \approx \tau_d$ the function $\frac{A_i'}{\sqrt{y}}\left[-\frac{t}{\tau_d}+y\right]$ has a broad plateau for $0 \le y \le 2$. The second integral is therefore approximately $\frac{\sqrt{\bar{z}^2+r_o^2}-r_o}{2c\tau_d}$ times the first (assuming this is less than unity); that is, it introduces a correction factor of about $C \equiv \left(1+\frac{\sqrt{\bar{z}^2+r_o^2}-r_o}{2c\tau_d}\right)$, to the far-field Lamb mode amplitude. According to the results of the next section $r_o \ge 9\left(\frac{Y_M}{P_b/P_s}\right)^{1/3} = 9\,e^{\bar{z}/3H}\,Y_M^{1/3}$ km, where Y_M is again the yield in megatons. For H=7 km we find that $\frac{\bar{z}^2}{r_o^2}$, which is

maximized at $\bar{z} = 3H$, is always less than $\frac{.565}{Y_M^{2/3}}$. Expanding C for $\left(\frac{\bar{z}}{r_o}\right)^2 < 1$ gives $C = \left(1 + \frac{\bar{z}^2}{4r_o c\tau_d}\right)$ which, for $c\tau_d = 30$ km, has a maximum value of $1 + \frac{.06}{Y_M^{1/3}}$ at $\bar{z} = \frac{3H}{2} = 10$ km.

Thus neglecting the second integral Eq. (A-43) becomes:

$$P_L = \frac{-P_s}{r_e^{\frac{1}{2}} \left(\sin \frac{r}{r_e}\right)^{\frac{1}{2}}} \sqrt{\frac{2}{\pi}} \frac{2-\gamma}{\gamma} \frac{c^{\frac{1}{2}}}{H\tau_d^{3/2}} \left(\frac{P_b}{P_s}\right)^{1/\gamma}$$

$$\bar{\pi}(r_o, \bar{z})\, t_+^2(r_o, \bar{z})\, r_o \int_o^\infty \frac{dy}{\sqrt{y}} A_1' \left(-\frac{t}{\tau_d} + y\right) \qquad \text{(A-44)}$$

Note that if we determine r_o in Eq. (A-44) in the "conventional" way, that is for a given $\bar{\pi}$ take $t_+(r_o, \bar{z}) \alpha \left(\frac{Y}{P_b}\right)^{1/3}$ and $r_o \alpha \left(\frac{Y}{P_b}\right)^{1/3}$ we obtain $P_L \alpha Y P_b^{1/\gamma - 1}$. This result has been previously obtained, as has the dependence $P_L \alpha \frac{1}{\left(\sin \frac{r}{r_e}\right)^{\frac{1}{2}}} \tau_d^{-3/2}$ by Pierce and Posey[1] and by Pierce, Posey, and Iliff.[4]

In the sequel we show that the above method of choosing r_o, while probably correct for small yields, is probably not correct for large ones. The main effect of this finding is to introduce a slightly different dependence of P_L on Y for large yields.

A.7 Determination of the Matching Radius, r_o

We need a physical criterion to obtain the matching radius r_o which occurs in Eq. (A-44). The basic concept in the analysis to determine this matching radius is as follows:

The low frequency components of the near-field disturbance, which eventually determine the far-field amplitudes, must become spatially separated from the higher frequency components before the linear Lamb mode propagation theory is appropriate. While the high and low frequency components are located in the same region of space they interact nonlinearly. In particular, the low frequencies gain energy from the higher frequencies as is demonstrated, for example, by the lengthening of positive phase with distance.

One way this spatial separation of frequencies could occur is the following. As the shock or Mach stem propagates along the ground it will lift up because of refraction associated with the normal atmospheric sound speed profile. This effect is responsible for the so-called zone of silence phenomenon at intermediate distances from an explosion. If the low frequencies are thought to exist in a Lamb mode at this time then they will continue to propagate along the ground and hence will become spatially separate from the higher frequencies.

Refraction of the weak shock may be an important part of source modeling but we do not believe the above description is the key to understanding how the Lamb mode is set up. The difficulties with the above explanation are first that it begs the question, and, second, that it relates to an effect peculiar to the shock front near the ground. In view of the fact that the shock extending up to at least about 60 km altitude is effective in exciting the Lamb mode we doubt that this type of refraction could by itself achieve the spatial separation of frequencies required.

The model we propose, which is discussed below, involves a

spatial separation of frequencies within the weak shock itself. To give the argument in the simplest form we assume that all atmospheric properties are independent of range. Then according to Eqs. (A-14) and (A-18):

$$\tau_d = \left(\frac{3h_{kk}}{c^4}\right)^{1/3} r^{1/3} \qquad \text{(A-45)}$$

According to what has been previously said this will be approximately the quarter period of the disturbance at range r.

If we start with a hypothetical far-field waveform, and extrapolate back toward the burst, the period will decrease according to Eq. (A-45). At the same time we may calculate the shock positive phase duration, which is approximately the quarter period of the near-field disturbance, at increasing distances from the burst. This is done by using Eq. (A-36) applied in the horizontal direction for an arbitrary radius r:

$$t_+(r,\bar{z}) = t_+(R_o)\left(1 + \beta \ln \frac{r}{R_o}\right)^{\frac{1}{2}} \qquad \text{(A-46)}$$

It turns out that there are two cases:

(a) $\tau_d \geq t_+$ for all radii at which the shock is weak.

(b) $\tau_d \leq t_+$ up to r_o, in spite of the fact that the shock is weak, and $\tau_d \geq t_+$ for $r \geq r_o$.

Consider the latter case first. We will show that the radius r_o has the following physical meaning: Up to r_o the Fourier component of period $\sim 4\tau_d$ observed in the far field is spatially located well behind the shock front. For radii greater than r_o this Fourier component has moved up to the front of the shock. While the long period

Fourier components are located behind the shock front they gain energy from the shorter period components as is manifested, for example, by the positive phase lengthening given by Eq. (A-46). Once these long period Fourier components move ahead to the shock front they propagate independently of the short period components.

On the basis of this physical picture we choose $r_o : \tau_d(r_o) = t_+(r_o)$, for case (b). For case (a) we choose the matching radius such that a continuous transition is made with case (b). When this is done it turns out that case (a) corresponds to the method of choosing r_o used by Pierce and Posey, that is, $r_o \propto Y^{1/3}$. The criterion for case (b), however, is not the conventional one and this introduces a far-field amplitude dependence which is not simply proportional to yield.

We now give a quantitative statement of these remarks. Again we take a Glasstone pulse form

$$\pi(t) = \bar{\pi}\, e^{-t/t_+}\,(1 - t/t_+),\ t \geq 0 \qquad \text{(A-47)}$$

To see where the low frequency components are located within the pulse we take the Fourier transform of only that part of the pulse between the front and a distance $\frac{\ell}{c} = \bar{t}$ behind the front:

$$S(\omega) \equiv \int_0^{\bar{t}} e^{-i\omega t}\,\pi(t)\,dt$$

$$= \frac{\bar{\pi}\left(\frac{1}{t_+} - i\omega\right)^2}{\left(\frac{1}{t_+^2} + \omega^2\right)^2}\left\{e^{-i\omega\bar{t}}\, e^{-\bar{t}/t_+}\left[-i\omega + i\omega\,\frac{\bar{t}}{t_+} + \frac{\bar{t}}{t_+^2} + i\omega\right]\right. \qquad \text{(A-48)}$$

For large $\frac{\bar{t}}{t_+}$ the last term dominates due to the factor $e^{-\bar{t}/t_+}$, and $|S| = \frac{\bar{\pi}\omega}{\frac{1}{t_+^2} + \omega^2}$. This will be essentially the value of $|S|$ when

$$\omega > e^{-\bar{t}/t_+} \left| -i\omega + i\omega \frac{\bar{t}}{t_+} + \frac{\bar{t}}{t_+^2} \right| , \qquad \text{(A-49)}$$

Under the assumption $\omega << \frac{1}{t_+}$ this reduces to $\omega > e^{-\bar{t}/t_+} \frac{\bar{t}}{t_+^2}$ or:

$$\bar{t} \gtrsim t_+ \ln \frac{1}{\omega t_+} \qquad \text{(A-50)}$$

This means that the dominant contribution to the Fourier amplitude of period $\frac{2\pi}{\omega}$ comes within a distance of about $ct_+ \ln \frac{1}{\omega t_+}$ of the pulse front. For example, we might have $\frac{2\pi}{\omega} \approx 600$ sec and t_+ the order of 6 seconds, then the dominant contribution comes within about $4ct_+$ of the pulse front. Under no circumstances is it necessary to go back more than a few ct_+.

The energy associated with a low-frequency component of period $4\tau_d(r)$ (the period observed in the far field) propagates at a group velocity given by Eq. (A-10):

$$V_g\left(\omega = \frac{\pi}{2\tau_d(r)}\right) = \frac{d\omega}{dk} \approx c - 3k^2 h_{kk}$$

$$\approx c - 3\frac{\omega^2}{c^2} h_{kk}$$

$$= c\left[1 - \frac{3}{c^3}\left(\frac{\pi}{2\tau_d(r)}\right)^2 h_{kk}\right] \qquad \text{(A-51)}$$

Similarly the energy associated with the largest amplitude Fourier component $\left(\omega = \frac{1}{t_+}\right)$ propagates at:

$$V_g\left(\omega = \frac{1}{t_+}\right) \approx c\left[1 - \frac{3}{c^3}\left(\frac{1}{t_+}\right)^2 h_{kk}\right] \qquad \text{(A-52)}$$

Justification for using the Lamb mode dispersion equation in deriving Eqs. (A-51) and (A-52) is given below.

At r_o therefore the low frequencies have moved ahead relative to the main pulse by an amount:

$$d(r_o) \approx \frac{r_o}{c}\frac{3}{c^2}\frac{1}{t_+^2} h_{kk} ,$$

since $\tau_d \gg t_+$. Using Eq. (A-45), under the assumption that the shock is weak over most of the distance to r_o, this becomes:

$$d(r_o) \approx \frac{c\tau_d(r_o)^3}{t_+^2} \qquad \text{(A-53)}$$

According to what has been said before, we must require $d(r_o)$ to be a few times ct_+ since this is how far within the pulse

the frequencies of interest $\left(\omega \simeq \frac{\pi}{2\tau_d}\right)$ are located. Thus we obtain the criterion:

$$t_+(r_o) \quad \tau_d(r_o) \tag{A-54}$$

The sound speed occurring in Eqs. (A-51) - (A-53) is the sound speed within the pulse which presumably is larger than ambient due to effects occurring at the front of the weak shock.

In deriving the frequency dependent group velocity in Eqs. (A-51) and (A-52) we used the Lamb mode dispersion equation, Eq. (A-10). We now justify this procedure. Equation (A-10) cannot be exactly correct within the shock because of nonlinear effects. That is, in the Fourier decomposition of the weak shock, $rS(\omega)\, e^{i(kx-\omega t)}$, $rS(\omega)$ is a function of space. The factor r is included to account for purely geometrical effects. According to Eq. (A-48) with $\bar{t} = \infty$

$$\begin{aligned} r|S(\omega,r)| &= \frac{\bar{\pi}\omega r}{\frac{1}{t_+^2} + \omega^2} \\ &\alpha\ \bar{\pi} r t_+^2 \quad \text{for} \quad \omega \lesssim t_+ \\ &\alpha\ t_+ \\ &\alpha\ \sqrt{1 + \beta\, \ell n \frac{r}{R_o}} \end{aligned} \tag{A-55}$$

where we have used the fact that $\bar{\pi} r t_+$ is a constant for a weak shock[6] and have used Eq. (A-46) to write the explicit r dependent of t_+.

Because of Eq. (A-55) it is appropriate to define an imaginary component of k which represents the spatial growth of frequencies $\omega \lesssim t_+$:

$$k_i \simeq \frac{\partial}{\partial r} \ell n \, |S(\omega, r) r| \simeq \frac{\beta}{r\sqrt{1 + \beta \, \ell n \, \frac{r}{R_o}}}$$

$$\simeq \frac{1}{r_o} \text{ , for } r = r_o \text{ .} \qquad \text{(A-56)}$$

The real part of k is of course $k_r \simeq \frac{\omega}{c}$. If $k_r >> k_i$ then the group velocity will be given by $\frac{d\omega}{dk_r}$ using the Lamb mode dispersion equation. This criterion amounts to:

$$\frac{c}{\omega} << r_o \text{ ,} \qquad \text{(A-57)}$$

or for the dominant Fourier components $\omega \simeq \frac{1}{t_+}$:

$$ct_+ << r_o, \qquad \text{(A-58)}$$

which simply means that the positive phase length must be much less than the matching radius. This will be the case since r_o is chosen to be a radius where the shock is weak and hence is much larger than a fireball dimension (ct_+ being the order of a fireball dimension).

For the very low frequencies observed in the far-field ($\omega \sim 1/\tau_d(r)$) the criterion is:

$$c\tau_d(r) << r_o \text{ ,} \qquad \text{(A-59)}$$

which is not automatically satisfied.

However, in deriving the matching criterion, Eq. (A-54), we only used the fact that the very low frequencies have a group velocity which is much nearer the local sound speed than that of the high

frequencies. This will still be the case since both k_r and k_i will be small for the low frequencies (as compared to $k_r \approx \frac{1}{t_+ c}$ for the high frequencies) and hence the term $h_{kk}\, k^3$ in the Lamb mode dispersion equation (A-10) may still be omitted in determining $d\omega/dk$ for the very low frequencies. Thus our use of Eq. (A-10) in deriving the matching criterion (A-54) is justified.

From Eqs. (A-45) and (A-46) this basic criterion (A-54) becomes:

$$\frac{3h_{kk}}{c^4} r_o = t_+(R_o)^3 \left\{ 1 + \beta \ln \frac{r_o}{R_o} \right\}^{3/2} \qquad \text{(A-60)}$$

According to Sachs scaling:

$$R_o = \varepsilon \left(\frac{Y}{P_b} \right)^{1/3}$$

$$t_+(R_o) = \alpha \left(\frac{Y}{P_b} \right)^{1/3}, \qquad \text{(A-61)}$$

where again using the problem M results, $\varepsilon \approx .9$ km, $\alpha = 1/3$ sec, and as before $\beta = 2/3$, when Y is measured in kT and P_b in atmospheres.

Putting $\frac{3h_{kk}}{c^4} = \sigma$ we obtain from Eq. (A-60):

$$\sigma r_o = \alpha^3 \left(\frac{Y}{P_b} \right) \left\{ 1 + \beta \ln \frac{r_o}{\varepsilon} \left(\frac{P_b}{Y} \right)^{1/3} \right\}^{3/2} \qquad \text{(A-62)}$$

We wish to solve Eq. (A-62) for $r_o \left(\frac{Y}{P_b} \right)$. It is convenient to define the parameter $x \equiv \frac{r_o}{\varepsilon} \left(\frac{P_b}{Y} \right)^{1/3}$ so that Eq. (A-62) becomes:

$$\varepsilon\sigma\left(\frac{Y}{P_b}\right)^{1/3} x = \alpha^3 \frac{Y}{P_b} \left(1 + \beta \ell n x\right)^{3/2} \qquad \text{(A-63)}$$

or:

$$\frac{Y}{P_b} = \left(\frac{\varepsilon\sigma}{\alpha^3}\right)^{3/2} \frac{x^{3/2}}{(1 + \beta \ell n x)^{9/4}} \qquad \text{(A-64)}$$

so that:

$$r_o = \left(\frac{\varepsilon}{\alpha}\right)^{3/2} \sigma^{1/2} \frac{x^{3/2}}{(1 + \beta \ell n x)^{3/4}} \quad . \qquad \text{(A-65)}$$

Now $\left(\frac{Y}{P_b}\right)$ has a minimum value at $x = \exp\left(\frac{3}{2} - \frac{1}{\beta}\right) \simeq 1$ where $\frac{Y}{P_b} = \left[\frac{2}{3\beta} \exp\left(1 - \frac{2}{3\beta}\right)\right]^{9/4} \left(\frac{\varepsilon\sigma}{\alpha^3}\right)^{3/2} \simeq \left(\frac{\varepsilon\sigma}{\alpha^3}\right)^{3/2} \simeq \left(\frac{Y^*}{P_b^*}\right)$, for $\beta = 2/3$. At this value of $x, r_o = R_o = \varepsilon \left(\frac{Y^*}{P_b^*}\right)^{1/3}$. To continue the solution $r_o \frac{Y}{P_b}$ to values of $\frac{Y^*}{P_b^*}$ which are smaller than can be obtained from Eq. (A-64) we take $r_o = \varepsilon \left(\frac{Y}{P_b}\right)^{1/3} = .9 \left(\frac{Y}{P_b}\right)^{1/3}$ km for $\frac{Y}{P_b} \leq \left(\frac{Y^*}{P_b^*}\right)$. This corresponds to the aforementioned case (a) for which $\tau_d > t_+$ at all radii for which the shock is weak.

To see what the net effect of the altered criterion contained in Eqs. (A-64) and A-65) is we return to Eq. (A-43). The far-field Lamb mode amplitude is proportional to $\bar{\pi}(r_o)\, t_+^2(r_o)\, r_o$. For $\frac{Y}{P_b} \leq \left(\frac{Y^*}{P_b^*}\right)$ this quantity is equal to $\simeq 10^{-2} \frac{Y}{P_b}$ km sec^2, when Y is in kT and P_b in atmospheres. For $\frac{Y}{P_b} \leq \frac{Y^*}{P_b^*}$ we may use the fact that according

to weak shock theory $\pi r t_+$ is independent of r.[2] Thus

$$\bar{\pi}(r_o)\, t_+^2(r_o)\, r_o = 10^{-2}\, \frac{Y}{P_b}\, \frac{t_+(r_o)}{t_+(R_o)}$$

$$= 10^{-2} \left(\frac{Y}{P_b}\right) \left[1 + \beta \ln x\right]^{1/2} \qquad \text{(A-66)}$$

The correction factor to the far-field amplitude when $\frac{Y}{P_b} > \frac{Y^*}{P_b^*}$ may therefore be defined for $\beta = 2/3$ as:

$$Q = \left[1 + \frac{2}{3} \ln x\right]^{1/2}, \quad x \geq 1 \qquad \text{(A-67)}$$

where x is given by Eq. (A-64)

$$\left(\frac{Y}{P_b}\right) = \left(\frac{Y^*}{P_b^*}\right) \frac{x^{3/2}}{\left(1 + \frac{2}{3} \ln x\right)^{9/4}} \qquad \text{(A-68)}$$

Using Eqs. (A-66) - (A-68) we may rewrite Eq. (A-44) as:

$$P_L = \frac{1}{r_e^{1/2}\left|\sin\frac{r}{r_e}\right|^{1/2}} 10^{-2} \sqrt{\frac{2}{\pi}} \frac{2-\gamma}{\gamma} \frac{c^{1/2}}{H\tau_d^{3/2}} \left(\frac{P_b}{P_s}\right)^{1/\gamma - 1}$$

$$\gamma\, Q\left(\frac{\gamma}{P_b}\right) \int_0^\infty \frac{dy}{\sqrt{y}}\, A_i'\left[-\frac{t}{\tau_d} + y\right] \qquad \text{(A-69)}$$

$$= -\frac{4.7 \times 10^{-5}}{r_e^{1/2}\left|\sin\frac{r}{r_e}\right|^{1/2}} \left(\frac{1}{c\tau_d}\right)^{3/2} \left(\frac{P_b}{P_s}\right)^{\frac{1}{\gamma}-1} \gamma\, Q\left(\frac{\gamma}{P_b}\right) \int_0^\infty \frac{dy}{\sqrt{y}}\, A_i'\left[-\frac{t}{\tau_d} + y\right],$$

where we have used $H = c^2/\gamma g$. The corresponding matching radius is given by Eq. (A-60):

$$r_o = \epsilon \left(\frac{\gamma^*}{P_b^*}\right)^{1/3} \frac{x^{3/2}}{(1 + \frac{2}{3}\ell nx)^{3/4}} \qquad \text{(A-70)}$$

and the critical yield to pressure ratio is:

$$\left(\frac{\gamma^*}{P_b^*}\right) = \left(\frac{c\sigma}{a^3}\right)^{3/2} = \left(\frac{3h_{kk}\epsilon}{c^4 a^3}\right)^{3/2}$$

$$= 400\ (h_{kk})^{3/2} \frac{Mt}{\text{atmosphere}} \frac{\text{sec}^{3/2}}{\text{km}^{9/2}} \qquad \text{(A-71)}$$

for $\epsilon = .9$ km, $c = .34$ km/sec, and $a = 1/3$ sec. Based on a particular model atmosphere and direction of propagation chosen to represent the signal received at Berkely, California, following the Housatonic

detonation at Johnston Island Pierce and Posey[1] find $h_{kk} = .13 \frac{km^3}{sec}$. Thus in this particular case $\left(\frac{Y^*}{P_b^*}\right) = 19 \frac{Mt}{atmosphere}$. For a different set of atmospheric conditions near the burst point or a different direction of propagation h_{kk} and thus $\left(\frac{Y^*}{P_b^*}\right)$ would be different.

We define the scaled yield to pressure ratio:

$$\Gamma = \left(\frac{Y}{P_b}\right) \Big/ \left(\frac{Y^*}{P_b^*}\right) = \left[\frac{\exp \frac{Q^2-1}{2}}{Q}\right]^{9/2}, \qquad \text{(A-72)}$$

where we have used Eqs. (A-67) and (A-68) to eliminate x. Similarly the scaled matching radius is:

$$\frac{r_o}{R_o} = \Gamma Q^3 \qquad \text{(A-73)}$$

For $Q \leq 1.6$ which corresponds to $\Gamma \leq 4$ we may derive a simple analytic form for $Q(\Gamma)$ from Eq. (A-72):

$$\begin{aligned} \ln \Gamma &= \frac{2}{9}\left[\frac{Q^2-1}{2} - \ln Q\right] \\ &= \frac{2}{9}\left\{\frac{Q^2-1}{2} - \left[(Q-1) - \frac{(Q-1)^2}{2}\right]\right\} \\ &= \frac{2}{9}(Q-1)^2 \end{aligned} \qquad \text{(A-74)}$$

and therefore:

$$Q = 1 + \frac{\sqrt{2 \ln \Gamma}}{3} \qquad \text{(A-75)}$$

which gives the correction factor directly in terms of the scaled yield to pressure ratio.

In Fig. A-4 we plot Q and $\frac{r_o}{R_o}$ vs. Γ based on Eqs. (A-72) and (A-73). In order to utilize Eq. (A-75) or Fig. A-4 for a particular detonation it is necessary to calculate the critical yield to pressure ratio $\left(\frac{Y^*}{P_b}\right)$. This quantity involves the dispersion coefficient h_{kk} near the detonation which can only be obtained from numerical calculations based on a detailed atmospheric model. It is important to note that $\left(\frac{Y^*}{P_b^*}\right)$ will differ in different directions from the burst.

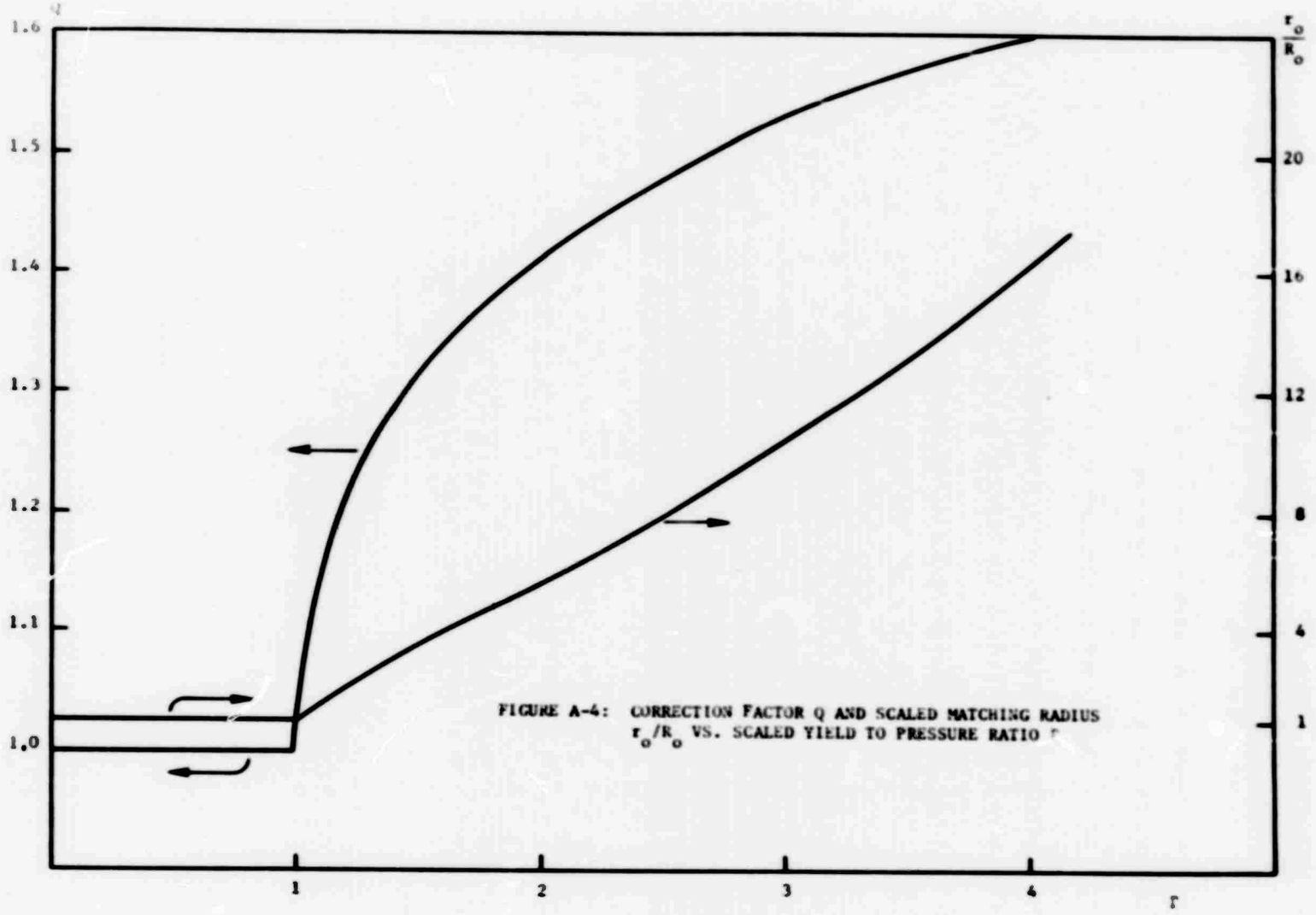

FIGURE A-4: CORRECTION FACTOR Q AND SCALED MATCHING RADIUS r_o/R_o VS. SCALED YIELD TO PRESSURE RATIO Γ

A.8 References

1. A. D. Pierce and J. W. Posey, Geophys. J. Roy. Astron. Soc. (to be published).

2. S. G. Reed, J. Acous. Soc. Am., 31, 1265, 1959.

3. "Problem M" results as contained in Nuclear Weapons Blast Phenomena Vol. 1, DASA 1200-1, compiled by P. A. Ellis, D. C. Sachs, F. H. Shelton, and J. F. Moulton, 1 March 1971 (S-RD).

4. A. D. Pierce, J. W. Posey, and E. F. Iliff, J. Geophys. Res., 76, 5025, 1971.

APPENDIX B: VARIATION OF RAYLEIGH WAVE AMPLITUDE WITH YIELD AND HEIGHT OF BURST FOR INTERMEDIATE ALTITUDE NUCLEAR DETONATIONS

B.1 Introduction

The shock wave from an atmospheric explosion can excite Rayleigh waves when it strikes the earth. In this appendix we derive a theory which predicts shock properties (overpressure and positive phase length) on the ground beneath a nuclear detonation. Using this theory we then compute the source strength for Rayleigh wave excitation as a function of yield and height of burst for intermediate altitude detonations. A more precise description of the altitude regime which we treat is given in Table B-2 and "source strength" is defined by Eq. (B-17) of the sequel. We do not consider any details of Rayleigh wave propagation, so that we are unable to provide absolute values of far-field Rayleigh wave amplitudes or phases. The present analysis is directly applicable only to estimating relative yields or heights of burst for situations in which source and receiver locations are the same for two or more detonations. However, the shock parameters at the earth's surface, which are calculated in the theory, are suitable as inputs to existing Rayleigh wave propagation models such as those of Harkrider and Flinn[1] and Nickel and Whitaker.[2]

It is in the inclusion of the influence of atmospheric structure on the shock parameters resulting at the earth's surface that the present treatment differs from previous work. Several authors have utilized a homogeneous model atmosphere in computing the time dependent overpressure at the earth's surface.[3,4,5] The assumption of atmospheric homogeneity can only be valid for detonation altitudes sufficiently less than an atmospheric scale height.

More recently, Harkrider and Flinn[1] have used a layered model atmosphere and have assumed that a given weak shock overpressure Δp relative to the ambient pressure at the source altitude p_c occurs at a distance r which scales as $p_c^{-1/3}$. The length of the positive

phase of the shock L at the distance r is also assumed to scale as $p_c^{-1/3}$. The scaling relations used by Harkrider and Flinn[1] are usually referred to as ordinary Sachs scaling.[6] This scaling law for the shock overpressure is known to be invalid for weak shocks which propagate downward through several atmospheric scale heights. Lutzky and Lehto[7] have shown that so-called modified Sachs scaling in which r scales as $p^{-1/3}$ (where p is the ambient pressure at a distance r from the explosion) for a given value of $\Delta p/p$ is a much more accurate scaling law for the overpressure of downward propagating shock than is ordinary Sachs scaling. It should be pointed out that Harkrider and Flinn[1] do not treat explosions above 4.88 km altitude. For low enough explosion altitudes quantitatively different results due to using different ambient pressure scaling laws should be small.

However, for intermediate altitude detonations the ordinary Sachs scaling laws are definitely inadequate for predicting shock parameters at the earth's surface. Nor does it appear that modified Sachs scaling is adequate for this purpose. This is for two reasons: (1) The validity of modified Sachs scaling at relative overpressures much lower than those which occur in the calculations of Lutzky and Lehto[7] is uncertain. (2) Modified Sachs scaling applies only to the relative overpressure and not to the positive phase length. In general the positive phase length is required in order to calculate the far-field Rayleigh wave amplitude, although for detonations well above 100 km altitude this may not be the case.[2]

In the absence of reliable height of burst scaling laws we have used the numerical calculations of Lutzky and Lehto[7] to predict the shock properties at the earth's surface. These authors have made calculations of the downward-going shock from a point explosion in an ideal gas, spherically symmetric, exponential atmosphere. Several factors must be assessed in applying these idealized calculations to the case of a nuclear explosion in the real atmosphere:

a. The assumption of an exponential atmosphere limits the theory, in its present form, to the 0-100 km altitude interval where the scale height may be assumed constant.

b. Application of results obtained for a spherically symmetric atmosphere (i.e. one-dimensional) to the real, horizontally stratified atmosphere involves the assumption of independent propagation of different portions of the shock front. It has been found that differences between one and two dimensional blast wave calculations in an isothermal atmosphere are in fact small.[8]

c. The calculations of Lutzky and Lehto are for an ideal gas with $\gamma=1.4$. Near the burst point this description of the equation of state of air is obviously lacking because of the high temperatures and pressures involved. Numerical calculations indicate that the net effect of this complication is the following: a nuclear explosion at sea level in real air is 0.7 times as effective in producing a given weak shock overpressure at large distances as the idealized point source with $\gamma=1.4$. That is, a 0.7 Mt idealized point source in the $\gamma=1.4$ medium produces the same given weak shock overpressure as a 1 Mt actual nuclear burst in real air.[9]

Even allowing these assumptions, the numerical calculations of Lutzky and Lehto are not entirely sufficient for our purposes because: (1) The do not extend to low enough relative overpressures. (2) They do not explicitly calculate the length of the positive phase.

In the next section we match these numerical calculations to an analytic weak shock theory in order to extend the relative overpressure range which may be treated. Also in the next section we use this analytic weak shock theory to relate the positive phase length to the spatial derivative of peak overpressure, a quantity which is calculated numerically. Thus by using weak shock theory in conjunction with the numerical calculations we are able to calculate shock parameters at

the earth's surface without using Sachs scaling laws. Having the shock parameters at the earth's surface we then compute the variation of far-field Rayleigh wave amplitude with yield and height of burst.

B.2 Determination of Shock Properties at the Earth's Surface

The calculations of Lutzky and Lehto[7] are parameterized by the quantities $\sigma_r = r(p_c/E)^{1/3}$ and $\sigma_h = h(p_c/E)^{1/3}$, where E is the energy released by the point explosion, p_c is the ambient pressure at burst altitude, h is the scale height and r is the distance from the explosion. Note that σ_h and σ_r are scale height and radius in units of the length $(E/p_c)^{1/3}$ characterizing the detonation.

We will match the numerical solution to an analytic one at a relative overpressure $\Delta p/p = 0.1$ (Δp is the overpressure and p is the ambient pressure at σ_r). Assume that in the neighborhood of the matching point we may write $\Delta p/p = a\,\sigma_r^n$, where a and n are constants. It turns out that matching of solutions can be conveniently done in terms of two quantities: $\bar{\sigma}_r = \sigma_r$ at $\Delta p/p = 0.1$, and $n = \bar{\sigma}_r \left(\frac{\partial}{\partial \sigma r} \ln \frac{\Delta p}{p}\right)_{\sigma_r = \bar{\sigma}_r}$. This amounts to prescribing Δp and its first derivative at $\bar{\sigma}_r$.

Values of $\bar{\sigma}_r$, n and the useful quantity $x = \bar{\sigma}_r/2\sigma_h$ obtained from the calculations of Lutzky and Lehto[7] are shown in Table B-1.

TABLE B-1

MATCHING PARAMETERS OBTAINED
FROM NUMERICAL CALCULATIONS

σ_h	$\bar{\sigma}_r$	n	x
0.05	0.311	-4.26	3.11
0.10	0.511	-3.84	2.55
0.20	0.786	-3.29	1.96
0.50	1.26	-2.82	1.26
2.0	2.10	-1.90	0.502

In Fig. B-1, n and σ_h are plotted vs x. We have also included the point n(x=0) corresponding to a homogeneous atmosphere ($\sigma_h = \infty$) based on Figure 3 of Lehto and Larson.[9]

Now according to the weak shock theory of Reed[10]

$$\frac{\Delta p}{p} = \frac{\Delta p_o}{p_o} \frac{r_o}{r} \frac{L_o}{L} \sqrt{\frac{p_o}{p}} \tag{B-1}$$

$$\frac{L}{L_o} = \left[1 + \frac{\gamma+1}{2\gamma} \frac{\Delta p_o}{p_o} \frac{r_o}{L_o} \int_{r_o}^{r} \sqrt{\frac{p_o}{p(r)}} \frac{dr}{r} \right]^{\frac{1}{2}} \tag{B-2}$$

where $\Delta p_o/p_o$ is the relative overpressure and L_o is the length of the positive phase at $r_o < r$ and where γ is the ratio of specific heats.

From Eq. (B-1) assuming an exponential atmosphere

$$\frac{\partial}{\partial r} \ln \frac{\Delta p}{p} = -\frac{1}{r} - \frac{1}{2h} - \frac{\partial}{\partial r} \ln \frac{L}{L_o} \tag{B-3}$$

where h is the atmospheric scale height.

Using Eq. (B-2) we find

$$\frac{\partial}{\partial r} \ln \frac{L}{L_o} = \frac{\frac{\gamma+1}{4\gamma} \frac{\Delta p_o}{p_o} \frac{r_o}{r} \sqrt{\frac{p_o}{p}} \frac{1}{L_o}}{\left(\frac{L}{L_o}\right)^2} = \frac{\gamma+1}{4\gamma} \frac{\Delta p}{p} \frac{1}{L} \tag{B-4}$$

where we have used (B-1) to eliminated $\Delta p_o/p_o$.

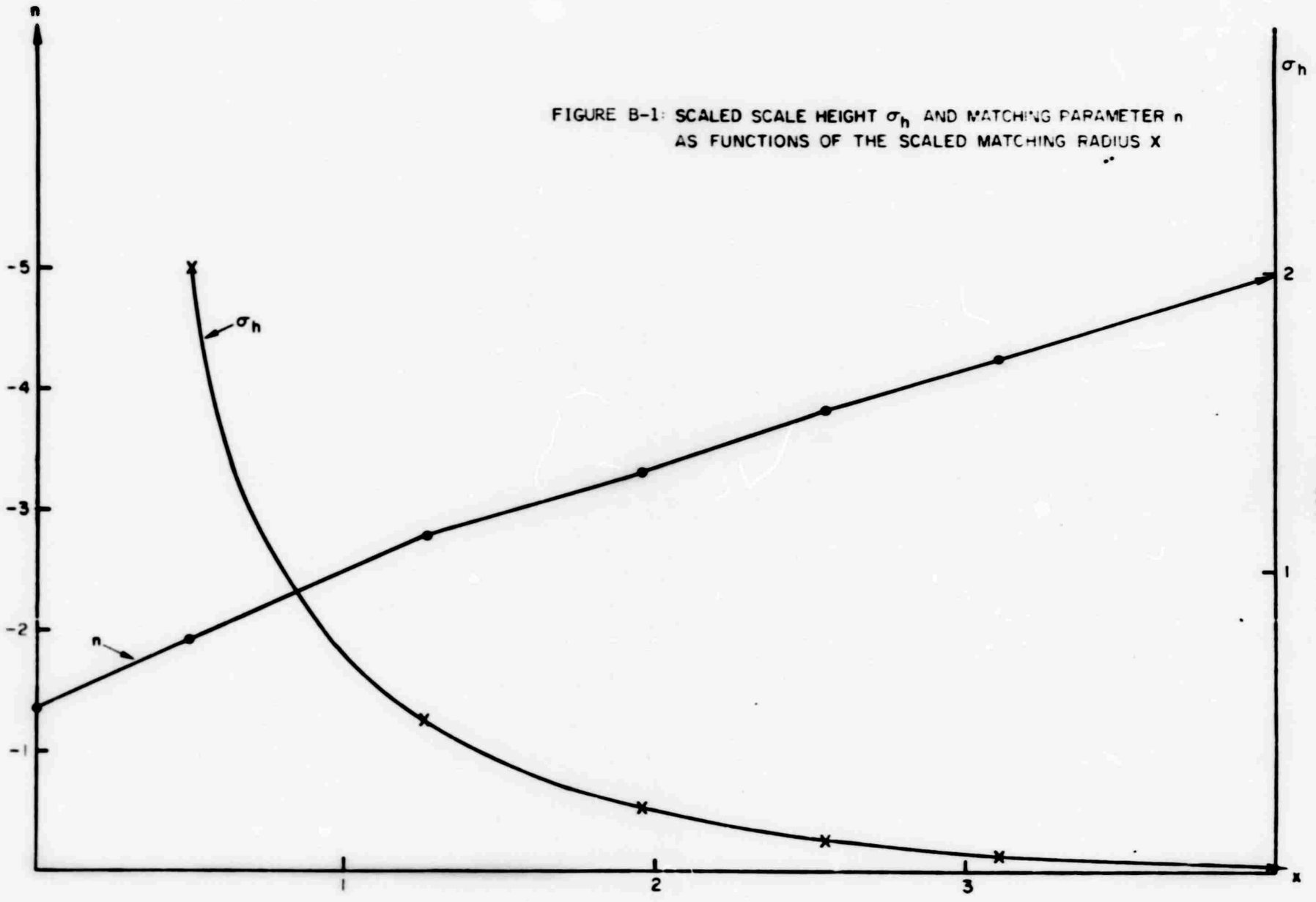

FIGURE B-1: SCALED SCALE HEIGHT σ_h AND MATCHING PARAMETER n AS FUNCTIONS OF THE SCALED MATCHING RADIUS X

Substituting (B-3) in (B-4) yields:

$$\frac{\partial}{\partial r} \ln \frac{\Delta p}{p} = -\frac{1}{r} - \frac{1}{2h} - \frac{\gamma+1}{4\gamma} \frac{\Delta p}{p} \frac{1}{L} \tag{B-5}$$

or

$$L = \frac{-\frac{\gamma+1}{4\gamma} \frac{\Delta p}{p} r}{\left[1 + \frac{r}{2h} + \frac{r\partial}{\partial r} \ln \frac{\Delta p}{p}\right]} \tag{B-6}$$

Taking γ=1.4 we find that at $\Delta p/p = 0.1$ ($\sigma_r = \bar{\sigma}_r$):

$$L(\bar{\sigma}_r) = \bar{L} = \frac{-0.0857\ h\ x}{1 + x + n} \tag{B-7}$$

While from (B-6)

$$\left[\frac{\gamma+1}{2\gamma} \frac{\Delta p}{p} \frac{r}{L}\right]_{\sigma_r=\bar{\sigma}_r} = -2\ (1 + x + n) \tag{B-8}$$

so that from (B-2)

$$\frac{L}{\bar{L}} = \left[1-2\ (1 + x + n) \int_{\bar{r}}^{r} \sqrt{\frac{p(\bar{r})}{p}}\ \frac{dr}{r}\right]^{\frac{1}{2}}$$

$$= \left\{1-2\ \left[1 + x + n\right] e^{x} \left[E_1(x) - E_1\left(\frac{r}{2h}\right)\right]\right\}^{\frac{1}{2}} \tag{B-9}$$

where E_1 is the exponential integral. Using (B-7), the length of the positive phase at distance r is found to be

$$L = \frac{-0.0857\, h\, x}{1 + x + n}\left\{1 - 2\left[1 + x + n\right] e^{x}\left[E_1(x) - E_1\left(\frac{r}{2h}\right)\right]^{\frac{1}{2}}\right\}_{r>\bar{r}} \qquad \text{(B-10)}$$

Finally, substituting (B-9) into (B-1) and taking $\Delta p_o/p_o = 0.1$ we find

$$\frac{\Delta p}{p} = \frac{0.2h\,\frac{x}{r}\, e^{x - \sqrt{\frac{p_c}{p}}}}{\left\{1 - 2\left[1 + x + n\right] e^{x}\left[E_1(x) - E_1\left(\frac{r}{2h}\right)\right]\right\}^{\frac{1}{2}}} \qquad \text{(B-11)}$$

For the class of detonations which we treat, the quantity $E_1(r/2h)$ can be neglected in (B-10) and (B-11). This is a valid approximation when the relative overpressure at the ground is somewhat smaller than 0.1 (corresponding to a reflected overpressure at the ground of about 200 mb). In terms of Eq. (B-10) this approximation is related to the fact that the length of the positive phase becomes "frozen" for downward propagation at a value independent of distance from the burst point. It is convenient for later use to define the dimensionless functions

$$f(x) \equiv \frac{0.2\, x\, e^{x}}{\left\{1 - 2\left[1 + x + n\right] e^{x} E_1(x)\right\}^{\frac{1}{2}}} = \frac{\Delta pr}{\sqrt{p_c p}\, h} \qquad \text{(B-12)}$$

$$g(x) \equiv \frac{-0.0857\, x}{1 + x + n}\left\{1 - 2\left[1 + x + n\right] e^{x} E_1(x)\right\}^{\frac{1}{2}} = \frac{L}{h} \qquad \text{(B-13)}$$

The functions f(x) and g(x) are shown in Figs. B-2 and B-3. Equations (B-12) and (B-13) form the basis for the subsequent analysis in which we consider the variation of Rayleigh wave amplitude with yield and height of burst.

First, however, in concluding this section it is useful to summarize the various factors which determine the altitude regime to which the present theory is applicable. According to what has been said previously, the point source equivalent energy E of a sea level nuclear explosion of yield Y is 0.7 Y. We therefore redefine the parameter σ_h

$$\sigma_h = h\left(\frac{p_c}{0.7\ Y}\right)^{1/3} = h(km)\left[\frac{p_c(mb)}{29.4\ Y(kT)}\right]^{1/3} \qquad (B-14)$$

Our treatment is essentially limited to the range of values of σ_h used in the numerical calculations of Lutzky and Lehto[7] (0.05-2.0). For a given yield, Eq. (B-14) therefore places constraints on the relevant pressure or altitude interval:

$$0.685\ Y(kT) \gtrsim p(mb) \gtrsim 1.07 \times 10^{-3}\ Y(kT) \qquad (B-15)$$

There are two additional restrictions on the relevant altitude interval which have been previously mentioned: (1) The theory is limited to detonations below 100 km, because above this altitude the isothermal atmosphere approximation is invalid. (2) We are also limited to sufficiently high altitude detonations that the relative overpressure on the ground is smaller than 0.1

Putting all of these factors together for the σ_h values at our disposal, we construct Table B-2, which shows the altitude interval

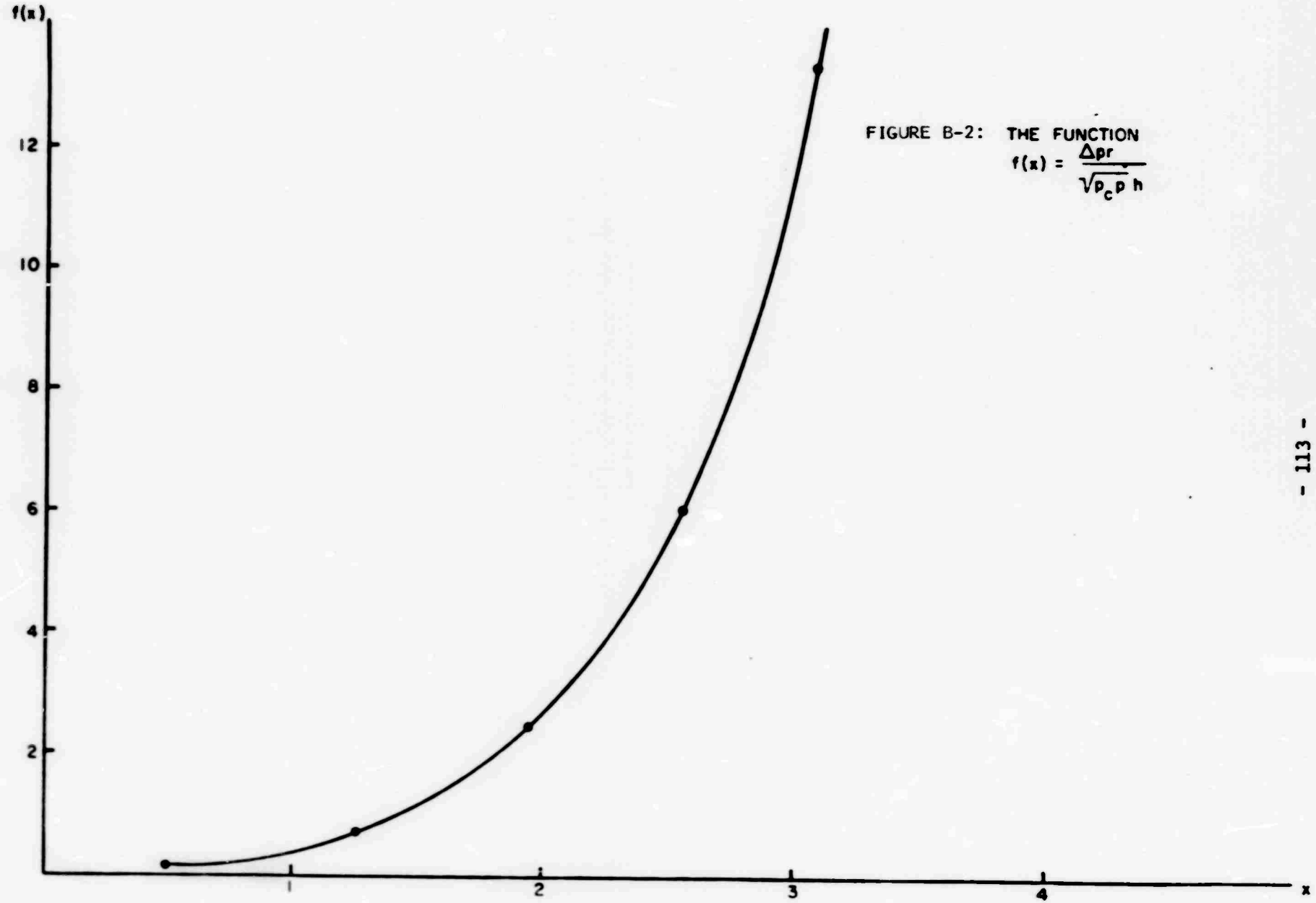

FIGURE B-2: THE FUNCTION $f(x) = \frac{\Delta pr}{\sqrt{\rho_c p}\, h}$

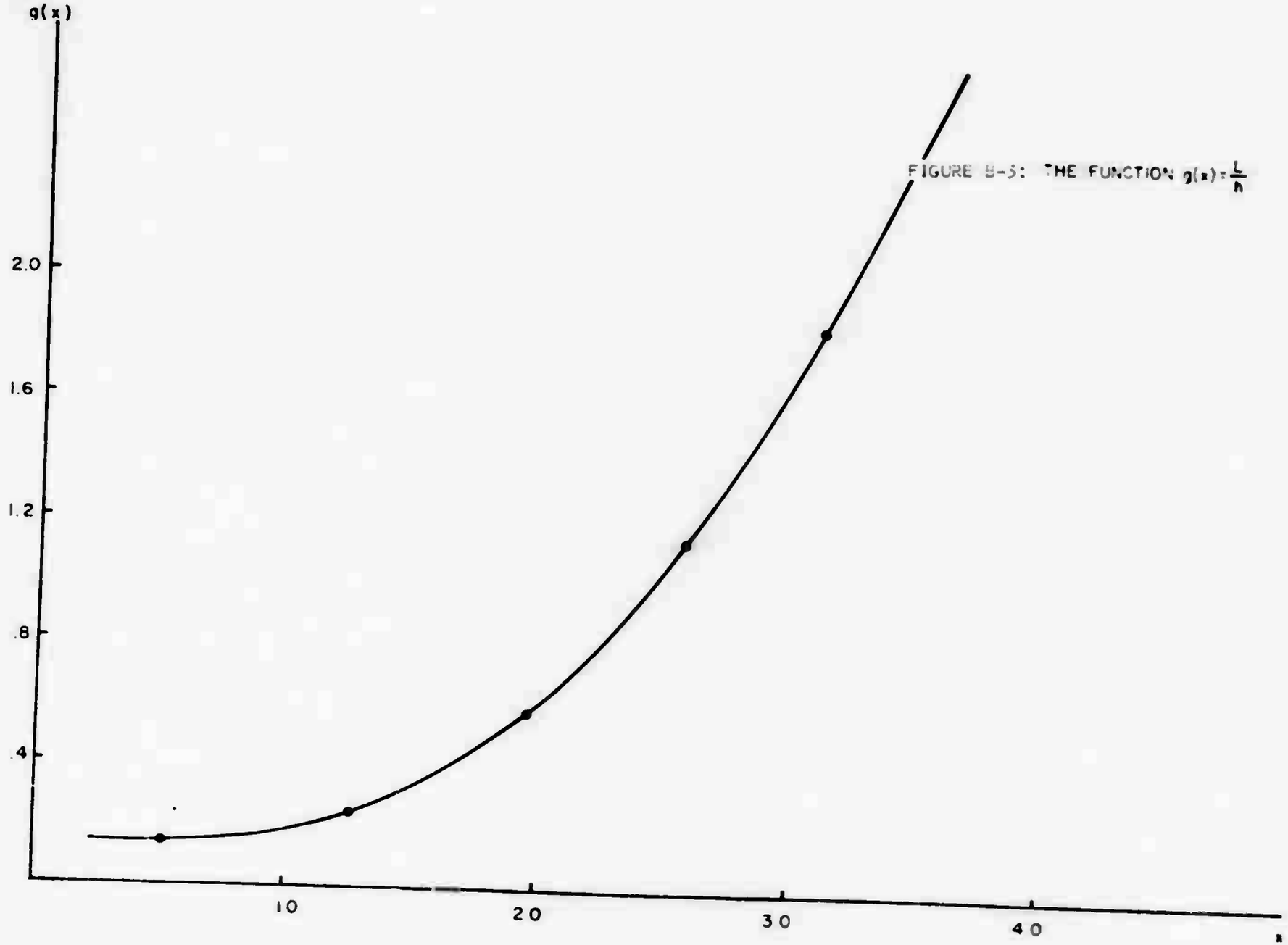

FIGURE B-3: THE FUNCTION $g(x) = \frac{L}{h}$

which can be treated for several yields. In deriving Table B-2, we have used the 1962 Standard Atmosphere and assumed a scale height h=7 km.

TABLE B-2

ALTITUDE INTERVALS TO
WHICH THE THEORY APPLIES

Yield	Altitude Interval
10 kT	33.8 - 93.5 km
100 kT	18.6 - 92.5 km
1 Mt	30.7 - 80.0 km

B.3 Source Strength for Rayleigh Wave Excitation as a Function of Yield and Height of Burst

Toksöz and Ben-Menahem[4] have considered the far-field Rayleigh wave amplitudes excited by a point source in a homogeneous atmosphere. For three-dimensional propagation in the absence of non-linear effects, the source parameters contribute to the amplitude almost entirely through a factor

$$|L(\omega)| = \left| \int_{-\infty}^{\infty} \delta p(t)\, e^{-i\omega t}\, dt \right| \qquad \text{(B-16)}$$

which is the Fourier transform of the point source pressure fluctuation $\delta p(t)$. As described by the above authors the far-field Rayleigh wave amplitude is proportional to $|L(\omega)|$ and also to a factor which lies between unity and $\exp -k_i r$, where k_i is the imaginary component of the seismic disturbance wave number, and r is the height of the source above

ground. These are the only factors which depend on source parameters. For the atmosphere-lithosphere contrast $k_i \approx (2\pi/\lambda_R) \times 10^{-5}$, where λ_R is the seismic wavelength. Thus, $\exp -k_i r$ is essentially unity, even when r is comparable to λ_R, and we may simply take the Rayleigh wave amplitude to be proportional to $|L(\omega)|$ with no other factors which depend on the source amplitude, time dependence, or height above ground.

In the case of linear pressure pulse propagation, $\delta p(t) \propto \delta p_g(t) r$, where $\delta p_g(t)$ is the time dependent pressure pulse on the ground a distance r beneath the source. Even in the case where the pressure propagation is nonlinear, because of pulse lengthening and dissipative effects we expect that the source strength for Rayleigh wave excitation will be proportional to the Fourier transform of $\delta p_g(t) r$. The reason is simply that the source strength can only depend on parameters at the ground and not on the previous history of the pulse propagation. That is, we may substitute an equivalent linear point source pressure fluctuation proportional to $\delta p_g(t) r$ for the actual nonlinear disturbance.

For reasons which will soon be evident, we therefore define the dimensionless source strength to be

$$S(T) = \frac{2\pi r}{T\, p_g h} \left| \int_0^\infty \delta p(t)\, e^{-i\omega t}\, dt \right| \qquad \text{(B-17)}$$

where $T = 2\pi/\omega$ is the Rayleigh wave period of interest, p_g is the sea level pressure, and h is the atmospheric scale height. Notice that S(T) does not contain any dependence on source parameters except through $|L(\omega)|$. The far-field Rayleigh wave amplitude is therefore proportional to S(T) with no other factors which depend on source amplitude, time dependence, or height above ground.

To continue we assume a pressure pulse at the ground

$$\delta p_g(t) = \Delta p \left(1 - \frac{t}{t_+}\right) e^{-t/t_+} \qquad \text{(B-18)}$$

where Δp is the peak overpressure and t_+ is the positive phase duration.[11] The weak shock theory employed in the previous section should be independent of pulse shape since nonlinear effects are governed by what happens at the shock front and not the shock interior. Thus, Eq. (B-17) becomes

$$S(T) = \frac{\Delta p\, r}{\left[1 + \left(\frac{T}{2\pi t_+}\right)^2\right] p_g h} \qquad \text{(B-19)}$$

Now $t_+ = L/c$, where c is the sea level sound speed and L, as in the previous section, is the positive phase length. Thus, in terms of the functions f(x) and g(x) of the previous section, Eq. (B-19) can be written

$$S = \frac{f(x)}{1 + \left[\frac{T}{\frac{2\pi h}{c}\, g(x)}\right]^2} \sqrt{\frac{p_c}{p_g}} = \frac{f(x)}{1 + \left[\frac{T}{129.36\, g(x)}\right]^2} \sqrt{\frac{p_c}{p_g}} \qquad \text{(B-20)}$$

for h=7 km, and c=0.34 km/sec. In writing (B-20) we have explicitly noted that the right sides of (B-12) and (B-13), defining f(x) and g(x), are to be evaluated at the ground where $p = p_g$.

According to Eq. (B-14)

$$\left(\frac{p_c}{p_g}\right)^{1/2} = \left(\frac{29.4}{p_g}\right)^{1/2} \left(\frac{\sigma_h}{h}\right)^{3/2} Y^{1/2} = 9.1975 \times 10^{-3}\ \sigma_h^{3/2}\ Y^{1/2} \qquad \text{(B-21)}$$

for $p_g = 1013.25$ mb. Thus, (B-20) becomes:

$$S = \frac{9.1975 \times 10^{-3}\ \sigma_h^{3/2}\ Y^{1/2}\ f(x)}{1 + \left[\frac{T}{129.36\ g(x)}\right]^2} \qquad \text{(B-22)}$$

We generate curves of source strength S versus height of burst r in the following way: Picking Y and σ_h determines p_c and hence r through Eq. (B-21) (again using the 1962 Standard Atmosphere). The quantity x is determined from Fig. B-1 or Table B-1, and f(x) and g(x) for use in Eq. (B-22) are found from Figs. B-2 and B-3.

Results for yields Y=10 kT, 100 kT, and 1 MT and Rayleigh wave periods T = 10, 20, and 40 seconds are shown in Figs. B-4, B-5, and B-6. The yields we refer to are effective yields which at high altitudes may be less than the nominal yields due to radiative or other energy loss mechanisms. There is a maximum in source strength which occurs at about 80-85 km for 10 kT, 65-70 km for 100 kT, and 50-60 for 1 MT. The strength of the maximum is greatest for the larger Rayleigh wave periods and for the shorter periods the maximum may disappear entirely. The altitude at which the maximum occurs increases slightly with Rayleigh wave period.

The variation of source strength with altitude can be appreciable. For example, the source strength for a Rayleigh wave period of 40 seconds and a yield of 100 kT increases by almost a factor of 3 as the height of burst is raised from 20 km to 70 km.

FIGURE B-4: SOURCE STRENGTH FOR RAYLEIGH WAVE EXCITATION VS HEIGHT OF BURST, Y = 10 KT

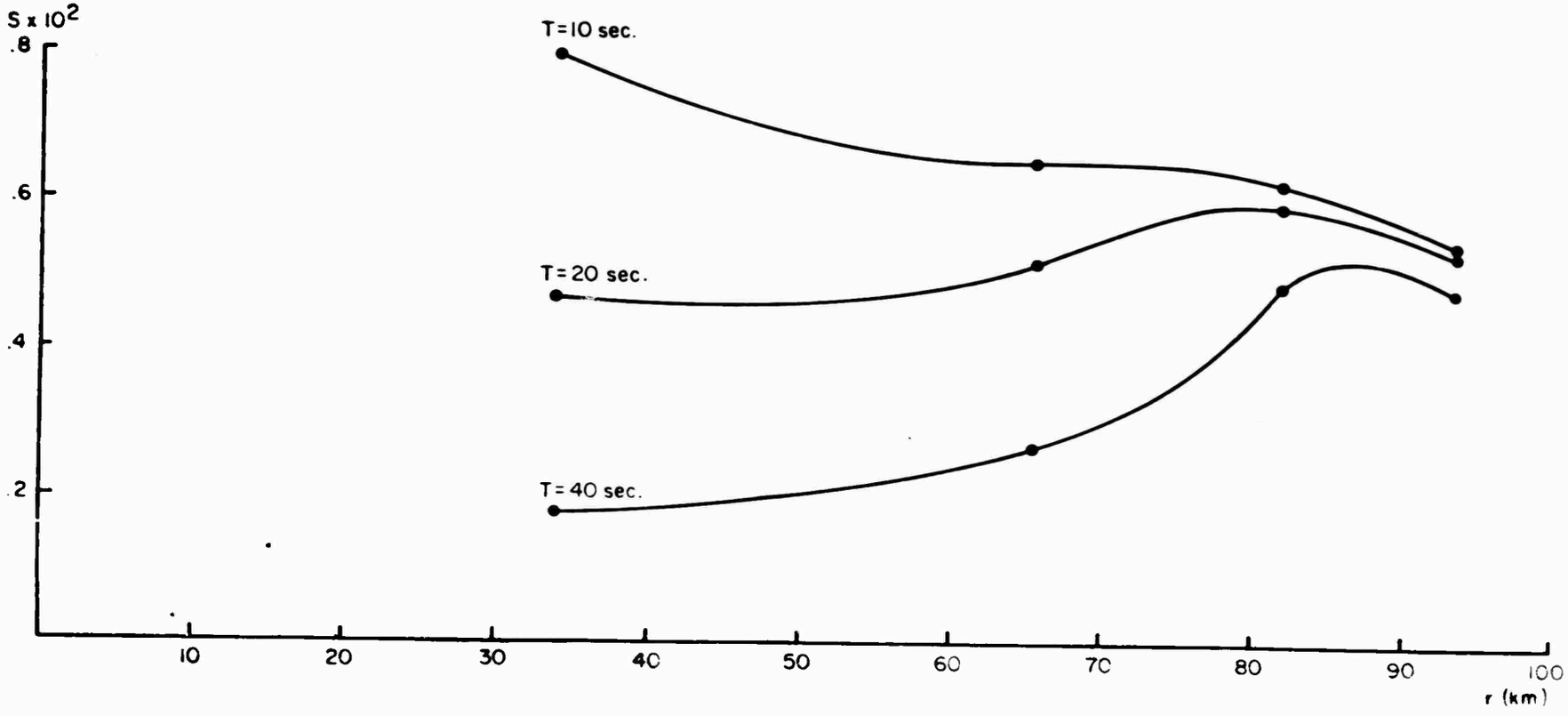

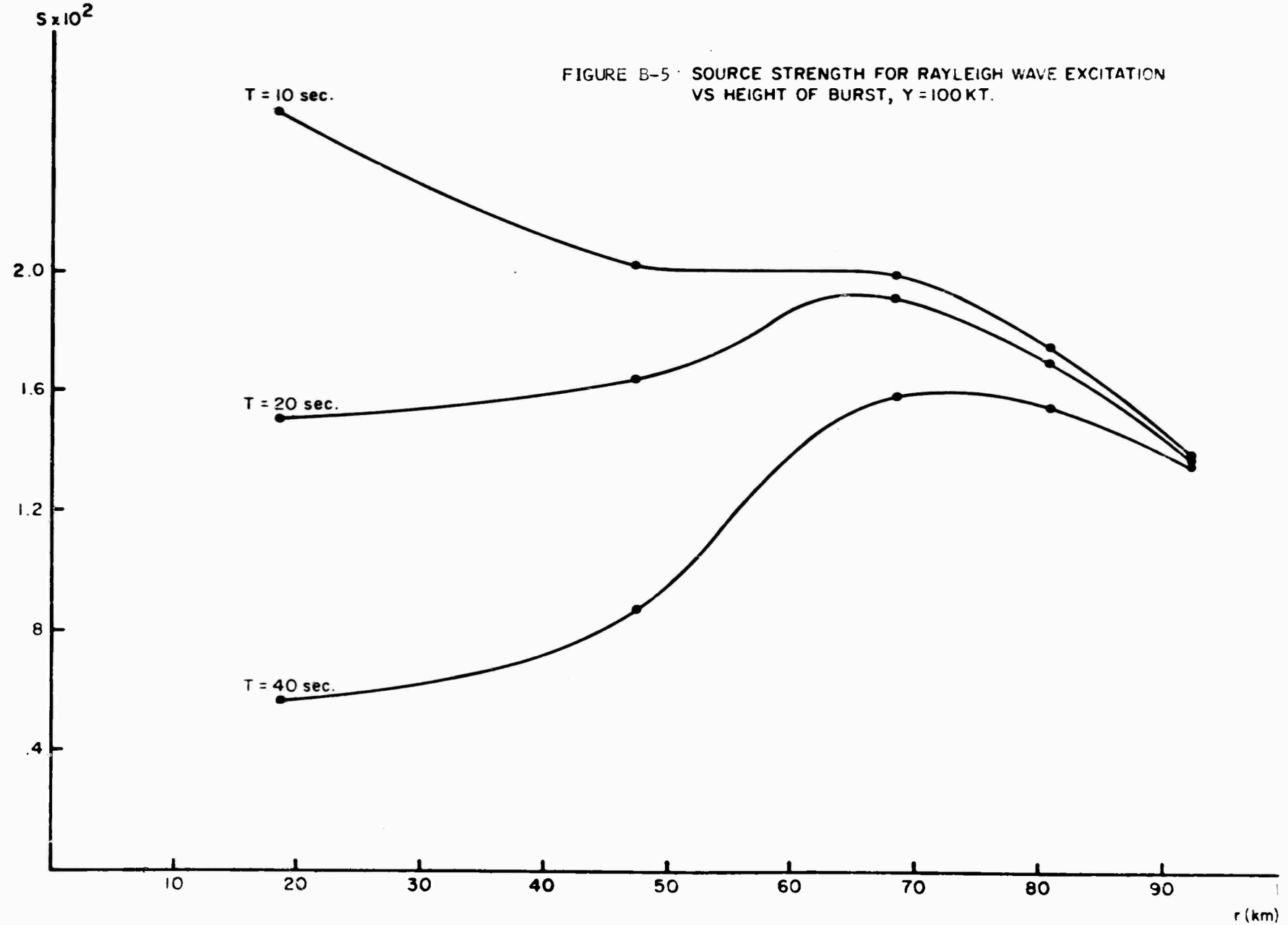

FIGURE B-5 · SOURCE STRENGTH FOR RAYLEIGH WAVE EXCITATION VS HEIGHT OF BURST, Y = 100 KT.

FIGURE B-6: SOURCE STRENGTH FOR RAYLEIGH WAVE EXCITATION VS HEIGHT OF BURST, Y = 1 MT

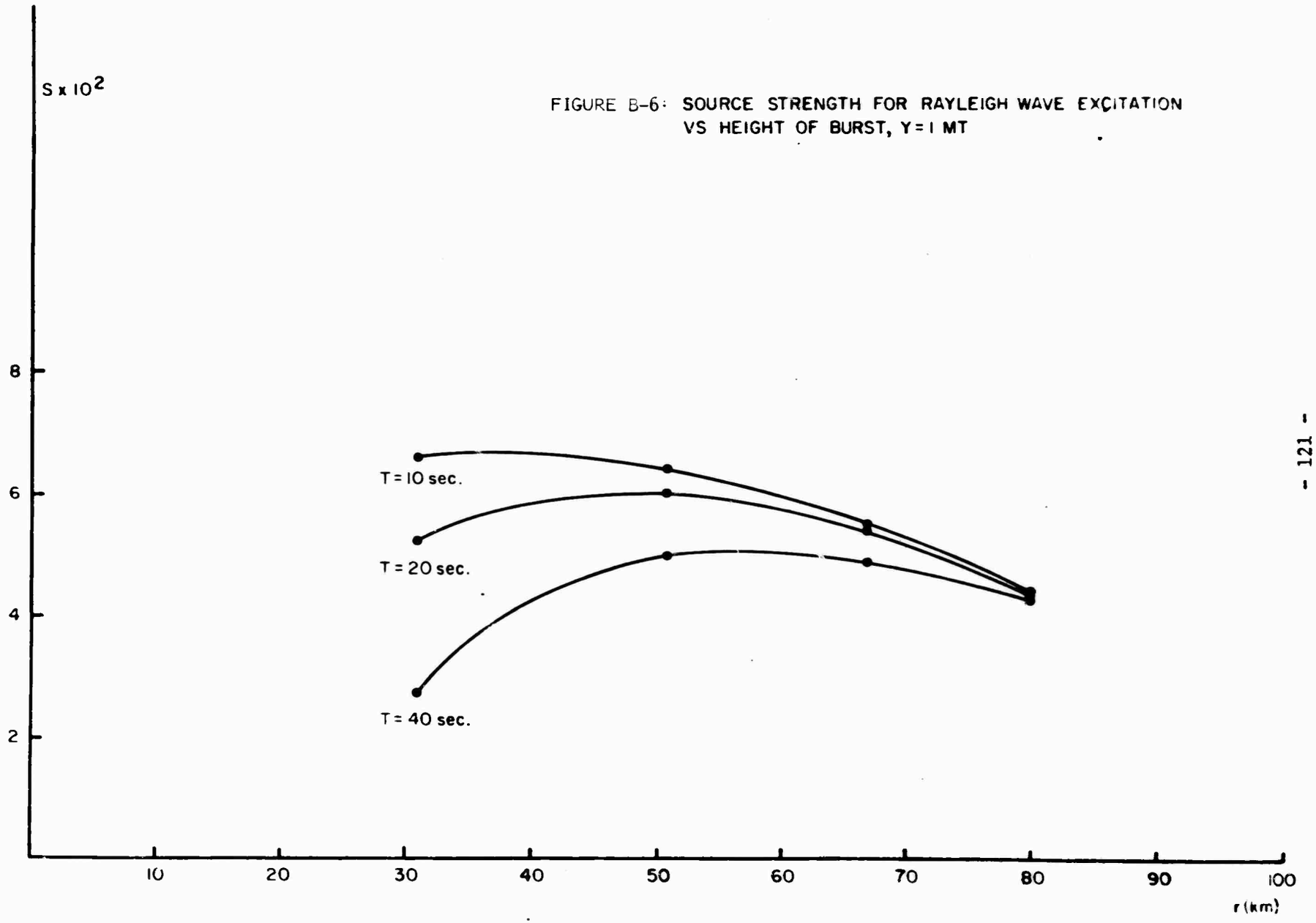

Figures B-7 and B-8 show source strength plotted against yield for Rayleigh wave periods of 10, 20, and 40 seconds and burst heights of 40 and 80 km. Within the range of parameters treated, the source strength increases with yield at a rate between $Y^{1/2}$ and $Y^{2/3}$.

B.4 Conclusions

a. Rayleigh wave amplitudes from intermediate altitude detonations vary with height of burst as well as yield.

b. The variation with yield appears to lie between the 1/2 and the 2/3 power, depending on burst height and the Rayleigh wave period being considered.

c. For a given yield the Rayleigh wave amplitude, at least for periods of 20 seconds or more, has a maximum at a particular burst height. The maximum occurs at 80-85 km for 10 kT, 65-70 km for 100 kT, and 50-60 km for 1 Mt. The strength of the maximum is greatest for the longer Rayleigh wave periods and the altitude at which the maximum occurs increases slightly with increasing Rayleigh wave period.

Acknowledgements

I wish to acknowledge useful discussions with S. L. Kahalas and D. L. Lehto, the latter of whom provided data on which Table B-1 is based.

This research was sponsored by the Advanced Research Projects Agency under Air Force Office of Scientific Research Contract No. F44620-71-C-0086.

FIGURE B-7: SOURCE STRENGTH FOR RAYLEIGH WAVE EXCITATION VS YIELD, 40 km HEIGHT OF BURST

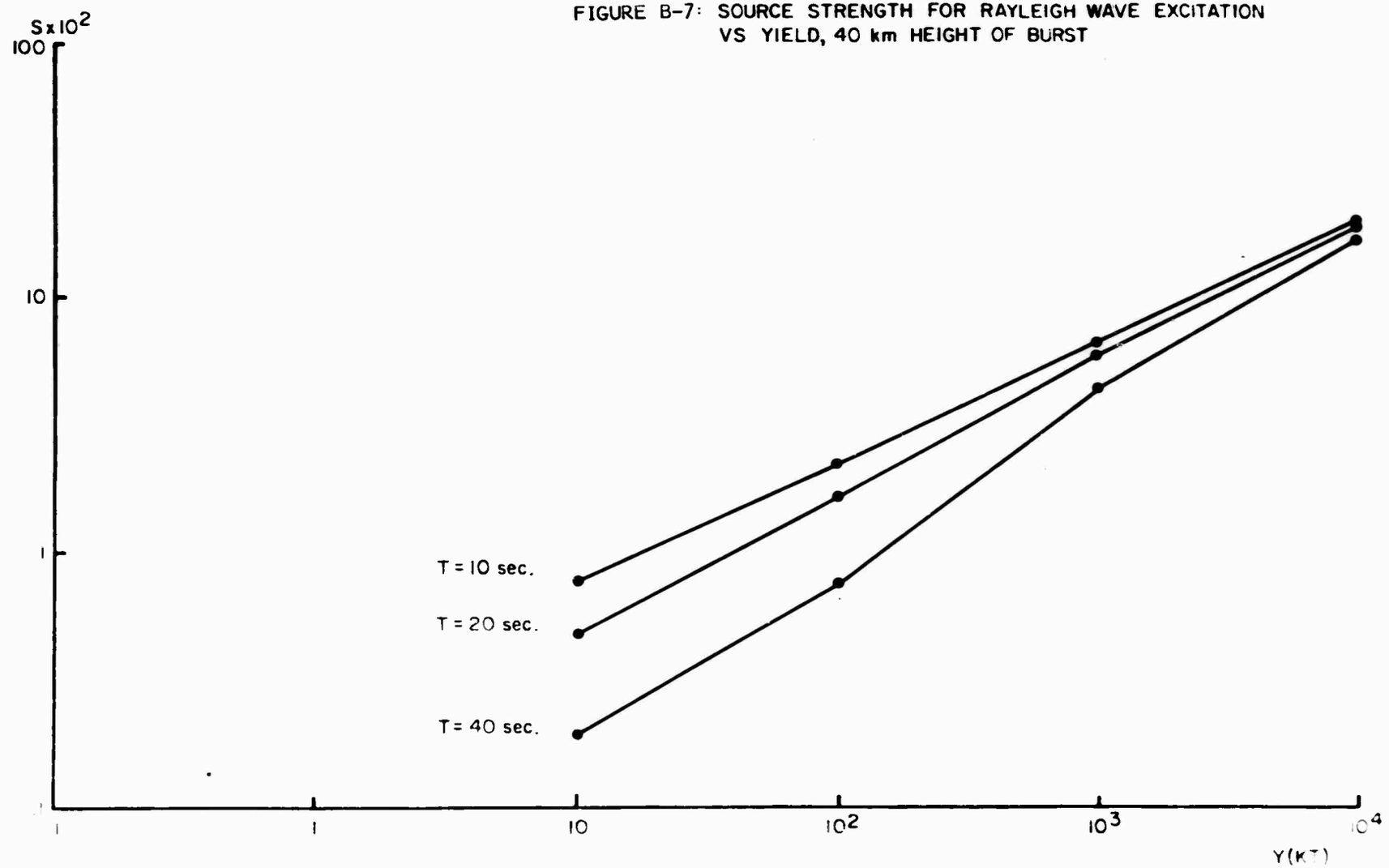

FIGURE B-8: SOURCE STRENGTH FOR RAYLEIGH WAVE EXCITATION VS YIELD, 80 km HEIGHT OF BURST

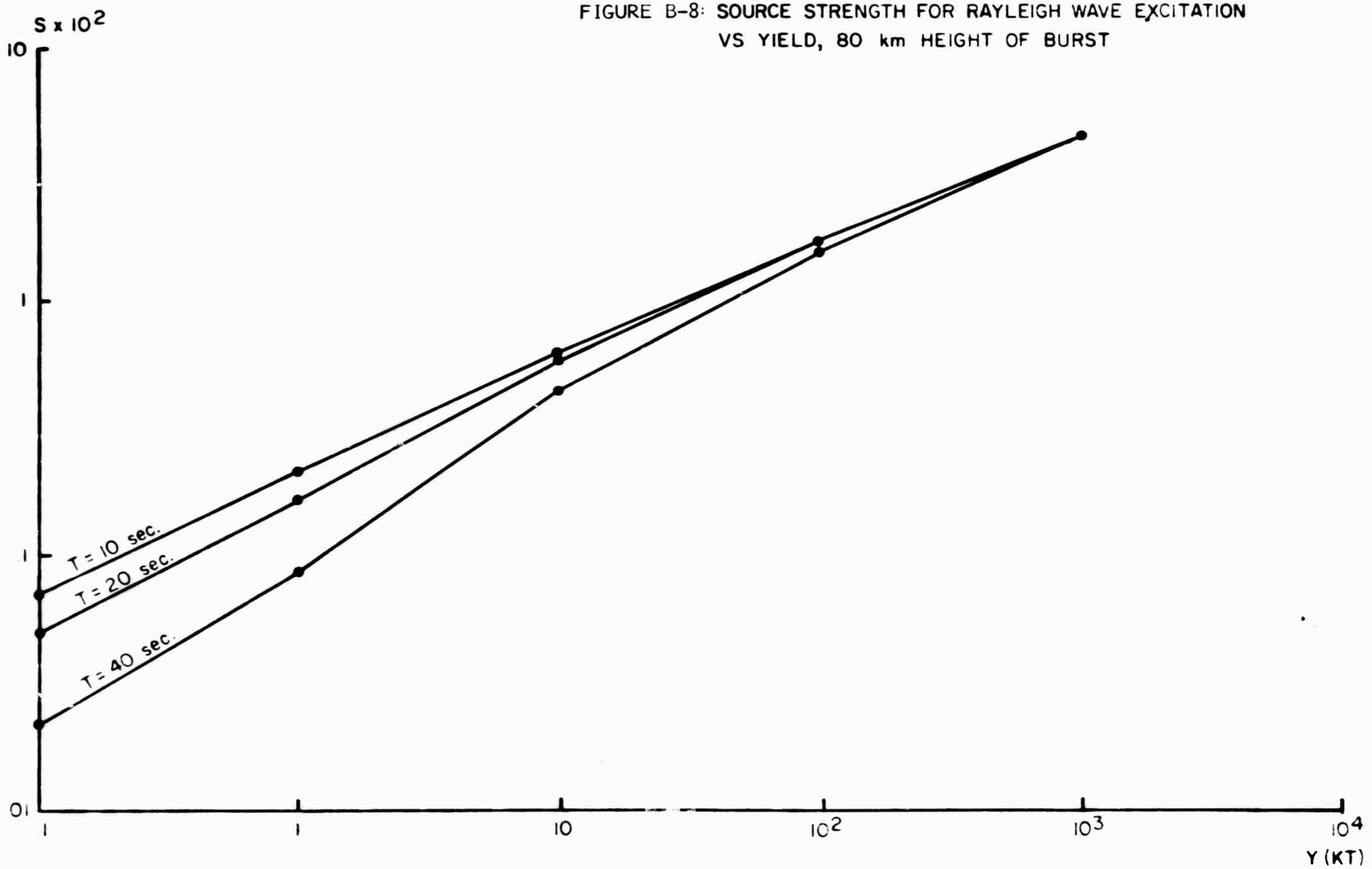

B.5 References

1. D. G. Harkrider and E. A. Flinn, Rev. Geophys. and Space Phys., 8, 501-516, 1970.

2. G. Nickel and W. Whitaker, "Distant Seismic Waves from a High Altitude Source," Air Force Weapons Laboratory Technical Report, AFWL-TR-67-125, 1968.

3. M. Bath, Seismic records of explosions - especially nuclear explosions, 3, Försvarets Forskningsanstalt Avdelning 4 rapports A 4270-4721, Uppsala, 116 pp., 1962.

4. M. N. Toksöz and A. Ben-Menahem, J. Geophys. Res., 69, 1639-1648, 1964.

5. S. Crampin, J. Geophys. Res., 71, 2951-2958, 1966.

6. R. G. Sachs, "The Dependence of Blast on Ambient Pressure and Temperature," Ballistic Research Laboratory Report No. 466, 1944.

7. M. Lutzky and D. L. Lehto, Phys. Fluids, 11, 1466-1472, 1968.

8. W. W. Troutman and C. W. Davis, Jr., "The Two-Dimensional Behavior of Shocks in the Atmosphere," Air Force Weapons Laboratory Technical Report, AFWL-TR-65-151, 1965.

9. D. L. Lehto and R. A. Larson, "Long Range Propagation of Spherical Shockwaves from Explosions in Air," Naval Ordnance Laboratory Technical Report 69-88, 1969.

10. S. G. Reed, Jr., J. Acous. Soc. Am., 31, 1265, 1959.

11. S. Glasstone, The Effects of Nuclear Weapons, U. S. Government Printing Office, Washington, D. C., 1962.

GLOSSARY OF SYMBOLS USED

Section 2 and Appendix A

A	amplitude function of Lamb mode
A_i	Airy function
A_i'	derivative of the Airy function
c	sound speed
C	correction factor due to $\Delta z \leq 0$ integration in Eq. (A-43)
d	distance moved by low frequencies relative to high frequencies
F	function containing time and horizontal distance dependence of Lamb mode
G	function defined by Eq. (A-40)
h_{kk}	dispersion coefficient due to deviations of wind and sound speeds from vertically averaged values
H	scale height
k	wave number
k_i	imaginary part of k
k_r	real part of k
ℓ	distance behind shock front
P_b	ambient pressure at burst altitude
P_b^*	critical ambient pressure for breakdown of yield-amplitude proportionality
P_L	Lamb mode pressure amplitude
P_s	sea level pressure
P_{fpt}	pressure amplitude, first peak to trough

ΔP overpressure

Q large yield amplitude correction factor

r great circle distance

r_e earth radius

r_o cylindrical radius for matching weak shock and Lamb mode

$\bar{r}$ parameter defined by Eq. (A-14)

R distance from burst

Re "real part of"

R_o small radius where $\bar{\pi}(R_o) = .1$ and atmospheric inhomogeneity is unimportant

$S(\omega)$ Fourier transform of Glasstone pulse

t time after signal arrival

t_+ positive phase duration

$\bar{t}$ parameter defined by Eq. (A-13)

T period of far-field disturbance

V_g group velocity

x $\dfrac{r_o}{\varepsilon}\left(\dfrac{P_b}{Y}\right)^{1/3} \equiv x$

y $\dfrac{\sqrt{\Delta z^2 + r_o^2} - r_o}{c\tau_d} \equiv y$

Y yield

Y_m yield in megatons

Y^* critical yield for breakdown of yield-amplitude proportionality

z altitude

z_m altitude of rigid ceiling in modal analysis

$\bar{z}$ height of burst

Δz vertical distance relative to height of burst

z_1 lowest altitude to which shock extends

z_2 highest altitude to which shock extends

α t_+ at $\bar{\pi} = .1$ for 1 kT at sea level

β $\frac{\gamma+1}{2\gamma} \frac{\bar{\pi}(R_o)\, R_o}{c t_+(R_o)} \equiv \beta$

γ ratio of specific heats

Γ scaled yield to pressure ratio defined by Eq. (A-72)

σ $\frac{3h_{kk}}{c^4} \equiv \sigma$

ϵ radius at which $\bar{\pi} = .1$ for 1 kT at sea level

$\pi(r_o, z, t_o)$ relative overpressure at r_o, z, t_o

$\bar{\pi}$ peak relative overpressure

τ time after passage of shock front

τ_a waveform arrival time

τ_d characteristic dispersion time

ψ waveform function of Lamb mode

$\hat{\psi}$ Fourier transform of $\psi(r)$

Ψ sum of modes other than the Lamb mode

ω frequency of disturbance

Section 3

$B_1, B_2, \ldots$ Bernoulli numbers

c	sound speed
d	distance between ground reflections
E_i	exponential integral given by Eq. (3-14)
E_1	exponential integral given by Eq. (3-13)
f	function giving relative overpressure vs. distance for 1 kT at sea level
H	effective scale height
H_s	atmospheric scale height
I	integral defined by Eq. (3-8)
I_ℓ	contribution to I from ℓth transit between ground and upper boundary
ℓ	index for each transit between ground and upper boundary
m	number of reflections at upper boundary
n	$r \frac{\partial}{\partial r} \ell n \frac{\Delta P}{P(r)}$
n_h	value of n for a homogeneous atmosphere
P	ambient pressure
P_b	ambient pressure at burst point
ΔP	overpressure
r	radial distance from burst
r_o	value of r at $\frac{\Delta p}{p} = .2$
R	range
t_+	positive phase duration
T	far-field disturbance period

Y	yield
z_o	altitude of upper reflecting boundary
$\bar{z}$	height of burst
γ	ratio of specific heats
Γ	Euler's constant

Section 4 and Appendix B

a	constant relating relative overpressure to radius at $\frac{\Delta p}{p} = .1$
c	sound speed
E	point source energy
E_1	exponential integral
$f(x)$	dimensionless function defined by Eq. (4-8)
$g(x)$	dimensionless function defined by Eq. (4-7)
h	scale height
$L(\omega)$	Fourier transform of point source pressure fluctuation
L_o	positive phase length at r_o
$\bar{L}$	positive phase length at $\frac{\Delta p}{p} = .1$
n	starting value defined by Eq. (4-10)
p	ambient pressure at r
p_b, p_c	ambient pressure at burst
p_g	sea level ambient pressure
p_o	ambient pressure at r_o
Δp	peak overpressure at the ground
Δp_o	overpressure at r_o

δp	point source pressure fluctuation
δp_g	pressure fluctuation at the ground from a point source
r	radius from burst point, also height of burst
r_o	arbitrary radius less than r, $\bar{r}$ in particular
$\bar{r}$	radius at $\frac{\Delta p}{p} = .1$
S	dimensionless source strength defined by Eq. (4-4)
t	time
t_+	positive phase duration at the ground
x	$\frac{r_o}{2h}$
Y	yield
γ	ratio of specific heats
σ_h	scaled scale height defined by Eq. (4-11)
σ_r	scaled radius
$\bar{\sigma}_r$	scaled radius at which $\frac{\Delta p}{p} = .1$
τ	Rayleigh wave period
ω	frequency of disturbance